PRASUN DASTIDAR

Volumetric Estimation of Structures and Lesions of the Respiratory, Reproductive and Central Nervous Systems

■

ACADEMIC DISSERTATION

To be presented, with the permission of
the Faculty of Medicine of the University of Tampere,
for public discussion in the main auditorium of Building K,
Medical School of the University of Tampere,
Teiskontie 35, Tampere, on April 15th, 2004, at 12 o'clock.

Acta Universitatis Tamperensis 995

ACADEMIC DISSERTATION
University of Tampere, Medical School
Tampere University Hospital, Department of Diagnostic Radiology
University of Technology, Ragnar Granit Institute
Finland

Supervised by
Professor Erkki Laasonen
University of Tampere
Professor Hannu Eskola
Tampere University of Technology

Reviewed by
Docent Kaarina Partanen
University of Kuopio
Docent Tapani Tikkakoski
University of Oulu

Distribution

University of Tampere
Bookshop TAJU
P.O. Box 617
33014 University of Tampere
Finland

Tel. +358 3 215 6055
Fax +358 3 215 7685
taju@uta.fi
http://granum.uta.fi

Cover design by
Juha Siro

Printed dissertation
Acta Universitatis Tamperensis 995
ISBN 951-44-5920-2
ISSN 1455-1616

Electronic dissertation
Acta Electronica Universitatis Tamperensis 328
ISBN 951-44-5921-0
ISSN 1456-954X
http://acta.uta.fi

Tampereen yliopistopaino Oy Juvenes Print
Tampere 2004

CONTENTS

ABBREVIATIONS **5**

LIST OF ORIGINAL COMMUNICATIONS **8**

ABSTRACT **9**

1 INTRODUCTION **11**

2 REVIEW OF THE LITERATURE **14**

2.1 PHYSICAL AND TECHNICAL BACKGROUNDS OF IMAGE PROCESSING **14**

2.1.1 IMAGE SEGMENTATION 15

2.1.1.1 EDGE DETECTION METHODS 17

2.1.1.2 REGION IDENTIFICATION METHODS 18

2.1.1.3 PROBLEMS INVOLVED IN SEGMENTATION 19

2.1.2 QUANTITATIVE MEASUREMENTS OF OBJECTS 19

2.2 RADIOLOGICAL PROCESSING OF MEDICAL IMAGES **20**

2.3 THREE-DIMENSIONAL VISUALIZATION **21**

2.4 CLINICAL APPLICATIONS OF IMAGE SEGMENTATION **23**

2.4.1 NASAL AIRWAY DISEASES 23

2.4.2 OVARIAN TUMORS 24

2.4.3 FETAL WEIGHT ABNORMALITIES 25

2.4.4 MULTIPLE SCLEROSIS 26

2.4.5 CEREBRAL INFARCTION 28

3 AIMS OF THE PRESENT STUDY **30**

4 PATIENTS AND METHODS **31**

4.1 PATIENTS (II-VI) **31**

4.1.1 NASAL AIRWAY DISEASES (II) 31

4.1.2 OVARIAN TUMORS (III) 32

4.1.3 FETAL WEIGHT ESTIMATION (IV) 32

4.1.4 MULTIPLE SCLEROSIS (V) 32

4.1.5 CEREBRAL INFARCTION (VI) 32

4.2. RADIOLOGICAL EXAMINATIONS **33**

4.2.1 FETAL ULTRASOUND (IV) 33

4.2.2 COMPUTED TOMOGRAPHY (II) 33
4.2.3 MAGNETIC RESONANCE IMAGING (III-VI) 33
4.2.3.1 OVARIAN TUMORS (III) 34
4.2.3.2 FETAL WEIGHT ESTIMATION (IV) 34
4.2.3.3 MULTIPLE SCLEROSIS (V) 35
4.2.3.4 CEREBRAL INFARCTION (VI) 36
4.3 OTHER PROCEDURES USED TO OBTAIN LESION VOLUMES (II-III) 37
4.3.1 RHINOMETRY (II) 37
4.3.2 LAPAROTOMY (III) 37
4.4 SEMIAUTOMATIC SEGMENTATION AND 3D RECONSTRUCTIONS 38
4.4.1 ANATOMATIC SOFTWARE (I) 38
4.4.1.1 CT 40
4.4.1.2 MRI 41
4.4.1.3 PHANTOM TEST (I) 45
4.4.2 MEDIMAG SOFTWARE (II, III, VI) 46
4.5 INTER- AND INTRA-OBSERVER STUDIES (II-VI) 47
4.5 INTER- AND INTRA-OBSERVER STUDIES (II-VI) 48
4.6 STATISTICAL ANALYSES (II-VI) 48
4.7 ETHICAL CONSIDERATIONS 49
5 RESULTS 50
5.1 TECHNICAL RESULTS (I-VI) 50
5.1.1 SEGMENTATION AND TIME CONSUMPTION (I-VI) 50
5.1.2 THREE-DIMENSIONAL REFORMATIONS (II-VI) 52
5.1.3 INTER- AND INTRA-OBSERVER STUDIES IN VARIOUS DISEASE GROUPS (III, V, VI) 54
5.2 CLINICAL RESULTS AND CORRELATIONS (II-VI) 55
5.2.1 NASAL AIRWAY DISEASES (II) 55
5.2.2 OVARIAN TUMORS (III) 56
5.2.3 FETAL WEIGHT ESTIMATION (IV) 58
5.2.4 MULTIPLE SCLEROSIS (V) 60
5.2.5 CEREBRAL INFARCTION (VI) 63
6 DISCUSSION 67
6.1 TECHNICAL CONSIDERATIONS (I-VI) 68
6.1.1 SEGMENTATION TECHNIQUES (I) 68

6.1.2 TIME USED TO PERFORM VOLUMETRIC ANALYSIS (I-VI) 69
6.1.3 SLICE THICKNESS AND GAP 69
6.1.4 INTER- AND INTRA-OBSERVER VARIATIONS (II-VI) 70
6.1.4.1 GENERAL 70
6.1.4.2 INTER-OBSERVER STUDIES: 70
6.1.4.3 INTRA-OBSERVER STUDIES: 71
6.1.5 USE OF DIFFERENT MRI SEQUENCES IN DISEASES STUDIED (II-VI) 72
6.2 MEDICAL IMAGING (II-VI) 73
6.2.1 NASAL AIRWAY DISEASES (II) 73
6.2.2 OVARIAN TUMORS (III) 75
6.2.3 FETAL WEIGHT ESTIMATION (IV) 75
6.2.4 MULTIPLE SCLEROSIS (V) 77
6.2.5 CEREBRAL INFARCTION (VI) 79
6.3 3D REPRESENTATION OF VOLUMETRIC MR IMAGES 81
6.4 TRENDS IN THE FUTURE 81
7 SUMMARY AND CONCLUSIONS 83
ACKNOWLEDGEMENTS 85
REFERENCES 87

ABBREVIATIONS

AD	Alzheimer's dementia
ADC	Apparent diffusion coefficient
AR	Acoustic rhinometry
ASSET	Array spatial sensitivity encoding
ABI	Barthel index
BIT	Behavioral inattention test
BITB	Behavioral subtests of BIT
BITC	Conventional subtests of BIT
BPF	Brain parenchymal fraction
CD	Color Doppler
CNS	Central nervous system
CSF	Cerebrospinal fluid
CT	Computerized tomography
CTA	Computerized tomography angiography
DCR	Dacro cysto rhinostomy
DICOM	Digital imaging and communications in medicine
DMSS	Directed multispectral segmentation
DSA	Digital subtraction angiography
DWI	Diffusion weighted imaging
EDSS	Expanded disability scoring scale
EPI	Echo planar imaging
ENT	Ear nose and throat
ERCP	Endoscopic retrograde cholangiopancreatography
ETL	Echo train length
FESS	Functional endoscopic sinus surgery
FH	Flow heterogeneity
FIGO	International Society of Gynecology and Obstetrics
FLAIR	Fluid attenuated inversion recovery
FORE	Fourier rebinning
FOV	Field of view
fMRI	Functional magnetic resonance imaging
FSD	Fletcher Suit Delclos
fGM	Fraction of gray matter
fWM	Fraction of white matter

fCSF	Fraction of cerebrospinal fluid
FSE	Fast spin echo
Gadolinium-DTPA	Gadolinium diethylenetriamine pentaacetic acid
GEORG	Geometrically constrained region growth
HCT	Helical computerized tomography
HIV	Human immunodeficiency virus
HR	High resolution
HRCT	High resolution computerized tomography
HMFT	Hand motor function test
IARD	Image enhancement, amplitude segmentation, region growing, decision making
ICH	Intracerebral hematoma
ISODATA	Interactive self organizing data analysis
Java	Platform independent programming language
MAPS	Posterior spatial probability
MB	Megabyte
MCHC	Multicontext fuzzy clustering
MHz	Megahertz
MIDAS	Medical Image Display and Analysis Software
MIP	Maximum intensity projection
MMSE	Mini-mental state examination
MPR	Multiplanar reformation
MRA	Magnetic resonance angiography
MRI	Magnetic resonance imaging
MRS	Magnetic resonance spectroscopy
MS	Multiple sclerosis
MSA	Multispectral automatic
MT	Magnetization transfer
MTC	Magnetization transfer contrast
MTR	Magnetization transfer ratio
MTT	Mean transit time
NEX	Number of excitations
NAWM	Normal-appearing white matter
NIHSS	National Institute of Health scoring scales
OMC	Osteomeatal complex
PC	Personal computer

PD	Proton density
PET	Positron emission tomography
PWI	Perfusion weighted imaging
RAM	Random access memory
RAVENS	Regional analysis of volumes examined in normalized space
RFSS	Regional functional scoring scale
RRMS	Relapsing remitting multiple sclerosis
SE	Spin echo
SEM	Standard error of means
SENSE	Sensitivity encoding (in MRI)
SIENA	Structural image evaluation using normalization of atrophy
SIENAX	An adaptation of SIENA for cross-sectional measurement
SIR	Signal intensity ratio
SMASH	Simultaneous acquisition of spatial harmonics
SPECT	Single photon emission computerized tomography
SPGR	Spoiled gradient
SPMS	Secondary progressive multiple sclerosis
TE	Time of excitation
T	Tesla
TM	Trade mark
TR	Time of repetition
TSE	Turbo spin echo
US	Ultrasound
VHM	Visible human man
WMH	White matter hyperintensities
1D	One-dimensional
2D	Two-dimensional
3D	Three-dimensional

LIST OF ORIGINAL COMMUNICATIONS

The thesis is based on the following original communications, referred to in the text by their Roman numerals I - VI.

I Heinonen T, Dastidar P, Kauppinen P, Malmivuo J, Eskola H (1998): Semi-automatic tool for segmentation and volumetric analysis of medical images. Medical and Biological Engineering and Computing 36: 291-296.

II Dastidar P, Numminen J, Heinonen T, Ryymin P, Rautiainen M, Laasonen E (1999): Nasal airway volumetric measurement using segmented HRCT images and acoustic rhinometry. American Journal of Rhinology 13: 97-103.

III Dastidar P, Mäenpää J, Heinonen T, Kuoppala T, Van Meer M, Punnonen R, Laasonen E: (2000): Magnetic resonance imaging based volume estimation of ovarian tumors: use of a segmentation and 3D reformation software. Computers in Biology and Medicine 30:329-340.

IV Uotila J, Dastidar P, Heinonen T, Ryymin P, Punnonen R, Laasonen E (2000): Magnetic resonance imaging compared to ultrasonography in fetal weight and volume estimation in diabetic and normal pregnancy. Acta Obstetrica et Gynecologica Scandinavica 79:255-259.

V Dastidar P, Heinonen T, Lehtimäki T, Ukkonen M, Peltola J, Erilä T, Laasonen E, Elovaara I (1999): Volumes of brain atrophy and plaques correlated with neurological disability in secondary progressive multiple sclerosis. Journal of the Neurological Sciences 165: 36-42.

VI Dastidar P, Heinonen T, Ahonen JP, Jehkonen M, Molnar G (2000): Volumetric measurements of right cerebral hemisphere infarction- use of a semiautomatic MRI segmentation technique. Computers in Biology and Medicine 30:41-54.

The publishers of the original articles have kindly granted permission to reprint the papers. In addition, some unpublished data are presented.

ABSTRACT

In the field of radiology today, computer-based quantification methods allowing measurement of tissue volumes and representation of lesions in various diseases have not been adequately studied. In the present study we evaluated the clinical use of a semiautomatic segmentation software, Anatomatic™, in volumetric measurements, and of Medimag™ software in 3D analysis in five different disease groups. A phantom test included volumetric analysis of five different-sized syringes imaged with MR and showed a relative error of 1.5%.

The volumes of the nasal airways were calculated on the basis of the segmentation of HCT sections of the paranasal sinuses and measured in acoustic rhinometry in 14 patients. Statistically significant correlations were found between HCT segmented and acoustic rhinometry-computed volumes of the anterior ($p=0.01$) and middle parts ($p=0.03$) but not in the posterior part of the nasal cavity.

MR imaging on a 1.5 Tesla MR unit was performed on six patients with ovarian tumors. The tumor volumes obtained with the segmentation of both T2-weighted and contrast-enhanced T1-weighted images were compared with those obtained during laparatomy. The computed volumes agreed well in four patients but did not agree in two cases with complex cystic tumors and ascites.

Fetal weight at the 39^{th} gestational week was estimated by routine ultrasonographic methods and with the segmentation of T1-weighted high-field MR images in 10 normal subjects and in 10 subjects suffering from diabetes. Significant correlation was found between the US-estimated and MRI-estimated fetal weights. Also the MRI-estimated fetal weights correlated better with the actual birth weights than US.

In 28 patients with multiple sclerosis, the high intensity lesions of the brain on 3D T2-weighted images scanned with a 0.5 Tesla MR scanner were segmented and the total plaque volume was found to correlate with the regional functional scoring scale (RFSS) ($p=0.03$). Also the volumes of relative ($p=0.005$) and total ($p=0.006$) intracranial CSF spaces and the total brain volume ($p=0.01$) were more significantly associated with neurological disability as expressed by extended disability scales (EDSS) than with other measures.

3D T2-weighted imaging of the brain with 0.5 Tesla MR scanner was performed on 40 patients with right hemisphere brain infarction at a subacute phase. The clinical examination included evaluation of National Institute of Health scoring scales (NIHSS), hand motor function test (HMFT), Barthel Index (BI) and neglect scores. The segmented volumes of the infarcts showed positive correlation with NIHSS (p less than 0.0001), HMFT (p less than 0.001), BI (p less than 0.0001) and degree of neglect (p less than 0.0001). Also, patients with higher quantified infarction volumes (cut off at +-10.5 cm3) showed slower recovery than patients with smaller infarctions at 3 months, 6 months and 1 year of clinical follow-up.

The inter-observer variations in the computed lesion volumes of the ovarian tumors, multiple sclerosis plaques and cerebral infarctions were 4%, 1.5%, and 7% respectively, and the corresponding intra-observer variations were 2.5%, 1% and 3% respectively. In addition, realistic 3D reformations were produced on the nasal airways and sinuses, MS plaques and brain infarctions. The Anatomatic^{TM} and Medimag^{TM} software packages provided a user-friendly tool for interactive image segmentation, volume computing and 3D reconstructions with an expanding role in various clinical applications of diagnostic imaging.

1 INTRODUCTION

A new era has dawned in radiology, where computer-based image processing is being increasingly used and made accessible not only to research centers but also to the majority of radiological practices. Computer-based volumetric methods have the capability to make accurate measurement of tissue volumes and to recognize qualitative changes in lesions (Kischell et al. 1995).

The use of volumetric analysis in radiology goes back as far as the early part of the 20th century. Visual assessment of organs and lesions of determined shape and size from conventional radiological examinations has been done since the invention of X-rays and is even used in the modern age with new imaging modalities such as ultrasound (US), computerized tomography (CT), magnetic resonance imaging (MRI) and positron emission tomography (PET). Volume estimation on the basis of longitudinal dimensions has been and is being done even today using X-rays (e.g. cardiac volume, lung volume, pleural cavity volume), ultrasound, CT and MRI (e.g. fetal volume estimation, tumor and organ volume). In the literature the earliest reports of lung volumetry from pulmonary X-rays for clinical purposes were made in the 1960s (Stepanek and Zavada, 1969). In the 70s and 80s human brains and temporal bones were studied by this method (Orthner and Seler 1975, Georgi et al. 1980, Igarashi et al. 1983, Brassow et al. 1984).

Segmentation of medical images is one of the most important steps in the volumetric estimation of imaging data (Sueten et al. 1993). This method, first introduced three decades ago (Ritman et al. 1979, Harris et al. 1979), entails formation of these acquired imaging data from a stack of images into homogenous regions of similar characteristics, finally reported as a sum of volume elements called voxels. Voxels are the imaging information received, processed and stored with computers. Mostly

these voxels resemble a short pencil, e.g. 1x1x10 mm on the side. They are reproduced on screen or film as two-dimensional picture elements (pixels), where one dimension of voxels is omitted. The application of this volumetric principle has since been modified, when the first generation of three-dimensional (3D) spiral-helical computed tomography (HCT) (Costello et al. 1991, Hollett et al. 1995, Quint et al. 1995) and 3D MRI were developed for clinical and diagnostic use.

In the central nervous system (CNS), changes in ventricular volume and brain tissue have been noted in various clinical conditions. Volumetric analysis of the intracranial cerebrospinal fluid (CSF) spaces helps in the differential diagnosis of normal pressure hydrocephalus from Alzheimer's disease (AD) (Matsumae et al. 1996). Volumetric estimation of the brain atrophy in several diseases helps make differential diagnosis and prognosis. MRI-based volumetry of the mid-brain differentiates Parkinson's syndrome from multiple system atrophy and progressive nuclear palsy (Schulz et al. 1999). Significantly reduced volumes of hippocampal formation and the entorhinal cortex are seen in AD compared with controls (Parnetti et al. 1996, Juottonen et al. 1999). In stroke, serial changes in the brain and infarct volume during the course of acute infarction are of prognostic importance (Strinska-Kus and Filipzcak, 1990). In herpes simplex encephalitis, volumetry of different parts of the limbic system helps predict the outcome of the disease (Yoneda et al. 1994). Lesion volumetry in various diseases helps evaluate medical therapy. In multiple sclerosis, especially in phase three treatment trials, serial studies of quantitated MRI-based multiple sclerosis (MS) plaques and brain atrophy is made to evaluate the effects of medical therapy (Filippi et al. 1995). In intracranial tumors, it has been applied successfully in the pre-and post-operative assessment of the solid tumor core, cystic, calcified or vascular components, areas of necrosis or hemorrhage and edema surrounding the tumor (Vinitski et al. 1997). Lesion volume analysis is also useful in measuring progress of disease with time. Volumetric measurements of the amygdohippocampal complex and extrahippocampal limbic system parts such as fornix and mamillary bodies in patients with temporal lobe epilepsy (Bilir et al. 1998) are important parameters in follow-up of this disease. Volume analysis of infarctions and demyelinating lesions in serial studies helps assess the clinical deterioration in systemic lupus erythematosus (Sibbitt et al. 1999). Serial volumetric estimation of endocrinal hypophyseal tumors (Benesch et al. 1996) following bromocriptine treatment shows a significant decrease in follow-up studies. Lesion volume estimation of subdural and extradural hematomas in severe head injuries has been identified as prognostically useful and is used in follow-up of such patients (Stocchetti et al. 2000).

In the respiratory system, the nasal fossa has previously been evaluated by CT and volumetric analysis in preoperative assessment (Corsten et al. 1996). Volumetric analysis has also been made using other modalities such as acoustic rhinometry (AR). AR estimation of volumes in the nasal cavity has been satisfactory in its anterior and middle thirds but has been found unsuitable in the posterior portion (Hilberg et al. 1989, Hilberg et al. 1993). In the head and neck area, the volumes of the pneumatized portion of the temporal bone have been found to be significantly decreased in chronic inflammatory diseases and congenital abnormalities (Brassow et al. 1984). A significant increase has been recorded in the CT volumes of the four recti muscles and orbital fat in Graves' disease (Krahe et al. 1989). An increase in orbital volume and severity of enopthalmus in post-traumatic patients helps plan the surgical reconstruction of the orbital walls (Carls et al. 1994). Serial studies of US-based volumes of the thyroid show a decrease after radioiodine treatment in hyperthyroidism (Peters et al. 1996). The

treatment effects of radiotherapy are evaluated using MR-based volume changes in neck lymph node metastases in malignant head and neck tumors (Liszka et al. 1997).

In the human reproductive system, volumetric analysis with CT/MRI has proved useful for diagnosis, clinical planning and therapy. For volume estimation of gynecologic masses and fetuses, on the other hand, US has been far from ideal especially in macrosomic fetuses (Hirata et al. 1990) and large pathological endometrial lesions (Senoh et al. 1999). Fetal weight estimation by volumetric analysis of the fetus using echo planar imaging (EPI) MRI technique has led to near-accurate estimation of actual birth weights (Baker et al. 1994a). Measurement of total fetal volume and different fetal organ volumes (brain, liver and lungs) and their differential growth by MRI forms a sensitive method of assessing intrauterine growth in normal and abnormal pregnancy (Garden and Roberts 1996). In cervical cancers, tumor volume measurement is a major prognostic factor and is superior to International Federation of Gynecology and Obstetrics (FIGO) staging as basis for classification of tumors preoperatively (Hofmann et al. 1988). Moreover, gynecologic malignancies have been classified into better therapy response categories when the 3D volume method of tumor bulk estimation (using pre and post therapy CT/MRI) has been used (Piver et al. 1993).

The 3D visualization method was developed to provide qualitative information on a tissue or tissue system from two-dimensional (2D) or 3D medical image sets (Udupa et al. 1999). In the 1980s, 3D information contained in cross-sectional images in CT was studied through analysis of multiple 2D images. Several methods for direct display of 3D gray-level data were investigated (Hoehne et al. 1987, Park and Lee, 1987, Herman, 1988, Robb et al. 1989, Sundaramoorthy et al. 1995). 3D visualization also necessitates the use of segmentation. This improves the depiction of structures which are oriented out of the plane of the original image acquisition (Apicella et al. 1995).

For this purpose, our research group has developed new, fast semiautomatic segmentation software, Anatomatic^{TM} (Heinonen et al. 1997) and Medimag^{TM} software (Heinonen et al. 1998b) for volume estimation and 3D visualization, respectively, in various diseases.

2 REVIEW OF THE LITERATURE

2.1 PHYSICAL AND TECHNICAL BACKGROUNDS OF IMAGE PROCESSING

An image is a collection of spatially ordered elements (pixels) representing a scene. The scene is usually assumed to consist of several objects in a background. Both the background and object parts generate a class of pixels to be characterized by its own statistical properties. In medical imaging, the pixels represent different information depending on the imaging modality, e.g., in CT the pixels represent CT numbers and in MRI a pixel represents different relaxation times. When medical images are sectional images of a particular thickness the image pixels are understood as voxels.

Images can be processed using techniques such as image enhancement (e.g., image windowing and levelling), restoration (e.g., filtering noise and artifacts), transformation (e.g., mathematical modeling and modification) and classification (e.g., recognition of structures) (Jain 1989). These techniques are often applied in improving image appearance and correcting artifacts and noise in the images. However, the classification technique can be applied in image analysis, in which homogenous structures in the images are detected and recognized. One of the important techniques allowing classification is segmentation (Ramac et al. 1997), where an image is divided into its constituents or classes (represented using pixels). Furthermore, a segmentation procedure can apply several image processing techniques consecutively, for example image enhancement and feature extraction (e.g.,

emphasis of region of interest using any of the image processing techniques), in addition to segmentation and classification (Figure 1).

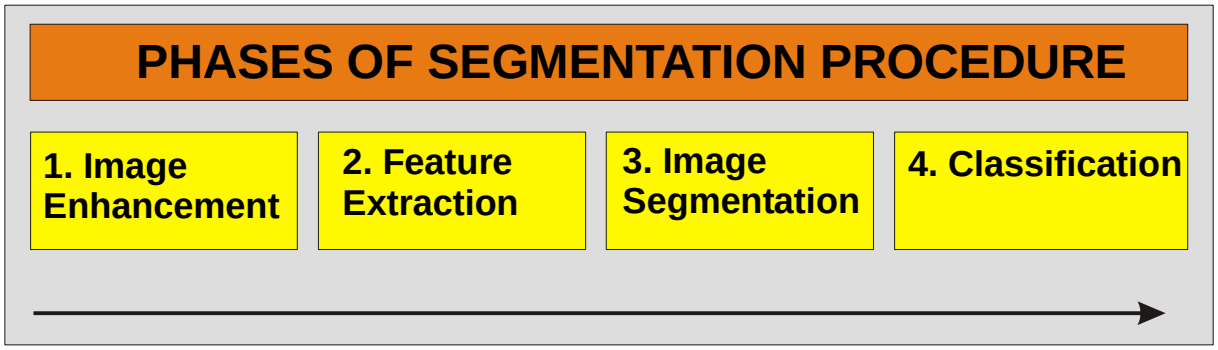

Figure 1. The segmentation procedure consists of four consecutive stages; first image enhancement aiming to improve image quality, feature extraction to emphasize region of interest, image segmentation to separate region of interest from other regions, and classification in order to detect/recognize segmented structures.

The ultimate goal of image segmentation in medicine is to extract important clinical information which will improve diagnosis and treatment of disease (Soltanian-Zadeh et al. 1996, Leung and Lam 1997) or even suppress the amount of non-relevant information from very large and poorly outlined datasets to make it easier to single out the important clinical information.

In conventional image diagnosis, the radiologist carries out visual segmentation; anatomical and pathological structures are separated from each other and thereafter recognized. When computerized segmentation is carried out, the result can be utilized further; volumetric analysis can be performed and segmented structures visualized separately using 3D techniques. Image segmentation consists of separating several lesions and structures from a medical image. The segmentation procedure consists of the whole procedure starting from the initial stage where the original CT/MRI image is enhanced, thereafter the different features of lesions and structures are noted and segmented, and finally these segmented lesions and structures are classified into specific classes, i.e. classification. The segmentation techniques consist of the different algorithms on the basis of which various segmentation softwares are constructed.

2.1.1 IMAGE SEGMENTATION

Image segmentation is an important research area in medical image processing (Zucker 1976, Haralick and Shapiro 1985, Pavlidis 1988, Anuweiri and Prasana 1992). The segmentation technique (software which allows image segmentation) classifies each voxel of an image (CT/MRI) into a particular class. It subdivides an image into its constituent (i.e., region of interest) parts or objects homogeneous in terms of some characteristics such as borders and homogenous intensities (e.g., the region of interest

appears with unique intensity range compared to other parts of the image) (Kwok and Constantinides 1997, Jacquelin et al. 1997). The segmentation techniques can be classified as manual (full manual interaction), semiautomatic (where the procedure is nearly automatic but allows human interaction to correct errors possibly arising due to different structures having similar intensities) and automatic (where no human interaction is possible). The various segmentation techniques can be classified according to level of interactivity and operation principle. On the basis of the level of interactivity they can be classified as manual, semiautomatic and automatic and by operation principle classified into: 1) statistical approach where different features of the image are grouped together using statistical analysis and 2) structural approach, where structures are identified on the basis of their intensities and shape (Lei and Sewchand 1992).

Segmentation techniques based on the statistical approach utilize mathematical feature variables or vectors in estimating properties of image details such as shape, texture, intensity, similarity etc. These computed parameters can be compared to particular model parameters, enabling statistical classification. The main aim of the statistical segmentation technique is to estimate statistically properties of different regions in MR images. Li and associates. in 1993 developed a knowledge-based system to detect and classify basic brain structure and possible abnormalities such as tumors. In 1993 Liang developed a conventional statistical technique by applying T1, T2 and PD MR images together with the distribution function of image intensities. This led to nearly automatic segmentation.

Segmentation techniques based on the structural approach can be further classified as 1) methods based on edge detection and 2) region identification methods based on homogenous intensities (Liang 1993). The following table enumerates different segmentation techniques (see Table 1).

Table 1. Classification of the structural image segmentation techniques.

EDGE DETECTION METHODS	REGION IDENTIFICATION METHODS
These methods seek borders between structures having homogenous intensities. The borders which are closed (i.e., surround an object) are detected and coded as chain links.	These methods seek regions of interest having homogenous intensities. These regions are labelled and separated from other parts of the image.
COMMON TECHNIQUES: Gradient operations Contour following Laplace derivatives Gaussian kernels	COMMON TECHNIQUES: Clustering Region growing Slit and merge Thresholding

2.1.1.1 EDGE DETECTION METHODS

Edge detection methods identify a class of objects with smooth boundaries which are continuously deformable. They search for edges between regions (Chen et al. 1991). These methods are often based on gradient operators (transformations which improve the appearance of borders on the image), followed by a threshold operation, in order to delineate edges and borderlines. The detected edges are stored as contour lines (chain links).

The most successful method in this category is the edge detection operator of the Laplacian derivative of a Gaussian kernel. This method has an adjustable parameter (depending on image quality and properties of region of interest) which requires interaction from the user (i.e., the person who carries out the segmentation procedure) (Bomans et al. 1990). The interaction causes difficulty in automating the segmentation procedure. These edge detection techniques produce boundaries (i.e., chain links surrounding the region of interest) which are often inaccurate, since the technique is sensitive to noise, particularly between regions with small contrast differences.

2.1.1.2 REGION IDENTIFICATION METHODS

Region identification methods classify an image into a number of regions or classes based on spatial properties of voxels. (Chakraborty et al. 1996). They can be divided into clustering schemes (based on partitioning an image into regions of similar features such as shapes, textures and intensities), region growing schemes (operates by merging neighbouring voxels of similar features), split and merge growing schemes (used as feature extractors to produce images with uniform intensities) (Revol and Jourlin 1997), and thresholding schemes (Jain 1983).

Clustering is also known as unsupervised classification and is a process by which a data set is divided into different clusters such that elements of the same cluster are as similar as possible and elements of different clusters as dissimilar as possible. These involve complex mathematics and statistical analysis in order to increase the performance and pattern recognition properties (Frigui and Krishnapuram 1997). The approach has been used in segmentation of medical images such as MR images of different pulse sequences (Taxt et al. 1994).

Region Growing looks for groups of voxels with similar intensities. It starts with one voxel and then examines its neighborhood in order to decide whether there are items having similar intensities. If they do, they are grouped together to form a region. In this way regions grow out of single voxels. More advanced forms do not start with voxels but with a partition of the image into a set of small regions. A uniformity test is then applied to each region and if the test fails the region is subdivided into smaller elements. This same earlier process is repeated for all regions until they are uniform (Yong and Fu, 1986, Sahoo et al. 1988). The region growing algorithm can also be implemented in 3D.

Split and merge is an extension of the region growing and uniformity testing method (Yong and Fu, 1986, Sahoo et al. 1988). It starts with the entire image being considered as the initial segment. The current segment is then successively split into quarters if the segment is not sufficiently homogenous. After the split, two quarters are merged into a region. This process goes on till when additional splitting or merging is no longer possible (Liang 1993).

Thresholding (i.e., amplitude segmentation) has been the most common and widely used segmentation technique since 1962. It is based on a simple image enhancement technique called noise clipping. The image histogram is analyzed and two seed values are selected: the minimum and maximum intensities representing the region of interest. All other gray scales in the histogram are set at zero. The selection of suitable threshold coefficients (thresholding) is ideally an automatic process requiring some criteria on which selection is based (Li et al. 1997). The thresholding selection techniques can be divided into bilevel and multilevel groups. In bilevel thresholding, one threshold value is used for segmenting an image into a background and an object. It is used if an image has an object distinct from the background. Multilevel thresholding is used when an image has several different objects distinct from the background. (Sahoo et al. 1997). For example the HBRS (histogram-based brain segmentation) technique has been found to be an accurate means of determining brain volume with high reproducibility (Shan et al. 2002). However, a fundamental limitation of thresholding as an approach to segmentation is that voxels having the same gray level value will always be segmented into the same

class. Either manual interaction is needed or highly accurate prior knowledge must be assimilated into the system to obtain proper segmentation.

Interactive algorithms (i.e., the user controls the segmentation procedure) are an attractive approach to the accurate segmentation of 3D brain scans, as they potentially improve the reliability of fully automated segmentation while avoiding the labour intensiveness and inaccuracies of manual segmentation. In recent times, numerous new image segmentation algorithms have been developed, based on gray level thresholding, edge detection, region growing, splitting and merging, relaxation and fuzzy set theory (Gupta et al. 1998). For example, the MCFC (multicontext fuzzy clustering) technique has been used for classifying 2D and 3D data into tissues of white matter, gray matter and cerebrospinal fluid automatically (Zhu et al. 2003). However, there is no single algorithm which can effectively segment all types of images. Different commercially available volume estimation techniques based on segmentation techniques are available today either along with the purchase of workstations connected to a CT/MRI machine and also on the internet. The application of different algorithms to the same image produces different results. The selection of an appropriate algorithm depends on the type of images and selection areas.

2.1.1.3 PROBLEMS INVOLVED IN SEGMENTATION

Every segmentation procedure has drawbacks, associated mainly with variations in the human anatomy, image artifacts, noise, processing time, and variations caused by the user interaction. With manual and semi-automatic methods, the reproducibility is usually poor because the operator involved in segmentation can affect the accuracy of the results considerably. Automatic methods are indeed operator-independent and there is thus a high reproducibility of results, but they are then sensitive to noise and unexpected situations in medical images leading to volume errors which will not be corrected in the absence of interactivity. Image features of abnormal tissues may be very close to those of their neighbouring normal tissues. Normal tissues may be found in an abnormal tissue component after segmentation. Second, image features of a tissue may vary. The effect on segmentation is that several components which have different labels then correspond to a single tissue. These problems motivate one to a knowledge-based approach where domain knowledge (i.e., prior information for anatomy) is applied to an initial segmentation to progressively identify landmarks (i.e., easily identified anatomical regions such as ventricles), to classify different tissues (as a result of image segmentation) and finally to determine normal or abnormal tissues (Li et al. 1993).

2.1.2 QUANTITATIVE MEASUREMENTS OF OBJECTS

When medical images have been segmented i.e., into voxels representing particular tissues, organs and pathological lesions, the number of voxels can be computed (e.g., how many voxels represent the region of interest). Because the physical dimensions of the image set are known (based on parameters of CT/MRI such as field of view, matrix, and slice thickness) it is possible to calculate the volume of a voxel. By multiplying the number of voxels and the voxel dimension one can achieve the real volume of the segmented structure.

In brain morphometry, a relationship exists between brain structure and function, both normal and abnormal. One descriptor of morphometric structure is volume. Lesion extraction has been achieved with the intention of quantitating and staging diseased brain parenchyma (Raff and Newman 1992). For example, MR-based volumetry establishes developmental characteristics of the temporal lobe such as hippocampal growth spurt, a growth difference between the hippocampal formation and the rest of the temporal lobe and right-left asymmetry, all of which aid in understanding abnormalities in children (Utsunomiya et al. 1999).

Volumetric accuracy differs with various imaging modalities. For example, in intracranial hematomas (ICH), when compared to CT volumetry, gradient echo T2 weighted MRI-based volumetric measurements overestimate the ICH size, whereas diffusion weighted MRI-based volumes correlate well with the ICH volume on CT (Schellinger et al. 1999). Also the thickness of a particular slice affects the final volume. Although in an earlier study with MRI-based hippocampal volumetry, no significant difference between the volumes of the hippocampus using different slice thicknesses of 1, 3 and 5 mm was observed it seems that the use of thin slices is more authorative and less vulnerable to interference by a single false estimate (Laakso et al. 1997).

An operator-independent technique has been developed for quantitating the volumes of white matter, gray matter and cerebrospinal fluid (Raff et al. 1994). For example, RAVENS (Regional Analysis of Volumes Examined in Normalized Space) and many other systems are presently being used for longitudinal data imaging in the context of quantitative volumetric analysis of brain images (Goldszal et al. 1998).

2.2 RADIOLOGICAL PROCESSING OF MEDICAL IMAGES

Different types of images are encountered in radiological practice. These images can be stored either in the form of still pictures, e.g. still single (anteroposterior or lateral radiograph), still spatial (CT and MRI), and still temporal (dynamic CT or MR imaging) or in the form of live pictures, e.g. on-line (fluoroscopy), stored (postprocessed video images) and constructed pseudo-live (animation from still images). The understanding of these medical images is a complex task, which depends on both the perceptual mechanism and high-level reasoning. Before the era of digital imaging radiological image processing was limited to analogic picture forms which needed to be converted to a digitized form before computers could process them. The latest developments in image processing amongst radiological modalities like those in US, have made possible volumetric estimation and 3D imaging (Meier et al. 1997). With computational CT and MRI analysis, realistic and useful simulations of surgical and endoscopic procedures, including "virtual dissection and resection" and "virtual biopsy", can be done in maxillofacial surgery. Surgical margins are accurately assessed and differential tissue diagnosis can be made (Robb et al. 1997). The use of positron emission tomography (PET) data quantitation has been evaluated in clinical research and patient studies in a new Java environment (Mikolajczyk et al. 1998).

There are several advantages of radiological image processing. The daily use of image processing in all digitized modes of imaging especially in digital radiographs, digital subtraction angiography (DSA),

CT, and MRI has rendered the mode of interpretation more accurate, diagnostically reliable and even three-dimensional. The advantages also include repeatability (good intra- and inter-observer variabilities), speed (faster image processing) and full automation (automatic final image reconstruction) (Cree et al. 1997). Image processing tools enable communication with storage devices such as the picture archival communication system (PACS) and can also itself act as a storage device allowing users to store selected image subsets and reformatted images from an original study without having to know on which server the original data are stored (Cox et al. 1999). New softwares like Medweb using high memory can manage, review and distribute DICOM images efficiently**.** Fully uncompressed 16-bit images (images consist of 65536 gray scales) allow different window settings to better assess the pathology, and cine viewing is possible (Ernst et al. 1999). In a virtual environment (e.g. virtual endoscopy) the advantages are interactive (user-controllable) editing, decrease in time used to create virtual cancer images used for surgical simulation, presurgical planning and 3D invasion diagnoses (Oyama et al. 1998). Also, it leads to a reduction in preoperative risk and the duration of surgical procedure, which in turn results in considerable stress reduction for the patient (Hassfield and Muhling, 1998).

However, there are also disadvantages with radiological image processing. For example, the quality of the stored and transferred medical images may suffer during image processing, leading to diagnostic problems. Some fundamental technological challenges for image processing are 1) cost-effective digital detectors and displays for imaging systems, 2) the need for novel algorithms for image processing and computer-aided diagnosis, and 3) high-performance low-cost digital networks to provide information for teleradiology (Winfield et al. 1994). All these requisites are of course easily available in large centers with high budget, but not in small-scale hospitals where high-standard surgery and therapy after high tech imaging is not possible. These challenges entail a substantial initial investment of millions of euros and cost-effective training of personnel in its use and maintenance (Price and Goldstein 1997). This also is feasible easily in large learning centers but is a problem in small centers.

2.3 THREE-DIMENSIONAL VISUALIZATION

Image representation modes based only on a single axial or coronal view alone do not always completely meet the requirements of diagnostic interpretation, therapeutic decisions or surgical operation. They require the radiologist to undertake sequential examinations of images with three-dimensional reconstructions. The availability of 3D volume and surface reconstructions in US, DSA, CT and MRI has prompted a new beginning to the regular use of these in clinical practices, not as a curiosity but as one of the possible useful ways of delivering diagnostic information and for assistance in treatment especially in the field of neurosurgery, head and neck surgery and intra-abdominal tumors.

3D image processing (i.e., a process aiming to produce photorealistic 3D images from a set of section images) includes several stages, namely image acquisition (i.e., patient imaging with an imaging device such as CT or MRI), image pre-processing (to improve the quality of original images), segmentation procedure (detect the region of interest to be displayed in 3D), surface reconstruction (i.e., a procedure where a surface is created in order to cover the region of interest), and rendering (i.e., the final stage,

where the surface is displayed in 3D) (see Figure 2). In addition, all these stages can be carried out using various techniques and parameters (Watt and Watt 1992). Such techniques have been incorporated into commercially available medical imaging software packages (Calhoun et al. 1999).

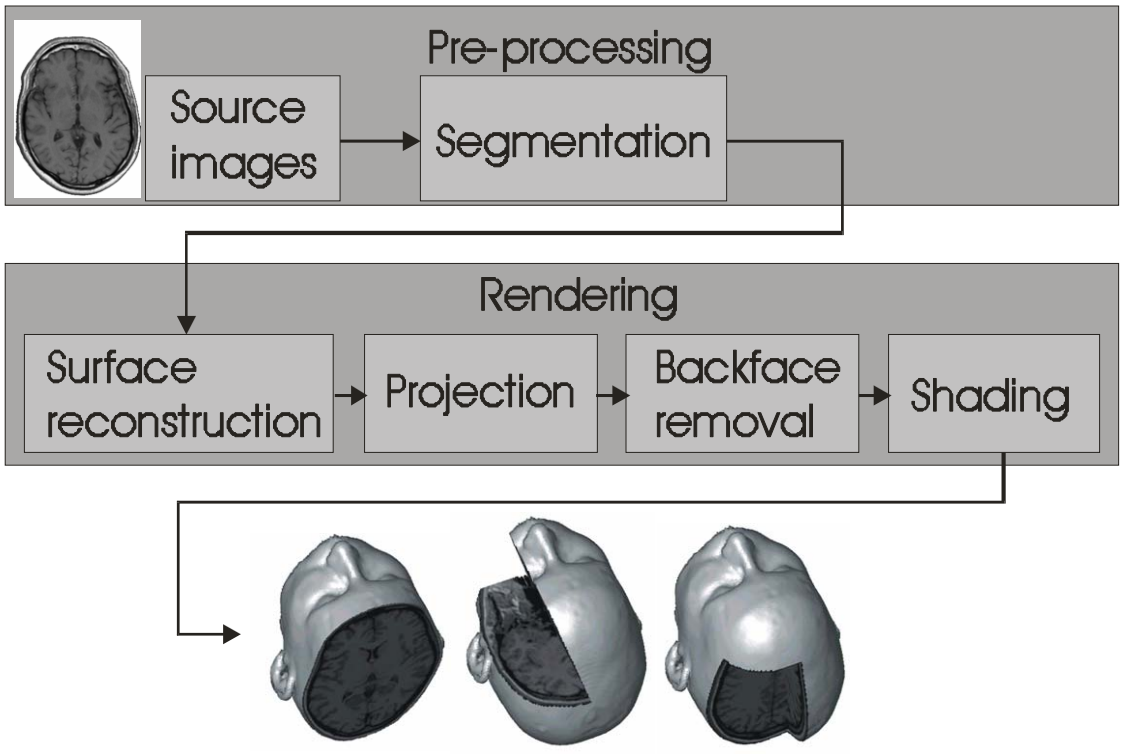

Figure 2. The general stages of 3D image reconstruction. First the acquired images are pre-processed and segmented to present a region of interest. Thereafter, a surface is created to cover the region of interest. Phases such as projection plane definition, backface removal (i.e., surface components such as triangles are drawn in correct order), and shading (i.e., to shade the surface photorealistically). The final 3D image can be projected in all planes and subplanes.

Two different approaches in reconstructing volumetric objects have been established in the area of 3D medical image visualization. One is the volume-based approach where objects are represented as continuous 3D volume data (e.g., segmented voxels). In this approach, 2D slices are stacked together and the missing data between slices usually estimated by interpolation (Choi et al. 1997). Such a dataset is thereafter surrounded with planar elements, which form the object surface. With some special techniques (cuberille and forward mapping), it is possible to display the original dataset directly without generating a surface (Watt 1993) and some specific hardwares (e.g., Silicon Graphics workstations) are capable of displaying such source data in 3D. Another approach is the surface-based

technique, where the surface of an object is approximated using a stack of two-dimensional contours surrounding the segmented structures. The contours are then connected to form a 3D mesh. In order to display the reconstructed surfaces on a computer monitor, several techniques can be applied, for example Phong shading and Ray tracing (Watt 1993).

Internal renderings (e.g., virtual endoscopy) are similar to the above-mentioned techniques, except that the vantage point is from within the imaged volume; this leading to so-called lumen rendering. By acquiring high-resolution digital images with helical CT or 3D MRI scans, individual organs can be graphically isolated or segmented into fully interactive 3-D reconstructions on a computer monitor. Applying sophisticated flight-tracking programs, the organs can be flown to and fro, giving a view identical to that in endoscopy (Satava 1996).

Recently, PC based low cost 3D imaging systems have been described for medical 3D imaging applications. These tools are known to produce easily and quickly relevant information from CT and MRI images in complex medical situations (Raya et al. 1990). New systems have been developed for medical image processing, which allow a multimodal dynamic 3D visualization interactively and in real time using MRI and SPECT (Santarelli et al. 1997). Radiation treatment planning was one of the first areas in which 3D information from imaging techniques were clinically applied (Pelizzari 1998).

2.4 CLINICAL APPLICATIONS OF IMAGE SEGMENTATION

Depending on the clinical query the choice of the appropriate segmentation technique is important. Reasonably fast computational and interaction times make the semiautomatic segmentation technique the optimal tool for segmentation in diseases of the intracranial cavity and head and neck area (Reittner et al. 2002, Ingle et al. 2002). Volumetric measures introduce a level of precision and reproducibility in the estimation of tissue size, not available simply by inspecting a set of MR or CT images (Jack, 1994, Goldszal et al. 1998). Correlating the qualitative and quantitative CT and MRI changes to clinical deficits has improved accuracy in diagnosis and follow-up in various diseases (Clanet et al. 2003).

2.4.1 NASAL AIRWAY DISEASES

The common diseases affecting the nasal airways are acute and chronic rhinosinusitis. The various specific tests are rhinogyrometry, rhinomanometry, acoustic rhinometry (AR), plain sinus X-ray, CT and MRI, of which most commonly used is AR. AR and CT have been used for making quantitative measurements.

Acoustic rhinometry is a noninvasive test performed within a short time, with minimal patient cooperation and in ordinary office settings (Corey et al. 1996). The technique provides a plot of nasal and nasopharyngeal airway cross-sectional area against distance, which again is achieved by comparison of an acoustic signal with its reflection from within the nose, and provides a volumetric estimate of the airway spaces (Hamilton et al. 1995). A significant negative, non-linear relationship has been found between nasal minimum cross-sectional area and nasal resistance. AR is useful when

rapidly repeated measurements are required, as in challenge investigations and also for precise measurement of the nasal valve area (Roithman et al. 1994). The reproducibility of the results of AR is related both to the dynamic mucosal effects on the nasal lumen (e.g. classical and non-alternating nasal cycle, effects of postures, body pressures and temperature changes) and to the method applied for data acquisition (e.g. wave tube- head angle, equipment calibration, nasal vestibule distortion by nasal adapter, sealing around the nostril, and number of curves collected) (Roithman et al. 1995).

Coronal HRCT is the optimal imaging modality for evaluating the nasal cavity and paranasal sinuses, especially in patients with chronic nasal obstruction (Zinreich 1992). This technique is used in preoperative planning of nasal surgery and in postoperative evaluation of results achieved. It is also possible to study the osteomeatal complex and paranasal sinuses simultaneously with the nasal cavities. However previous studies have shown that it can be difficult to evaluate the nasal fossa quantitatively with CT (Corsten et al. 1996). Environmental and postural effects similar to those on AR measurements also affect CT (Kase et al. 1994). The accuracy of HRCT-based measurements and their reproducibility also depends on the thickness, field of view and matrix size of the images**.** The application of CT to explore the volume-function relationship in the nasal cavity has been limited by lack of methods producing a measure of volumes with documented accuracy and validity. In a preliminary study it has been found that with the advent of 3D helical CT (HCT), accurate estimations of volumes can be now obtained in the sinonasal area (Dastidar et al. 1999 a).

In the treatment of chronic rhinosinusitis, functional endoscopic sinus surgery (FESS) has become a practical and successful therapeutic approach (Kennedy et al. 1985). The goal of FESS is to maintain the normal mucosa of the sinonasal cavity to preserve the normal pathway of mucociliary clearance while endoscopically enlarging the passageways of the paranasal sinuses and enlarging the natural ostia. In the process amputation of the uncinate process, enlargement of the infundibulum, resection of anatomical and pathological obstructions in the nasal cavity is done. With the widespread use of FESS, coronal CT has become the study mode of choice since it simulates the endoscopic view of the sinonasal cavity and provides a road map of bone for surgery (Youssem 1993). The use of segmentation has not been evaluated in the diagnosis of sinonasal diseases.

2.4.2. OVARIAN TUMORS

At initial diagnosis, more than 2/3rd of ovarian cancers have metastasized outside the true pelvis (Piver et al. 1993). Though primary surgery aims at clearance of all tumors (Hoskins 1994) residual disease is still seen in at least 50% of cases (Hunter et al. 1992). Levels of CA 125 tell the clinician of the tumor burden but not the location (Berek and Bast 1995). In these cases second-look operations increase morbidity and costs without affecting the final result (Creasman 1994). Noninvasive means of evaluation have been disappointing.

Imaging methods like US, CT and MRI have so far proved disappointing in evaluating the location and quantification of disease. US has proved easy and relatively inexpensive in diagnosis of these tumors but is not ideal for volume measurements. Large irregular shaped ovarian tumors cannot be accurately evaluated due to the limitations set by the transducers in regard to the volume size which can be visualized on the screen. MRI is superior to Doppler US and CT in the diagnosis of malignant ovarian

tumors, but there is very little variation regarding its staging (Forstner and Graf 1999, Kurtz et al.1999). However, neither of these examinations can replace surgery in detection of microscopic peritoneal seeding (Kubik-Huch et al. 2000a).

MRI can predict cyst contents and evaluate potential for malignancy by detecting an irregular solid portion or a papillary nodule within the cyst in ovarian tumors. Fat suppressed post Gadolinium chelate images show an enhancing solid mass reflecting the neoplastic nature of the growth (Kinoshita et al. 2000). Fast spin echo imaging sequences are routinely used in imaging the female pelvis but EPI due to its heavily T2-weighted contrast is a valuable adjunct to FSE images in detection of the uterus, ovary and ovarian tumors (Yamamoto et al. 1999). Diffusion-weighted MRI is useful in evaluating the cystic contents of ovarian tumors. The fluid in the serous cystadenomas shows larger apparent diffusion coefficient (ADC) values than in the cystic contents of malignant ovarian tumors (Moteki and Ishiazaka 2000). A normal CA-125 value but a pathological Gd-chelate enhanced-MRI in favor of a tumor is a strong indication of residual tumor or recurrent ovarian malignancy, proving MRI to be superior in detecting malignancy. The sensitivity, specificity and accuracy of PET, CT and MRI in characterization and detection of recurrent ovarian cancers are comparable and show no statistical difference (Kubik-Huch et al. 2000a).

Only volumetric data can be used for evaluation of response to chemotherapy in gynecologic masses like ovarian tumors (Miller et al. 1981). Earlier, 2D CT and MR imaging were performed where the largest diameter plus its greatest perpendicular for each section provided the best overall representation of the amount of tumor. These were then multiplied together, yielding a 2D area of tumor focus in each section whereafter the areas of all tumor foci were added together to yield the overall tumor bulk (Fornage 1993). Now, however with the help of 3D MRI and segmentation methods more accurate volumetric analysis can be performed in gynecologic malignancies (Hricak 1996). They may even be classified into better or poorer response categories (Hopper et al.1998). The use of segmentation, volumetric analysis and 3D-image reconstruction in cystic ovarian tumors has not previously been mentioned in the literature.

2.4.3. FETAL WEIGHT ABNORMALITIES

Fetal weight estimations constitute a particularly important clinical analysis for obstetricians. Hitherto US-based fetal weight estimations have had an acceptable accuracy clinically if the fetal borders are clearly distinguished and if the growth distribution is normal. However a number of clinical conditions such as maternal obesity, oligohydroamnios and unfavorable fetal positions may result in false measurements and consequently inaccurate weight estimations (Benaceraff et al. 1988).

With ultrasound, fetal weight estimations have been made based on two different formulas. The first, devised by Hadlock and associates in 1935, is based on measurements of biparietal diameter, abdominal circumference and length of femoral diaphysis and the second, by Shepard and group in 1982, is based on measurements of biparietal diameter and abdominal circumference. However, if the distribution of fetal growth is abnormal as in diabetes, these formulas are not optimal (Tamura and Dooley 1991). Later two new formulas were developed by Shinozuka and colleagues in 1987 which gave a smaller range of errors than the former methods. These formulas were based on first, actual

measurements of the volumes of the neonatal head and trunk with limbs, second, on analysis of the relationship between the sizes of the parts of the fetal body measured by US before birth and the volumes of the parts of the neonatal body, and third, on the calculation of the specific gravities of the parts of the neonatal body.

However, MRI has now proved to be a safe and useful technique for evaluation of the fetus in utero (Laptook 1990, Baker et al. 1994b). It does not involve ionizing radiation, has no significant adverse biologic effects and produces high-resolution cross-sectional images of the fetus and maternal parts (Lowe et al. 1985). It is used to diagnose high-risk fetuses as in cases of poor fetal growth, maternal depressive psychosis, maternal systemic lupus erythematosus, habitual intrauterine fetal death, twin pregnancy with one fetus in distress, and fetal hydrocephalus (Hata et al. 1990). However, fetal weight estimations by conventional MRI techniques have been faced with image blurring due to fetal movements (Johnson 1995). In the initial period of EPI development high resolution MRI with T1 weighted images allowed very good detection of fetal borders (clearly distinguishes between subcutaneous fat from the surrounding amniotic fluid) with an acquisition time comparable to that with EPI (Hata et al. 1990). But with the new high-speed EPI the problem of image blurring has largely been obviated (Johnson et al. 1990, Stehling et al. 1990). Ultrafast interleaved gradient-echo-planar imaging (where multiple excitations with multiple gradient echoes are employed) can image even the fetal heart with good resolution within 110 milliseconds (McKinnon et al. 1993). Half-Fourier acquisition single shot turbo spin echo (HASTE) is a sequence that enables high T2 weighted contrast imaging within a few seconds (430 msec) limiting artifacts from maternal and fetal motion. (Levine et al. 1996, Tsuchiya et al. 1996, Yamashita et al. 1997). With half-Fourier single shot rapid acquisition with relaxation enhancement (RARE), fetal anatomy can be well depicted in fetuses over 20 weeks age. Changes in brain maturation in an orderly and predictable fashion can be evaluated reliably. Also RARE images evaluate better fetal abnormalities not well depicted on US (Levine et al. 1998, Huppert et al 1999, Lan et al. 2000) Ultrafast MR imaging is superior to sonography in characterizing cerebral abnormalities though inferior in imaging abnormalities of the heart and extremities.

A volumetric analysis of the fetal sac and its contents requires accurate and reproducible identification of tissues. The Cavalieri method of stereology gives an accurate estimation of the volume of an arbitrary object only from a few systematic sections obtained with MRI. The fetal volume in utero can be estimated with a coefficient error of less than 5% from three or four sampled MRI sections (Roberts et al. 1994). Nowadays, computer-based image processing allows easy and accurate volumetric estimation of tissue volumes and hence fetal volumes. To our knowledge the use of segmentation and volumetric analysis and subsequent fetal weight estimation has not previously been described in ´the literature.

2.4.4 MULTIPLE SCLEROSIS

MS is the most common demyelinating disorder of the CNS. The expanded disability status scale (EDSS) has conventionally been used to study the grading of neurological dysfunction in this disease (Kurtzke 1983). In addition, the new Scandinavian regional functional scoring system (RFSS) has been applied in longitudinal clinical studies but as yet not in correlation studies with MRI (Runmarker and

Andersen 1993, Andersen et al. 1996). Both scoring scales involve examination of the visual, motor, sensory, brain stem, cerebellar, bladder, bowel and sex and higher cerebral function systems and appointing certain scores.

MRI provides an objective means of evaluating MS clinical trials and is at least five times more sensitive to disease activity than clinical parameters and is approximately twice as sensitive as clinical measurements to the treatment effect of drugs (Paty et al. 1994). Quantitative brain MRI is helpful in selecting patients with early clinical MS for treatment trials and for subsequent monitoring of response to treatment (Filippi et al. 1994). Measurements and 3D volume rendering of MS lesions clearly show changes in lesion shape, size, volume, and position (Mitchell et al. 1994). An increase in MRI lesion load correlates positively with an increase in disability, while the number of active lesions correlates significantly with the number of relapses (Van Walderveen et al. 1995).

Most MR studies have been focused on the assessment of MS plaques and their correlation with neurological disability (Franklin et al.1988, Kiel et al. 1988, Baum et al.1990, Filippi et al.1995 a, Filippi et al. 1995b). It has been observed that hyperintense lesions on T2-weighted images (T2 weighted plaques) cannot differentiate the separate pathological stages of MS lesion development and represent both active and inactive disease (Barkhof et al. 1992). They display the overall lesion load. A correlation has been found between disability and total plaques volume on MRI in MS but its strength is moderate (Mammi et al. 1996). It has on the other hand emerged that the degree of hypointensity of MS plaques on T1-weighted images (T1-weighted plaques) correlates well with the extent of axonal damage, extracellular edema and the degree of demyelination or remyelination and clinical disability (Bruck et al. 1997). Hence quantification of hypointense lesion load on T1-weighted spin-echo MRI has helped resolve the clinical-radiological paradox (poor correlation between clinical disability and the total plaques volume on MRI) and has the potential to be a surrogate marker of disability in MS (Truyen et al. 1996). The number and volume of Gadolinium chelate-enhancing lesions at a single examination are strong predictors of subsequent clinical activity and the active enhancing plaques in the future, as seen on MRI (Koudriavtseva et al. 1997). Newer MRI techniques such as fast FLAIR (van Vaesberghe et al. 1996), triple-dose Gadolinium chelate T1 imaging (Filippi et al. 1996b), DWI (Trievsky et al. 1997), MTR (Filippi et al 1995e, Filippi et al. 1998b), MRS (Davie et al. 1994) and fMRI (Clanet et al.1997) have substantially improved the correlations between MRI findings and clinical disability and their capability to visualize normal-appearing white matter (NAWM). Also dirty appearing white matter (DAWM), representing a intermediate stage between NAWM and a full blown acute demyelinating plaque, can be studied with these new MRI techniques and T2–weighted images (Ropele et al. 2000,Ge et al. 2003).

Cerebral (Hageleit et al. 1987, Comi et al. 1993) and spinal atrophy (Filippi et al. 1996a) are important new findings which correlate with disability measures in MS. The magnitude of change in atrophies provides an objective marker for evaluation of the effect of treatment. The atrophy can be measured in two ways either by estimating the brain volume or by estimating the volumes of CSF spaces (Quarantelli et al. 2003). Since the volume of the intracranial and spinal cavity is not uniform in all subjects, the total volume of the intracranial/intraspinal fluid spaces is compared to the intracranial/spinal cavity volume in every single subject, whereby a conception can be formed of

relative CSF spaces. However, not many studies with atrophy in MS have used quantitated segmented CSF space volumes in correlating MRI and neurological deficits.

2.4.5 CEREBRAL INFARCTION

Cerebral stroke is one of the leading causes of morbidity and mortality in the western world. Infarctions involving the right cerebral hemisphere cause neglect. Patients with neglect syndrome ignore relevant stimuli on the side contralateral to the lesion when performing everyday tasks (Heilman et al. 1985). Neglect in the acute stage after a stroke is an important predictor of patient recovery (Denes et al. 1982, Wade et al. 1983a, Kinsella and Ford 1985, Fullerton et al. 1988).

Detailed examination of the neurological impairment in brain infarctions includes National Institute of Health Scoring Scales (NIHSS), hand motor function test (HMFT) and Barthel Index (BI) scores. The neglect syndrome is assessed by the behavioral Inattention Test (BIT). The NIHSS assessment includes questions measuring levels of consciousness, response to commands, best gaze, visual fields, motor and sensory functions, best language, dysarthria, extinction, and inattention. The performance scales are recorded from 0 (normal) onwards to varying higher levels (Brott et al. 1889). HMFT entails testing motor functions ranging from normal function to total hand paresis in stroke and predicts the residual hand paresis (Holmberg et al. 1991). It follows the principles laid down in an earlier study (Elliott and Connolly 1984). The testing includes extension of fingers, squeeze, and pinch grip force, independent finger movements, holding a pen, pushing a syringe, unscrewing a small nut, and rotating a round term. A force transducer is used to measure the strength of hand squeeze and pinch grip force. The performance scale is recorded from 0 (normal function) to 24 (total hand paresis). BI predicts the length of hospital stay, the odds of independent daily living and the final outcome (Granger et al. 1979). BI assessment comprises several items measuring feeding, bathing, grooming, dressing, bowel and toilet control, chair transfer, ambulating and staircase climbing. The performance scale is recorded from 100 (normal) to lower values (Mahoney et al. 1965).

Acute neglect in BIT is the best predictor of functional outcome (Jehkonen et al. 2000). It consists of 9 behavioral subtests considered to assess neglect in an ecologically valid way and 6 conventional subtests. The behavioral subtest (BITB) includes, picture scanning, telephone dialing, menu reading, article reading, telling and setting time, coin sorting, address and sentence copying, map navigation and card sorting. The 6 conventional subtests (BITC) are line crossing, letter cancellation, star cancellation, figure and shape copying, line bisection and representational drawing. Infarct patients are separated into neglect and non-neglect group on the basis of the original cut-off scores of BITB and BITC (Wilson et al. 1987).

CT and MRI are now routinely used in the investigation of acute disease**.** Infarctions can be seen on CT as early as 6 hours after the onset of symptoms. CT in the acute phase is used to rule out hemorrhage before starting anticoagulant therapy. Diffusion (DWI) and perfusion (PWI) imaging provide powerful noninvasive means to evaluate pathologic and metabolic changes which occur in acute cerebral ischemia (Mathews et al. 1992). The combination of DWI and PWI can identify patients who might benefit from thrombolytic therapy, for example those with hypoperfused but viable tissue (Schlaug et al. 1999, Jansen et al. 1999). The severity of ADC abnormalities detected by DWI predicts the areas of

reversible and irreversible infarction within DWI demarcated lesions (Hasegawa et al. 1994). Spontaneous or induced reperfusion of an area of initial PWI hypoperfusion has been associated with reduced infarct expansion and favorable clinical outcome (Barker et al. 1998). Magnetization transfer contrast (MTC) imaging improves lesion conspicuity in acute infarction (Thomas JD 1996). In the subacute phase, both CT and MRI show either an increase or decrease in infarction size and in some cases, signs of hemorrhage. In the chronic phase, the fluid attenuation inversion recovery (FLAIR) sequence improves the characterization of infarction and microangiopathic deep hemisphere changes (Brant-Zawadski et al. 1996). More recently, with multiphasic perfusion CT, peak perfusion maps have demonstrated strong correlations between lesion volume and final infarct volume and accurately predicted final infarct volumes (Yi et al.2002).

NIHSS assessment has high criterion validity by predicting infarct size on brain CT (Brott et al. 1989). A direct relationship has been found between infarct size and post-stroke neurological dysfunction in cortically located infarctions (Beleoosesky et al. 1995). Patients with large infarctions detected after acute stroke are at greater risk of developing life-threatening cerebral edema and at greater risk of subsequent hemorrhagic conversion with or without heparin (Lodder 1984, Ropper 1986). These infarct sizes in the earlier studies were reported as diameters and as areas, whereas volumes were not measured. The presence of edema, atrophy, old lesions and periventricular hypodensity on the CT scan has no prognostic influence on survival within the first 3 weeks (Rasmussen et al. 1992). Patients with infarctions of the temporal lobe have a poor prognosis with respect to survival.

Correlation between infarct size and aphasia severity (Kertesz et al.1979) and upper limb weakness (Knopman and Rubens 1986) has been reported. The quantitative assessment of CT infarction volume for acute stroke patients provides an objective measure of an ischemic cerebral infarction. The clinical deficit-infarction size correlation also provides incentive for further analysis (Brott et al. 1989). However, these earlier measurements have not been based on accurate segmented techniques. In the later studies in the 1990s accurate computer-assisted infarct volumetric estimation was done. Infarct volume correlates negatively with the global outcome as estimated by the Barthel Index and positively with the occurrence of psychiatric alterations and disturbances of consciousness (Mauch et al. 1994). Subacute CT infarct volumes correlate with the 3-month clinical outcome. Reduction in infarct volume acts as a biological surrogate for human stroke clinical trials to replace or supplement deficit, disability and global clinical scales (Saver et al. 1999). Few studies have investigated correlations between infarct volumes quantified by segmentation techniques and clinical end points in acute ischemic stroke (Swanson et al. 1990, Mauch et al. 1994). There have also been only a few previous studies on the correlation between quantified right cerebral hemisphere infarct volumes and neurological scores.

3 AIMS OF THE PRESENT STUDY

1. To evaluate the use of Anatomatic™ in volumetric measurements and that of Medimag™ software in 3D-image analysis in five different disease groups, i.e. respiratory system (nasal airway diseases), reproductive system (ovarian tumors and fetal weight estimation) and central nervous system (multiple sclerosis and cerebral infarctions) (I-VI)

2. To correlate the volumetric measurements obtained by segmented CT/MRI and the volumetric measurements made by acoustic rhinometry (nasal airway diseases), laparotomy (ovarian tumors) and abdominal ultrasound (fetal weight estimation) (II-IV)

3. To correlate the volumetric measurements obtained with segmented MR images with neurological deficits in multiple sclerosis and cerebral infarctions (V-VI)

4 PATIENTS AND METHODS

4.1 PATIENTS (II-VI)

To evaluate the new semiautomatic segmentation software and correlate the volumetric findings with those obtained by other techniques and also with clinical findings, we selected five different disease groups: nasal airway diseases (14 patients), ovarian tumors (6 patients), fetal weight estimations (20 subjects), multiple sclerosis (28 patients), and cerebral infarctions (40 patients). The patients were selected from the outpatient units and inpatient wards of the Departments of Otorhinolaryngology, Obstetrics and Gynecology and Neurology.

4.1.1 NASAL AIRWAY DISEASES (II)

Fourteen consecutive patients (9 males and 5 females) with a median age of 39 years (range 19-69 years) with nasal stuffiness associated with chronic rhinosinusitis were recruited. All patients were studied by coronal helical computerized tomography (HCT) and acoustic rhinometry. Acoustic rhinometry was performed within 30 minutes from HCT examination to avoid the problems associated with the nasal cycle. Nasal cavity profiles were generated from the computed cross sections of nasal cavities using segmented CT slices and were compared to those obtained by AR.

4.1.2 OVARIAN TUMORS (III)

Six female patients with an average age of 59.5 years (range 35-72 years) with ovarian tumors suspected on the basis of clinical examination and ultrasound findings were recruited. A surgical laparotomy was performed on the day immediately following MRI examination. Computed volumes of the tumors and components generated from segmented MRI slices were compared to volumes obtained at laparotomy.

4.1.3 FETAL WEIGHT ESTIMATION (IV)

Ten women with insulin-dependent diabetes mellitus (average age 31±5 years) and ten healthy women without disturbances in glucose metabolism (average age 33 ±4.2 years) underwent an ultrasound and MRI examination in late pregnancy within 48 hours before delivery. Most of the fetuses were large for gestational age in both groups and in most cases delivery was accomplished by cesarean section. Four out of ten were nulliparous in the insulin-dependent diabetic group and five out of ten were nulliparous in the healthy women group. The gestational age at delivery was 39.0 ±0.9 and 40.0 ±1.0 weeks in the insulin-dependent diabetic women and healthy women groups, respectively. The MRI-based weight estimations of the fetuses were compared to those obtained by ultrasound and with actual birth weights.

4.1.4 MULTIPLE SCLEROSIS (V)

Twenty-eight patients (14 females and 14 males) with an average age of 46 years (range 35-58 years) and with secondary progressive MS underwent a detailed neurological examination and MRI. Detailed examination of the neurological disability included evaluation of EDSS and total RFSS scores. The neurological examination and MRI were performed within a two-week period and no changes in clinical conditions occurred during that time. The total volumes of T1-, T2- weighted plaques and the measure of cerebral atrophy were correlated to the clinical parameters, EDSS and RFSS. Inclusion criteria for patients were a diagnosis of definite MS and fulfillment of Poser's criteria A1 or A2 (Poser et al. 1983). None of the patients received any kind of steroids during the study and the minimum period from the last steroid administration to the examination was six months. No changes in clinical condition occurred during the time from administration of steroids to the date of examination.

4.1.5 CEREBRAL INFARCTION (VI)

Forty patients (27 males and 13 females) with an average age of 46 years (range 34 to 59 years) and with signs and symptoms of acute right cerebral hemisphere infarctions underwent detailed neurological and CT examinations within 3-6 hours from the onset of symptoms to exclude hemorrhage. MRI was performed in all cases within 2 weeks (a time range between 9 and 14 days) from the onset of stroke. The neurological examinations included NIHSS, HMFT, BI and BIT tests. All neurological examinations were performed on admission, 4-14 days, 3 months, 6 months and 1 year from the onset of symptoms. MRI-computed volumes of infarctions were correlated to the different neurological examinations. The inclusion criteria included age below 75 years, an NIHSS of 0 or 1,

representing the orientation and level of consciousness, right cerebral hemisphere infarction, no earlier neurological dysfunctions, right-handedness and no significant deterioration of eyesight or hearing.

4.2. RADIOLOGICAL EXAMINATIONS

4.2.1 FETAL ULTRASOUND (IV)

Ultrasound examinations were performed by one experienced obstetrician sonographist on a US machine (Aloka 2000, Japan). The subjects were examined in supine and lateral recumbent positions using a 3.5 MHz ultrasound probe. The fetal weights were estimated by two different formulas, one according to the formula presented by Hadlock and associates in 1935 (based on measurements of biparietal diameter and abdominal circumference) and the other according to Shepard and associates in. 1982 (based on measurements of biparietal diameter, abdominal circumference and length of femoral diaphyses).

4.2.2 COMPUTED TOMOGRAPHY (II)

HCT examinations of the nasal airways were performed using the third-generation scanner Pro Speed PLUS (General Electric, Milwaukee, Wisconsin, USA) using a tube voltage of 120 kV and a tube current of 250 mA. Coronal CT imaging of the nasal airways and air sinuses was performed from the tip of the nose to the posterior wall of the nasopharynx. These coronal HCT sections (3mm) were perpendicular to the axis of the floor of the nasal cavity (hard palate). The total number of slice images (1mm) generated from the reformatted 3mm HCT slices for each case varied from 80 to 100 depending on the length of the nasal airways in every individual case. Since AR measurements can be made only up to 7 cm from the tip of the nose, only 70 image slices were selected in HCT. The collimation of the coronal slices was 3mm with a pitch of 1, a field of view of 25 cm and a matrix of 512 x 512. These images were then transmitted through an Ethernet connection to another microcomputer containing Anatomatic^{TM} segmentation software. Segmented CT slices were used to compute cross sections of the nasal cavities in addition to the analysis of volumes of detected anatomical structures such as left and right nasal cavity, paranasal sinuses, and concha bullosa. The slice-dependent volumes were displayed as graphs. Since the slice thickness was known, cross-sectional profiles similar to that in acoustic rhinometry were generated in addition to volumetric profiles. The nasal cavity volumes were divided into a) anterior volume (from the tip of the nose to the range of 1 cm in anteroposterior direction), b) middle volume (from 1 cm to 4 cm), c) posterior volume (from 4 cm to 7 cm) and d) total volume (from the tip of the nose to the range of 7 cm).

4.2.3 MAGNETIC RESONANCE IMAGING (III-VI)

MRI examinations were performed on two different MRI units, 0.5 Tesla (Vectra, General Electric, Wisconsin, USA) and 1.5 Tesla (Signa Horizon Echospeed, General Electric, Wisconsin, USA). The

digital images were then subjected to image segmentation, computerized volumetric estimation and 3D visualization.

4.2.3.1 OVARIAN TUMORS (III)

The MRI protocol is shown in Table 2. Gadolinium DTPA was administered intravenously in a bolus of 0.2 mmol/kg. Axial 3D T2 fast spin echo (FSE) and gadolinium DTPA-enhanced 3D T1 SPGR (spoiled GRASS) images were used for segmentation, volumetric estimation and 3D reformations.

Table 2. MRI protocol for ovarian tumors (1.5 Tesla GE Signa Horizon Echospeed, Wisconsin, USA).

Sequence	TR (ms)	TE (ms)	NEX	FOV (cm)	Matrix	ETL	Thickness (mm)	Gap (mm)
Sagittal T1	200	9	1	35	128/256	-	8	2
Axial T1 SE	200	9	1	35	128/256	-	6	2
Coronal T2 SE	4700	104	3	36	224/512	-	6	2
Axial 3D T2 FSE	2000	150	1	22	192/224	16	3	0
Axial 3D T1 SPGR	42	14	2	22	212/256	-	1.8	0
Gd- DTPA Axial 3D T1 SPGR	42	14	2	22	212/256	-	1.8	0

SE=spin echo, FSE=fast spin echo, SPGR=spoiled grass, Gd-DTPA=Gadolinium DTPA

4.2.3.2 FETAL WEIGHT ESTIMATION (IV)

The MRI protocol is shown in Table 3. MRI examinations were performed on a 1.5 Tesla machine. The sagittal T1-weighted spin echo (SE) images were used for segmentation, volumetric analysis and 3D reformations.

Table 3. MRI protocol for fetal weight estimation (1.5 Tesla GE Signa Horizon Echospeed, Wisconsin, USA).

Sequence	TR (ms)	TE (ms)	NEX	FOV (cm)	Matrix	ETL	Thickness (mm)	Gap (mm)
Sagittal T1	200	10	1	48	128/256	-	10	2
Axial T1 SE	200	10	1	40	128/256	-	10	0
Sagittal T1 SE	200	10	1	40	128/256	-	10	0

4.2.3.3 MULTIPLE SCLEROSIS (V)

The MRI protocol is shown in Table 4. Gadolinium DTPA was administered intravenously in a bolus of 0.2 mmol/kg. Axial T1 SE, T2 and 3D T2 FSE images were used for segmentation, volumetric analysis, and 3D reformations. Hypointense plaques, CSF volumes and hyperintense plaques were evaluated from T1 FSE, T2 and 3D T2 FSE images respectively. Axial 3D T2 FSE images covered a range of 42 mm from the floor of the fourth ventricle to the level of the corona radiata by reason of the technical restrictions on the 0.5 Tesla MRI machine.

Table 4. MRI protocol for multiple sclerosis (0.5 Tesla GE Vectra, Wisconsin, USA).

Sequence	TR (ms)	TE (ms)	NEX	FOV (cm)	Matrix	ETL	Thickness (mm)	Gap (mm)
Sagittal T1	300	25	3	22	160/256	-	5	2
Axial T1 SE	300	20	5	22	160/256	5	5	2
Axial T2 Dual echo	2000	150	1	22	192/224	-	6	1
Axial PD Dual echo	2000	150	1	22	192/224	-	6	1
Axial 3D T2 FSE	2000	150	1	22	192/224	16	2	0
Axial FLAIR	6000	150 TI=2400	1	22	192/224	-	7	1
Gd-DTPA Axial T1 FSE	300	20	5	22	160/256	5	5	2

4.2.3.4 CEREBRAL INFARCTION (VI)

The MRI protocol is shown in Table 5. Gadolinium DTPA was administered intravenously in a bolus of 0.2 mmol/kg. Axial 3D T2 FSE images were used for segmentation, volumetric analysis and 3D reformations.

Table 5. MRI protocol for cerebral infarctions (0.5 Tesla GE Vectra, Wisconsin, USA)

Sequence	TR (ms)	TE (ms)	NEX	FOV (cm)	Matrix	ETL	Thickness (mm)	Gap (mm)
Sagittal T1	300	25	3	22	160/256	-	6	2
Axial T1	300	20	5	22	160/256	-	6	2
Axial T2 Dual echo	2000	150	1	22	160/256	-	6	2
Axial PD Dual echo	2000	150	1	22	160/256	-	6	2
Axial 3D T2 FSE	2000	150	1	22	192/224	16	5	0
Gd-DTPA Axial T1	300	20	5	22	160/256	-	6	2

4.3 OTHER PROCEDURES USED TO OBTAIN LESION VOLUMES (II-III)

4.3.1 RHINOMETRY (II)

The 1/2 Acoustic Rhinometry (G.M. Instruments Ltd., Glasgow U.K.) was used to measure nasal cavity volumes. An anatomically sculptured 5-cm, long nosepiece was inserted into the nostril. AR measurements were made during a breathing pause while the patients were in sitting position. The 1/2 AR produced several volume and cross-sectional area measurements. The following volume parameters were emphasized: anterior volume (from the tip of the nose to the range of 1 cm in anteroposterior direction), middle volume (from 1 cm to 4 cm), posterior volume (from 4 cm to 7 cm) and total volume (from the tip of the nose to the range of 7 cm).

4.3.2 LAPAROTOMY (III)

Laparotomy was performed on six patients within 24 hours of MRI examination. Tumors were measured in situ with a tape measure. For round tumors the circumference was measured and the volumes calculated using the formula, circumference = 2 r (radius) and volume = 4/3 r^3. If the tumor

was oval in shape, two circumferences were measured and their mean used for the radius formula. The volume of irregular tumors was estimated by multiplying three perpendicular dimensions.

4.4 SEMIAUTOMATIC SEGMENTATION AND 3D RECONSTRUCTIONS

During this study, two separate softwares, Anatomatic™ (Heinonen et al. 1997) and Medimag™ (Heinonen et al. 1998b), were developed. The former enables segmentation and volumetric analysis. Volumetric accuracy was tested using inter- and intra-observer studies and also by performing a calibration test using a phantom (Heinonen et al. 1998a). Medimag™ was developed for 3D-visualization of original and segmented images and is based on Ray casting and Phong shading methods (Watt 1993).

The original dynamics of the CT and MR image is 12 bits covering 4096 gray scales. However, normal PC computers are not capable of displaying more than 8 bits covering 256 gray scales. The original 12 bit images therefore have to be compressed to 8 bits before processing. The compression is based on histogram modification in order to emphasize the region of interest, e.g. lesions in different diseases. Due to the histogram equalization of the region of interest, the compression can even increase the accuracy of volumetric estimation. However, if the region of interest covers large portions of gray scales, compression can indeed cause some errors, e.g. in the cases of tumors having solid and cystic components. Also the normal human can distinguish only 64 gray scales at a time. Hence the information in these images obtained in 8 bits in the workstation does not lose information. In all our studies 8-bit images were used.

4.4.1 ANATOMATIC SOFTWARE (I)

Anatomatic™ software was developed for a 32-bit Windows system (Win95™, Win98™ and WinNT™) using ANSI C and C++ programming languages (Figure 3). It requires at least 16MB of RAM; minimum 16-bit colors and a minimum resolution of 1024x768 pixels. However, it is recommended to use 32 MB RAM, 24-bit colors and 1280x1024 resolution for optimal operations. It can open, produce, save and display medical images and segmented data. The data can be observed in all three (sagittal, coronal and axial) planes.

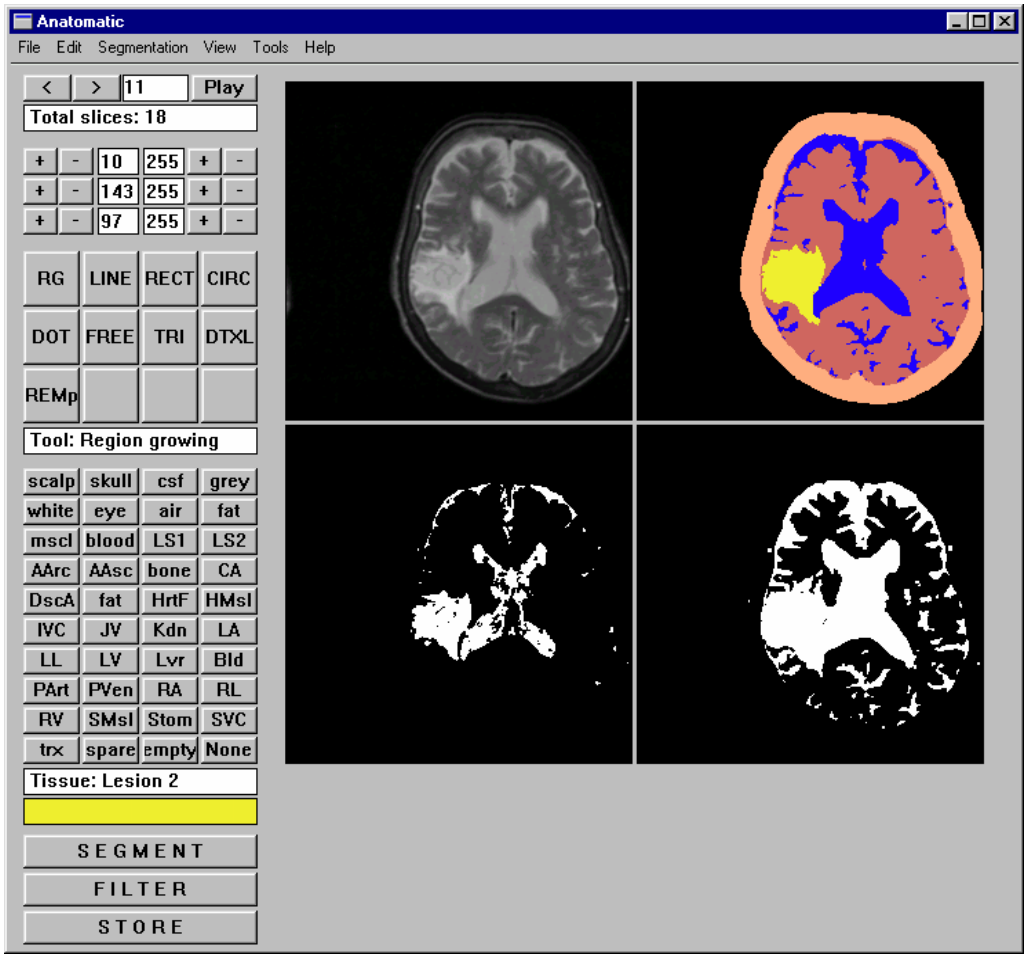

Figure 3. The user interface of Anatomatic™ software used in volumetric analysis of lesions in various diseases. The left upper figure represents the original MR image with an infarction seen as high signal intensity on a T2-weighted image. The right upper figure represents the segmented image of the infarct; also other structures of the brain like the cerebrospinal fluid, and the rest of the parenchyma have been segmented. The lower two figures represent the amplitude-segmented pictures, where using different threshold intensities the images have been modified to look similar to the original MR image in the left upper corner.

Using Anatomatic™ segmentation is carried out as follows: first an image stack of MR or CT images is opened and displayed on the screen. The current slice (i.e., the slice containing the region of interest) is defined and appropriate threshold coefficients are selected. Thereafter a segmentation tool (e.g., region growing, line drawing and other simple drawing tools) and a color representing a tissue are selected and the images modified appropriately. Once the results appear realistic, the user stores the segmented

data and begins to process the next image. The above-mentioned steps are repeated as many times as there are images in the data set.

The software is capable of processing only one image set at a time. If multiple imaging sets are used simultaneously, the sets must be matched (i.e., the same orientation and image resolution), this entailing additional work and more sources of error.

Volumes of the segmented images in all 5 disease groups were received directly in the form of voxels automatically, later converted to volumes via a factor derived from voxel dimensions in the original HCT or MR images. The volumetric analyses are reported automatically. In nasal airways, ovarian tumors and MS disease groups (hyperintense plaques on T2-weighted images), because the images were volumetric in nature, the volumes obtained from the images were considered as the final volumes. In fetal weight estimation the sagittal SE images had a zero gap between two slices and hence simulated a volumetric MR examination. In MS disease (gliotic plaques on T1 weighted images), howe ver, the segmented lesion volumes in the gaps between two consecutive images was estimated separately based on the segmented volumes of the consecutive slices. This was done by multiplying the average cross-sectional area of the plaques in two consecutive slices by the gap thickness and this volume was then added to the total lesion volume.

4.4.1.1 CT

Nasal airway diseases: in the segmentation procedure, the first step consisted of three amplitude segmentation operations in order to emphasize nasal cavities and paranasal sinuses. The threshold coefficients were obtained manually from the image histogram. The three resulting images were presented simultaneously on the screen. The air spaces in the nasal cavities and paranasal sinuses were marked (i.e., segmented) using different colors. The segmentation procedure operated nearly automatically in areas of the nasal cavity where there are sharp boundaries. Since the air spaces in the nasal cavity, paranasal sinuses and the pharynx are connected to each other at different levels, to avoid overestimation of the volumes, the boundaries between these three regions were modified manually and determined using tools such as line or rectangle drawing and filled with connectivity (i.e., region growing). The images were modified till the segmented structures looked similar to that in the original CT image. Thereafter they were integrated into one final segmented image (Figure 4)

A B C D E

Figure 4. Segmentation of nasal airways involves four stages: The original image (A) is first amplitude segmented to represent nasal airways (B). Thereafter the nasal sinuses (C) and cavities (D) are marked by using particular colors and a region-growing tool. Lastly, all the images are integrated (E).

4.4.1.2 MRI

With MRI, various colors represented the different parts of the brain, white and gray matter, cerebrospinal fluid and lesions like MS plaques, white matter hyperintensities and infarctions. These structures and lesions were segmented using different intensities measured in gray scale by the software.

Ovarian tumors: Segmentation was performed using axial 3D T2 FSE and Gadolinium-DTPA enhanced 3D T1 SPGR images. Separation of the ovarian tumors from the surrounding tissue was a semiautomatic process, but depending on the shape and size of the tumors was also done manually. The separation of the cystic and solid parts of the tumors was fully automatic. Separation between the cyst and the surrounding ascites proved to be an impossible task, as the extremely thin wall of the cyst could not be discerned. The volumes of cysts and the solid part of the tumor were calculated separately and by adding these together, the total volume of the tumor was arrived at (Figure 5).

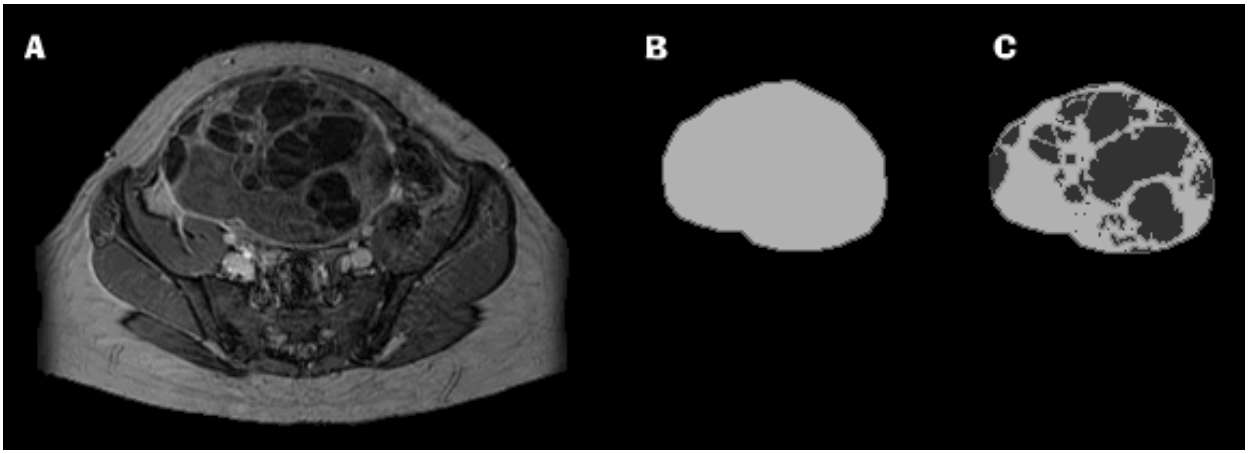

Figure 5. Segmentation of ovarian tumors consists of the following stages: The original image (A) is first amplitude-segmented to represent the whole tumor (B). Thereafter the solid and cystic components (C) are marked using particular colors and a region-growing tool and the segmented image of the tumor is obtained.

Fetal weight estimation*:* Segmentation was performed using sagittal T1-weighted SE images. The borders of the fetuses were distinguished in all but two cases where a motion artifact prevented accurate segmentation. The different components of the amniotic sac, i.e. fetus, placenta and amniotic fluid, were clearly delineated. Only the volumes of fetuses were calculated. The segmented volumes in the gaps between the slices were estimated based on the volumes of the consecutive slices. The fetal volumes were then converted into fetal weight using a multiplication factor 1.07 (density coefficient obtained from the slope of the regression line when birth weight and fetal volumes were compared) (Figure 6)

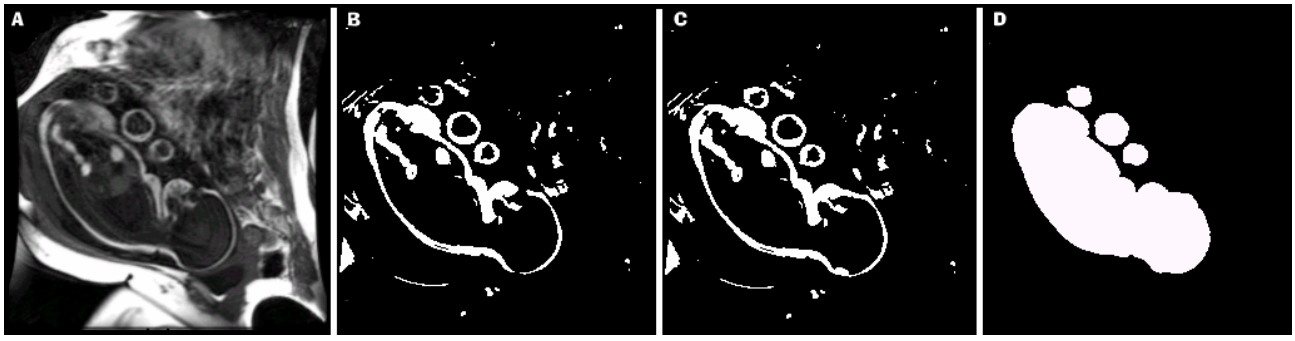

Figure 6. Segmentation of the fetus consists of four stages: The original image (A) is first amplitude-segmented to represent an amplitude-segmented image of the fetus (B). Thereafter the filtered image is demonstrated (C), different structures being marked using particular colors and a region-growing tool. Lastly, the segmented image of the fetus is obtained (D).

***Multiple sclerosis**:* With MS patients, segmentation of hypointense plaques was performed from the axial T1-weighted SE images and hyperintense plaques were segmented from axial 3D T2 FSE-weighted images. The CSF and brain volumes were segmented from axial T2 images. The criteria for a lesion to be labeled an MS plaque were the shape and lesion location. Those lesions classically situated in the brachium pontis of the brain stem area, anterior periventricular region of the temporal horns and corpus callosum were regarded as most probable MS plaques. Those situated elsewhere were labeled MS plaques on the basis of their gross morphology on MRI, i.e. lesions with their long axis towards the cortex. If the lesions were immediately adjacent to the ventricles or the sulci, which had similar intensities to the lesions, manual editing was performed. Depending on the proximity of the plaques to the ventricles and peripheral CSF spaces, the segmentation varied from fully automatic to varying amounts of manual interaction. Also other changes in the brain such as white matter hyperintensities related to age were manually edited so as to avoid errors in volumetric estimation. CSF segmentation and volume estimation done from the axial T2 FSE images was automatic in most cases. FLAIR images were not analyzed volumetrically because they were not volumetric in nature (Figure 7).

Volumetric measurement of the brain parenchyma (total brain volume) was made by assessing the volumes of the segmented gray and white matter. Volumetric measurement of total intracranial CSF spaces assessed the total volume of the ventricular and peripheral CSF spaces. Total intracranial volume was measured by calculating together the volumes of segmented brain parenchyma and total intracranial CSF spaces. Relative brain atrophy was measured by dividing the total brain volume (B) by the total intracranial volume (B+L, where L represents the total intracranial CSF volume) (the mention of it being achieved dividing the total intracranial CSF volume by total brain volume on page 38 of article V is due to human error) (B/B+L). Volumetric measurement of relative intracranial CSF spaces was made as a ratio, i.e. by dividing the total intracranial CSF volume by total intracranial volume so as

to avoid the errors in estimation caused by different sizes of the skull in individual patients (L/B+L)(Figure 7).

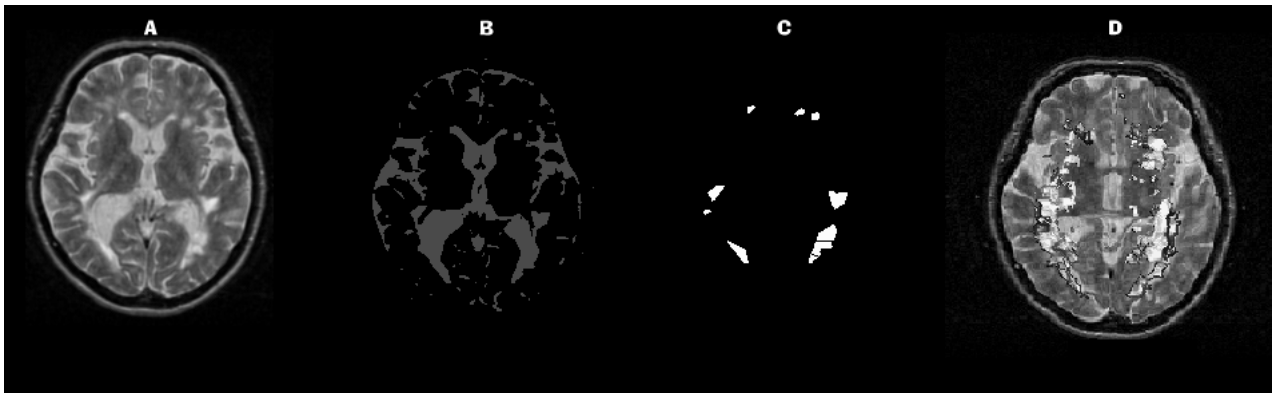

Figure 7. Segmentation of MS lesions consists of four stages: The original image (A) is first amplitude-segmented to represent the cerebrospinal fluid spaces and MS plaques (B). Thereafter the MS plaques (C) are marked separately using a particular color and a region-growing tool. Lastly, all images are integrated (D).

Cerebral infarctions: Segmentation of subacute infarctions was done from axial 3D T2 FSE images. Segmentation was performed using both manual and semiautomatic segmentation softwares. The infarcted areas were brought out from the surrounding anatomical structures and other age-related white matter hyperintensities using specific colors. Those infarctions adjacent to the ventricles or the sulci or other nonrelated hyperintensities underwent manual editing to avoid overestimation of infarction volumes. If there were multiple infarctions each infarction was segmented separately and the volumes added at the end of the operation. In cases where it was possible, the surrounding edema, if seen around the actual infarction as a less hyperintense area on proton density images, was segmented separately (Figure 8).

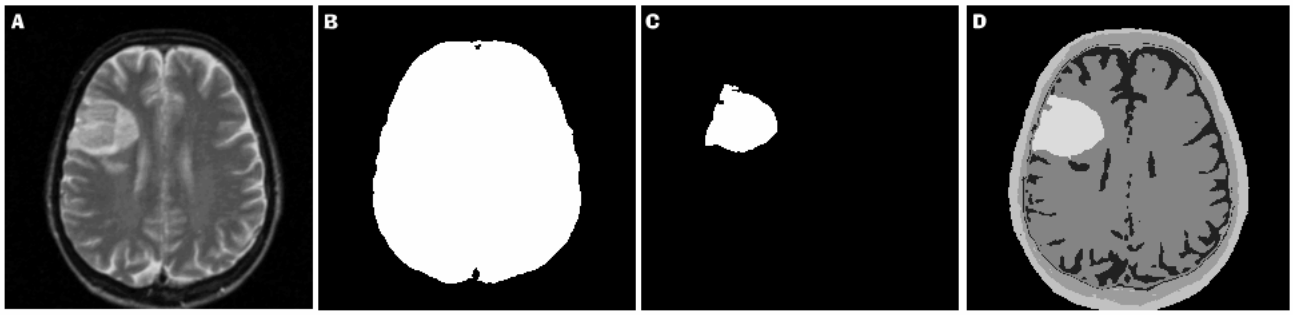

Figure 8. Segmentation of cerebral infarction consists of four stages: The original image (A) is first amplitude-segmented to represent the whole intracranial cavity (B). Thereafter the infarct (C) is marked using a particular color and a region-growing tool. Lastly, all images are integrated (E).

4.4.1.3 PHANTOM TEST (I)

Demonstration of the accuracy of the Anatomatic^{TM} was accomplished by performing the segmentation of MR images of five fluid-filled syringes with known volumes (1, 2, 5, 10 and 20 cm^3) of water. The syringes were imaged on a 0.5 T MRI using the T2-weighted sequences (35 slices, 250x250 pixels each, FOV=220x220mm, slice thickness=2mm with no intervening gap). The syringes were fixed on the surface of a quality-assurance phantom at an angle of 0 to 5 degrees to the surface. The syringes were located in the center of the imaging field; thus the border areas did not create artifacts in validation. The phantom (filled with 2000 cm^3 cupric sulfate) volume simulated well the head coil loading during normal head scan. Also the long relaxation time of the phantom was similar to the relaxation times of lesions in MS and infarctions. The images were histogram-modified in order to emphasize the border of the syringes with 8-bit gray scales. MR images thus produced were segmented using thresholding. According to the measured volumes, the relative error of the total volume based on the syringe images was 1.5%. For the smallest syringe the error was 4.0 % and for the largest, 0.3 % (Figure 9).

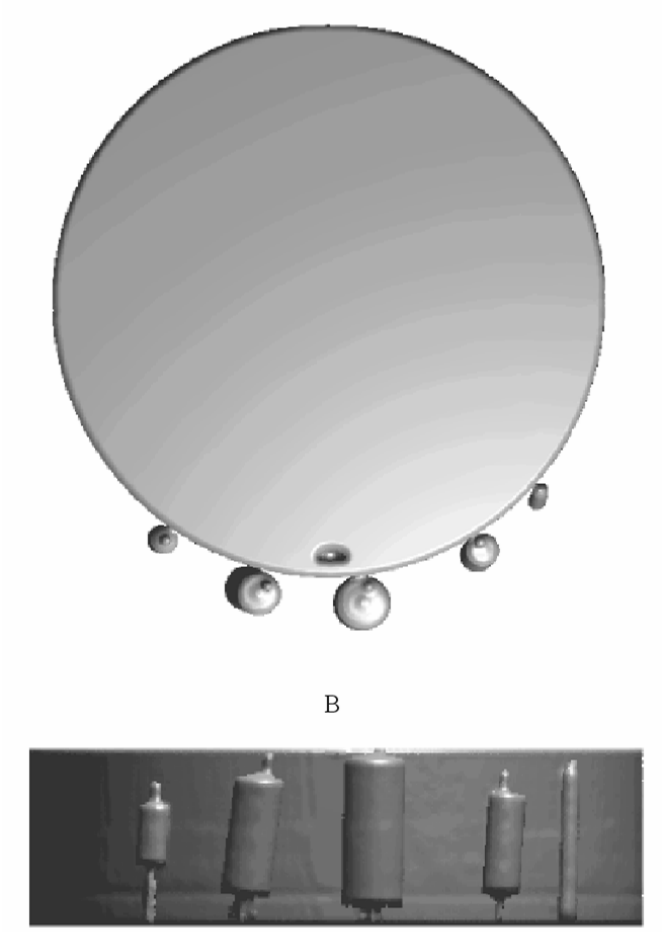

Figure 9. 3D-figures demonstrating the segmented images of five syringes fixed on the surface of a quality assurance phantom A) in the axial plane and B) in the sagittal plane

4.4.2 MEDIMAG SOFTWARE (II, III, VI)

The Medimag™ software was employed in the visualization of original MR/CT images, and produced 3D images (Heinonen et al., 1998b). With the help of Medimag™ software and a C++ visualization library, 3D visualization of segmented and raw MR images was performed. The visualization library consisted of two different surface reconstruction techniques based on Ray casting and Flood filling. Shading was carried out using Phong shading. The visualization capabilities of the software were tested in the nasal airway diseases, ovarian tumors, fetal weight estimations and cerebral infarctions. It uses a simple data format to open MR/CT image sets. Any digital image format can be easily converted to this format of a header and data. The header contains image stack dimensions (x-, y-, and z), physical dimensions, imaging techniques and projection planes. Image data are stored as a 3D matrix using 8 bits per voxel. The software is shown in Figure 10.

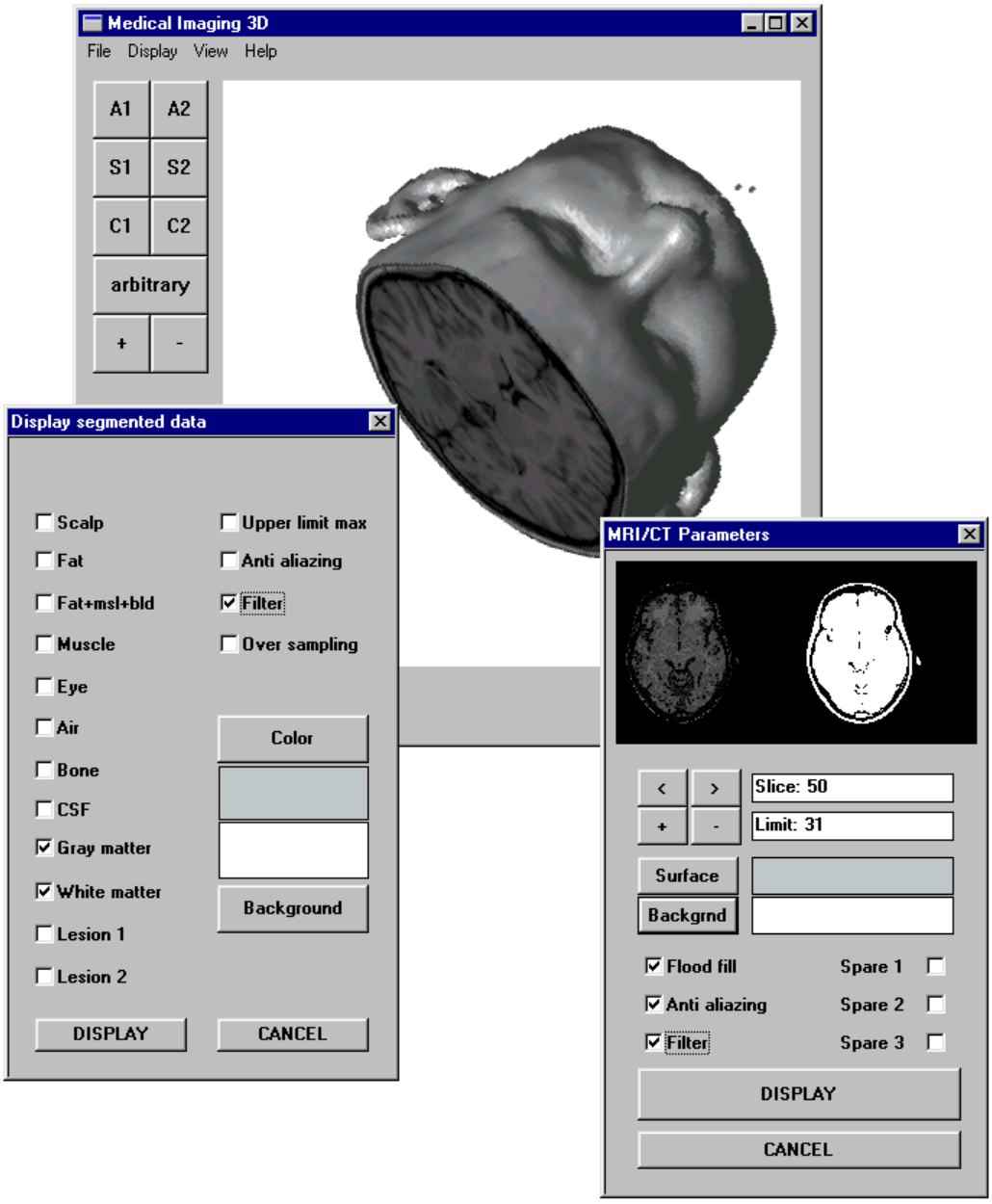

Figure 10. The user interface of the Medimag^{TM} 3D software. The generated 3D image is presented on the main window, which enables definition of projection planes, zoom factor, sections, etc. If the source data consist of raw information like the original CT or MR images, the "MRI/CT parameters" window appears and requires threshold coefficients, surface and background colors and some additional parameters for displaying the images. If the source data are preprocessed (segmented), the display-segmented window appears, by means of which appropriate tissues are then displayed.

4.5 INTER- AND INTRA-OBSERVER STUDIES (II-VI)

Inter- and intra-observer studies were undertaken separately in three disease groups (ovarian tumors, multiple sclerosis and cerebral infarction) studied to establish the reproducibility of the volume estimations in each case. The observers were blinded to the clinical findings in individual cases. The measured volumes of lesions and anatomic structures were compared and the variability of these results computed. The inter- and intra-observer variabilities were calculated as percentile differences between the measured average volumes and individual measures. The results were expressed as percentage difference between the measured and average volumes.

4.6 STATISTICAL ANALYSES (II-VI)

The statistical analyses in all five disease groups were performed using two different methods. In nasal airways and fetal weight estimations, the statistical program SPSS for Windows Release 5 was used. No statistical analysis was made in the case of ovarian tumors. In multiple sclerosis and right cerebral hemisphere infarctions, the STATISTICA for Windows program package (Statsoft, Inc. Tusla, OK, USA) was used. Since all these five studies form a part of a larger study in their respective disease groups, application of different statistical programs was inevitable.

Nasal airways: The results were expressed as mean values ± standard deviation. To study associations between the volumes obtained by CT segmentation and that by AR, Pearson's correlation coefficients were calculated. Values of p less than 0.05 were considered statistically significant. To study the association between the right versus left nasal cavity volumes by CT segmentation and AR, simple correlation coefficients were calculated.

Fetal weight estimation: To evaluate the accuracy of weight estimations both the US-based weight estimations and the MRI-based estimated fetal volumes were plotted against the actual birth weights of the infants. Linear regression analysis was used to determine the correlation between the US and MRI weight estimations and actual birth weights. These regressions were evaluated by backward stepwise multiple regression analyses.

Multiple sclerosis: Spearman's rank correlations were used to describe the dependence between two variables at a time supported by the p values. Multiple regression analyses were used to identify explanatory variables amongst the MRI measures for neurological disability. Due to the multiple comparisons, the criterion for the statistical significance was a p value less than 0.01. All p values between 0.05 and 0.01 were regarded as a tendency to association.

Cerebral infarctions: To study associations between the segmented infarction volumes and neurological impairment (NIHSS, HMFT and BI), Pearson's correlation coefficients were calculated in all 40 data sets. The criterion for statistical significance was a p value less than 0.05.

4.7 ETHICAL CONSIDERATIONS

Institutional guidelines of the University of Tampere, Finland were followed. All study protocols were approved by the Ethics Committee of Tampere University Hospital, Tampere, Finland. Participation in the studies was dependent on informed consent obtained from the patients and healthy controls after an explanation of the aims of the study and the study protocol.

5 RESULTS

5.1 TECHNICAL RESULTS (I-VI)

Anatomatic™ and Medimag™ softwares performed optimally in a simple 120 MHz Pentium-based computer running on the Windows 95 operating environment. Owing to the interactive character of the segmentation procedure, time consumption depended on the person controlling the segmentation. Experts on diseases of the nasal cavities, reproductive organs and central nervous system and on segmentation techniques analyzed the segmentation findings in the five disease groups under study and found the computer segmentation accurate enough for volumetric estimations of the different lesions and anatomic structures.

5.1.1 SEGMENTATION AND TIME CONSUMPTION (I-VI)

As a pilot study for technical feasibility, 118 visible human man (VHM) cryosection images of the thorax (converted to a set of 250x250 gray scale images) were segmented in to 32 different tissues including fat, muscles, heart, liver etc. for application in electrophysiological stimulation of electrocardiogram and impedance cardiogram. The time taken for segmentation was 16 hours.

In the 14 HCT sinonasal airways patients (70 slices) the air spaces of the nasal cavity and paranasal sinuses, pathological lesions such as sinonasal polyps, mucosal thickening and air spaces in such anatomical variations as concha bullosa, and Haller's sinuses were segmented. For correlations with AR measurements, however, only 70 slices were taken into consideration (1-7 cm in the AP direction) as

we found this area most optimal for comparison. The time used for segmentation was dependent on the variability in anatomic details of the nasal cavities and paranasal sinuses. In the six MRI patients with ovarian tumors, the cystic and solid components of the tumors were segmented. In the twenty pregnant subjects, the borders of the fetuses were clearly distinguished in all but two cases, where motion artifacts prevented accurate segmentation. The different components of the amniotic sac, i.e. fetus, placenta and amniotic fluid were clearly delineated. In the 28 MRI patients with multiple sclerosis the white and gray matter, CSF spaces and MS plaques were segmented. Good discrimination was obtained between these, and the margins of the MS plaques were accurately delineated. In 40 patients with right hemisphere cerebral infarction the brain tissue was successfully segmented using lesion tracking to obtain infarct volumes. The time used for segmentation and volumetric measurements of the infarctions depended on the quality of images and the number of infarctions.

The time involved in making segmentation and volumetric segmentation in nasal airways, ovarian tumors, fetal weight estimation, multiple sclerosis and cerebral infarction was 30-50 minutes, 15-20 minutes, 5-10 minutes, 5-20 minutes and 5-10 minutes respectively. In cerebral infarctions, comparing between manual segmentation and Anatomatic^{TM} softwares, the average manual segmentation and volume estimation time was 20-30 minutes. The times taken for segmentation and manual interaction in all 5 disease groups are given in Table 6.

Table 6. Time consumed in completing segmentation (including semiautomatic segmentation and manual interaction), volumetric estimation, manual interaction and 3D reformations and the total times measured in the five disease groups.

Disease group	Type of examination	Tissues segmented	Segmentation time (incl. man inter. time)	Manual interaction time
Nasal airway diseaes	HCT	Nasal cavities, paranasal sinuses	30-50 min	10 min
Ovarian tumors	MRI	Cysts, solid tumor, ascites	15-20 min	2-5 min
Fetal weight estimation	MRI	Fetus, placenta amniotic sac	5-10 min	2-5 min
Multiple sclerosis	MRI	Plaques, CSF, brain	5-20 min	1-5 min
Cerebral infarction	MRI	Infarct	5-10 min	2-5 min

5.1.2 THREE-DIMENSIONAL REFORMATIONS (II, III, VI)

3D visualization of segmented and raw images was achieved using Medimag^{TM} software equipped with Ray Casting and Flood Filling. Shading using Phong shading added to the depth of the images. This allowed piecewise definition of surface color enabling multi-modal visualization. 3D visualization was performed in three clinical situations (Figures 11. A-D). Precise and realistic 3D images were achieved. The time involved in making 3D reformations varied from 1-3 minutes depending on the number of images in the data set.

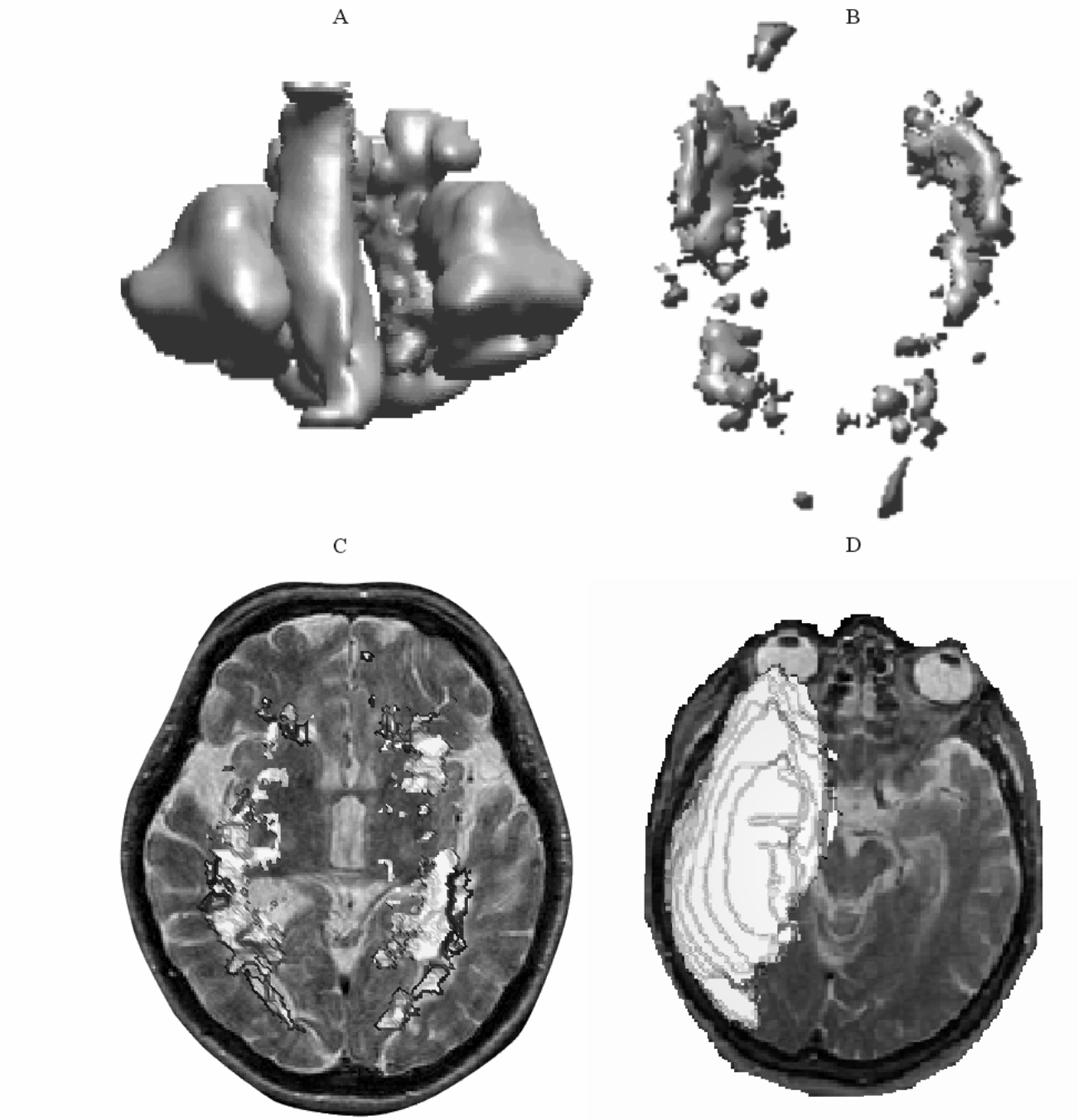

Figure 11. Three-dimensional presentations of: A) nasal air cavities and paranasal sinuses (coronal plane), B) hyperintense MS plaques (axial plane), C) hyperintense MS plaques in 3D integrated on an axial T2-weighted image (axial plane), and D) right hemisphere cerebral infarction (axial planes piled on each other).

5.1.3 INTER- AND INTRA-OBSERVER STUDIES IN VARIOUS DISEASE GROUPS (III, V, VI)

In all inter-observer studies, 3 experienced observers well acquainted with semiautomatic segmentation and the disease involved in the specific study carried out the segmentation independently. All observers underwent detailed training in the process of segmentation. In all intra-observer studies, a single experienced neuroradiologist carried out the segmentation twice at an interval of 2-3 weeks.

In nasal airway diseases, no inter- or intra-observer studies were made. In ovarian tumors, two radiologists and one researcher undertook the inter-observer study. In the fetal weight estimation study, no inter- or intra-observer studies were performed. In MS, three neurologists carried out the inter-observer study. The results demonstrated a variability between the observers of 0.5 cm^3 in the segmented T2-weighted hyperintense MS plaque volumes. In the intra-observer study the total variability was 0.3 cm^3. The range of deviations from the mean values was maximally 23% (0.16 cm^3) between the observers and 7% (0.05 cm^3) in the intra-observer readings. No inter- or intra-observer studies were performed for T1-weighted gliotic plaques. In cerebral infarctions, two neurologists and one neuroradiologist carried out the inter-observer studies. The variabilities were measured for the volumetric estimation of segmented infarctions from T2-weighted images.

The inter-observer variations in the computed lesion volumes of the ovarian tumors, multiple sclerosis plaques and cerebral infarctions were 4%, 7%% and 4% respectively and the corresponding intra-observer variations 2.5%, 3.0 % and 3.0 %. The results of inter- and intra-observer studies in the three disease groups are given in Table 7.

Table 7. Inter- and intra-observer variations in segmented structures in the three disease groups

Disease group (Segmented structure/lesion)	Type of exam.	Inter-observer variation	Intra-observer variation
Ovarian tumors	MRI	4.0 %	2.5 %
Multiple Sclerosis (Intracranial CSF spaces)	MRI	1.5 %	1.0 %
Multiple sclerosis (T2 weighted MS plaques)	MRI	7.0 %	3.0 %
Cerebral infarction	MRI	4.0 %	3.0 %

5.2 CLINICAL RESULTS AND CORRELATIONS (II-VI)

5.2.1 NASAL AIRWAY DISEASES (II)

The values and correlations between volumes of air spaces in the nasal cavities computed from the acoustic rhinometry and HCT segmentation method are set out in Table 8.

Table 8. Volumes of air spaces in the nasal cavities measured by AR and HCT segmentation volumetry. Volumes are in mean cm^3 ± standard deviations

Volumes (cm3) of different parts of the nasal cavity	AR	CT	p-value
Anterior	0.83 ± 0.20	1.71 ± 0.72	0.017
Middle	4.62 ± 3.39	7.23 ± 2.01	0.031
Posterior	10.30 ± 9.54	7.93 ± 2.34	0.107

When the anterior, middle and posterior air space volumes of 28 nasal cavities (14 patients), computed by either technique were compared, an increasingly distinct pattern of volume differences was found in the anterior to posterior portion of the nasal cavity. Statistically significant correlations between volumes computed by AR and HCT segmentation were found in the anterior and the middle parts of the nasal cavity. No significant correlation was found in the posterior part of the nasal cavity. No statistically significant correlations were found between these two methods in recognizing the volume correlation between the right and left nasal cavities. Likewise no correlation was found between the volumes of paranasal sinuses and the nasal cavities as measured by HCT-segmentation volumetric method.

5.2.2 OVARIAN TUMORS (III)

Using Anatomatic^{TM}, the volumes of segmented ovarian tumors ranged from 548 cm3 (patient 4) to 2812 cm^3 (patient 1). The volumetric estimations made separately on T1- and T2- weighted images on MRI showed no significant difference. For the four solitary tumors volumetric and laparotomy-based volumes agreed fairly well in patients 2, 3 and 4. Patient 1 had an oval-shaped tumor and the segmented volume was double that of the volume measured at laparotomy. For the two patients with multiple tumors and significant ascites the segmentation and laparotomy-based volumes did not agree. The correlations between the volumes on MRI and that at laparotomy are given in Table 9.

Table 9 Tumor volume estimations in cm^3:s at MRI (T2-weighted images) and at laparotomy in six ovarian tumors.

	MRI volume estimation (cm^3)			Volumes at laparotomy (cm^3)	
Patient number	Total volume	Cystic part	Solid part	Total volume	Ascites
1.	2812	577	2235	1207	-
2.	2014	1487	527	1753	400
3.	672	235	437	556	-
4.	548	482	66	580	-
5.	1264	1043	221	362	1500
6.	2479	1760	719	383	11000

Out of the six tumors, four were solitary and two multiple. Of the two benign tumors, one was mucinous and the other serous cystadenoma. Four of the tumors were malignant. For the malignant tumors, one was International Federation of Gynecology and Obstetrics (FIGO) stage I A (confined to the uteral adnexa) and three were III C (extend outside the uteral adnexa but not outside the true pelvis) ovarian carcinomas. Two patients with stage IIIC had in addition marked ascites. The detailed characteristics of the tumors are given in Table 10.

Table 10. The gross and histological characteristics of the six ovarian tumors at laparotomy

Patient number	Side	Nature at laparotomy	Histology	FIGO staging
1.	right	mucinous	Mucinous cystadenoma	-
2.	left	mixed	Serous cystadenoma	-
3.	left	1/3 rd solid 2/3 rd cystic	Clear cell adenocarcinoma	IA
4.	left	mixed	Serous cystadeno-carcinoma	IIIC
5.	bilateral	solid	Serous cystadeno-carcinoma	IIIC
6.	bilateral	solid	Serous cystadeno-carcinoma + large omental tumor	IIIC

5.2.3 FETAL WEIGHT ESTIMATION (IV)

When US and actual birth weights were compared, a correlation coefficient of r =0.77 was achieved. There was one serious overestimation in the normal pregnancy group where the estimated weight was 5000 g. and the actual weight was 3930 g. This resulted in an unnecessary cesarean section. Four estimations had a deviation of more than 10% from the actual birth weight. Hadlock's formula was slightly better than Shepard's in predicting birth weight. Differences between these two methods had no statistical significance. The correlations between the fetal weight estimation by conventional US and the actual birth weights are seen in Figure 12.

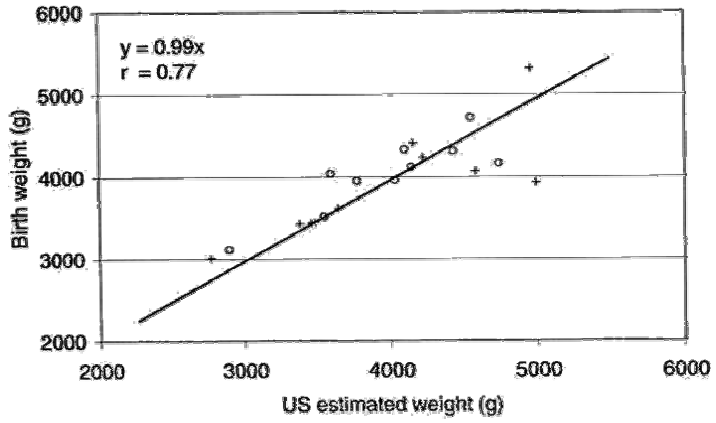

Figure 12. Ultrasound-based weight estimation (Hadlock's formula) compared with actual birth weight. o = diabetic mother, + = non-diabetic mother.

Using the obtained data with US and MRI it was possible to determine the density coefficient (taken from the slope of the regression line) of 1.07, which then multiplied by the fetal volume led to the fetal birth weights. When MRI and actual birth weight estimations were compared, a correlation coefficient of r = 0.95 was achieved. Backward stepwise multiple regression analyses showed 90% explanation of MRI estimation for the variation in actual birth weight ($p < 0.001$). US estimate as an additional determining variable did not improve the explanation of the model ($p = 0.32$). The correlation between the MRI-based fetal volume (cm^3) and the actual birth weight is shown in Figure13.

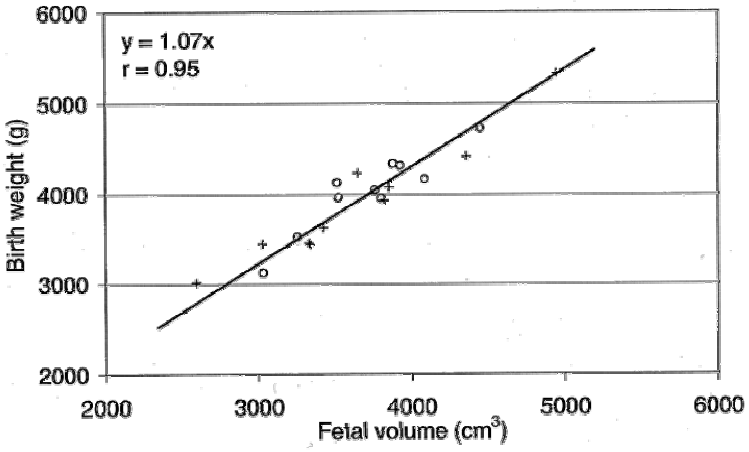

Figure 13. MRI-based estimate of fetal volume (cm^3) compared with the actual birth weight (gram). The slope of the regression line indicates average fetal density. o = diabetic mother, + = non-diabetic mother.

When the US-estimated and MRI-estimated fetal weights were compared, a significant correlation was found (p less than 0.005; r=0.99) and MRI fetal weight estimations proved to be more accurate. The correlation between the US-based fetal weights (g) and MRI-based fetal weights is shown in Figure 14.

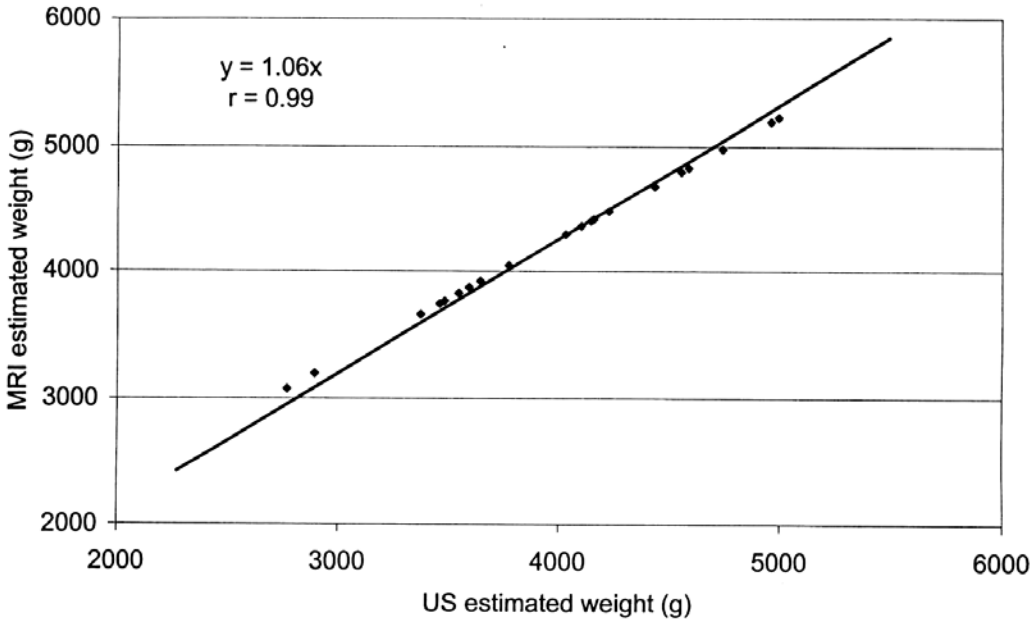

Figure 14. The graph showing correlations between the US-based fetal weights (g) and MRI-based fetal weights

5.2.4 MULTIPLE SCLEROSIS (V)

Using Anatomatic^{TM}, the median total brain lesion volumes of SPMS patients for hyperintense plaques on T2- weighted images and hypointense gliotic plaques on T1-weighted images were 5.21 cm^3 (range 4.22-5.86) and 0.60 cm^3 (0.54-0.66), respectively. In the assessment of brain atrophy, brain volume, total intracranial cerebrospinal fluid volume and the total intracranial volume were estimated. The median volume of the brain parenchyma (white matter and gray matter) was 982 cm^3 (range 921 cm^3-1002 cm^3). The median volume of total intracranial cerebrospinal fluid spaces (total volume of ventricles and peripheral cerebrospinal fluid spaces) was 131.9 cm^3 (range 112 cm^3-137 cm^3) The median total intracranial volume was 1113.9 cm^3 (range 1059-1239 cm^3). The relation of brain volume to total intracranial volume was on an average 0.88 (range 0.82-0.91) and that of total intracranial CSF volumes to total intracranial volume was on an average 0.12 (range 0.9-0.19).

Detailed examination of neurological disability included evaluation of EDSS scores (range 3.5-6.5, mean 4.8) and total RFSS scores (range 5.6-23.7, mean 13.9). The mean duration of the relapsing-

remitting phase was 132 ±12.4 SD (standard deviation) months (range 27-240) and that of the progressive phase 49 ± 6.0 (SD) months (range 2-132). In multiple regression analysis, the brain atrophy, i.e. volumes of relative (p=0.005) and total (p=0.006) intracranial CSF spaces were more significantly associated with neurological disability as expressed by EDSS than other measures. The total brain volume showed a significant inverse association with neurological disability as expressed by EDSS (p=0.010). No associations were found between MRI volumes of hypointense gliotic plaques on T1-weighted images and hyperintense plaques on T2-weighted images and neurological disability as expressed by EDSS (Table 11).

Table 11. Explanatory factors at MRI for neurological disability as expressed by EDSS in multiple regression analysis in 28 patients with secondary progressive multiple sclerosis

Explanatory variables CSF, brain and lesion volumes (cm^3)	p-value
Relative intracranial cerebrospinal fluid spaces	0.005
Total intracranial cerebrospinal fluid spaces	0.006
Total brain	0.010
Hypointense gliotic plaques on T1- weighted images	0.067
Hyperintense plaques on T2-weighted images	0.355

An association was found between the mean volumes of hyperintense plaques on T2-weighted images and total RFSS scores (r=0.40, p=0.03). The associations between the mean volumes of hypointense plaques on T1-weighted images and total RFSS scores were not significant. No associations were detected between the total brain volumes and total RFSS scores. No associations were found between the total or relative intracranial CSF space volumes and total RFSS scores. No significant associations emerged between the different volumes measured on MRI and EDSS scores (Table 12).

Table 12. Correlations between EDSS, RFSS and quantitative MRI volumes in 28 patients with secondary progressive multiple sclerosis

MRI parameter volume (cm^3)	EDSS score R	p-level	RFSS score R	p-level
Hyperintense plaques on T2-weighted images	0.16	0.38	0.40	0.03
Hypointense gliotic plaques on T1- weighted images	0.27	0.15	0.33	0.08
Total brain	-0.08	0.68	-0.15	0.44
Total intracranial CSF spaces	0.006	0.97	0.07	0.74
Relative intracranial CSF spaces	0.03	0.87	0.03	0.86

The duration of the progressive phase of secondary progressive MS showed a tendency to association with the EDSS score (r=0.37, p=0.05). The duration of the progressive phase of MS also showed a tendency to be associated with the volumes of lesions on T1-weighted images (r=0.38, p=0.05), but no associations were found with CSF space volumes or the volumes of lesions on T2-weighted images.

In a continued study with primary progressive MS (PPMS) patients (Ukkonen et al. 2003) the brain atrophy changes were controlled by studying a cohort of 20 normal individuals matched for age, sex and intelligence (with PPMS and SPMS patients). Using the same cohort of controls in an SPMS study the total brain volumes in patients with SPMS were smaller than in controls (10 %). The brain atrophy was also more pronounced in SPMS patients compared to the controls, i.e. significant differences were found in the degree of relative brain atrophy between SPMS and controls (p=0.004). Results also showed that PPMS patients had significantly smaller total brain and spinal cord volumes than controls (p=0.001 and p=0.000 respectively), and significant differences were found in the degree of relative brain and spinal cord atrophy between the groups (p=0.002 and p=0.000 respectively).

5.2.5 CEREBRAL INFARCTION (VI)

The means and standard error of means and ranges for age, NIHSS, HMFT and BI amongst patients suffering from right cerebral hemisphere infractions are shown in Table 13.

Table 13. Clinical characteristics of patients with right cerebral hemisphere infarctions

Variable and units	Mean SEM ± SD	Range
Age, years	63.3 ± 1.72	25-75
NIHSS	6.88 ± 0.87	0-18
HMFT	12.5 ± 1.61	0-24
BI	59.8 ± 5.74	5-100

SEM= standard error of means, SD= standard deviation, NIHSS=National Institute of Health Stroke Scale, HMFT= Hand motor function test, BI=Barthel Index

Most of the infarctions were situated in the anterior portion of the right cerebral hemisphere (frontal temporal and parietal lobes) and in the deep regions (corona radiata and internal capsule). Cortical infarctions showed a tendency to involve also the subcortical region. In only two cases, did these infarctions involve the deep gray matter. The regional distribution of infarctions is given in Table 14.

Table 14. Regional distribution of right cerebral infarctions in 40 patients

Location of infarction in the right cerebral hemisphere	Number of patients
Frontal, temporal, parietal	9
Frontal, temporal	4
Temporal	3
Parietal/temporoparietal	10
Corona radiata and or internal capsule	8
Thalamus	2
Parietooccipital	2
Temporooccipital	2

Using Anatomatic^{TM}, the mean volume of infarctions in 40 patients was 104.2 cm^3, the volumes ranging from 7.8 cm^3 to 200.6 cm^3. However, using the manual segmentation technique the mean volume of infarctions was lower, i.e. 85.9 cm^3, ranging from 8.5 cm^3 to 163.3 cm^3. All infarction volumes used in construing correlations were those measured by semiautomatic segmentation technique. Using Spearman rank order correlations the volumes of the infarctions showed positive correlation with the neurological function scores, NIHSS, HMFT and degree of neglect studied. four to 14 days after onset of symptoms (Table 15). The volumes showed a significant inverse correlation with BI (Table 15).

Table 15. Correlation between infarction volumes and neurological scores (NIHSS, HMFT, BI and BIT) using Spearman rank order correlations

Infarction volumes (cm3)		
Neurological scores	R values	p-values
NIHSS	0.737	< 0.0001
HMFT	0.492	< 0.0011
BI	- 0.576	< 0.0001
BIT (neglect)	0.762	< 0.0001

In a current study not yet published, clinical evaluation of NIHSS, HMFT and BI scores was done at three months, six months and one year from the onset of symptoms. However, due to resource problems MRI was not performed in this later period. An arbiratory cut-off value for infarction volume was calculated as 10.5 cm^3, values below this being considered small infarction and values above large infarction. The reason why this cut-off value was kept at 10.5 cm^3 is that this was a mean value of lacunar type infarctions. When the MRI results were correlated, in the analysis of variance and covariance for the repeated measures at these five time points (at admission, 4-14 days, 3 months, 6 months and 1 year), there was a significant time to infarct group (small infarction and large infarction groups) reaction for NIHSS ($p=0.011$), HMFT ($p=0.055$) and BI ($p=0.054$), indicating that patients who had a higher quantified infarction volume showed slower recovery than those patients with smaller infarction volume. From the onset of symptoms to three months there was a significant difference between the patients with small and large infarctions in NIHSS and BI (Figure 15), whereafter the differences between the two infarct groups diminished during the follow-up. In contrast, the differences in HMFT between the two groups increased with time (Figure 16).

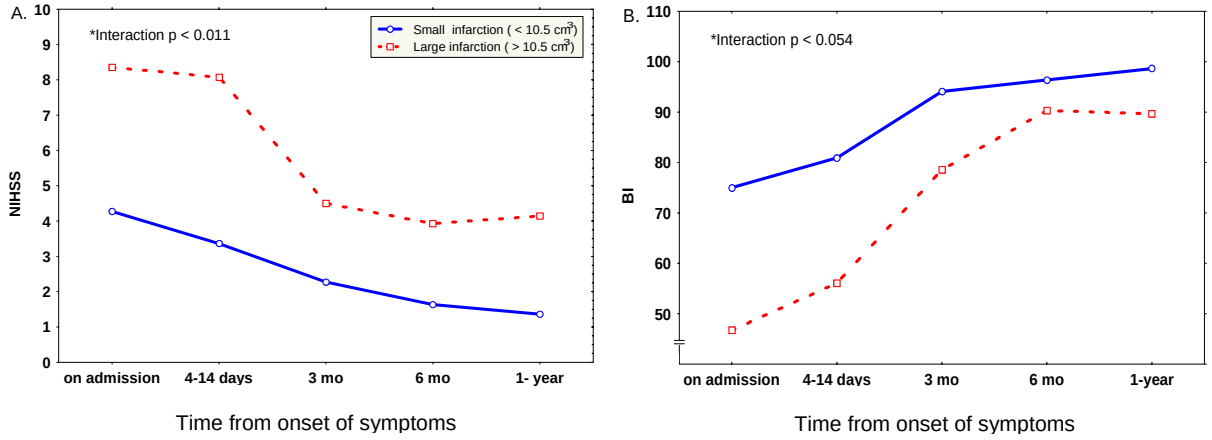

Figure 15. Neurological disability as measured by National Institute of Health Stroke Scale (NIHSS) and Barthel Index (BI), on admission, after 4-14 days, after 3 months, after six months and after one year from onset of symptoms. In analysis of variance and covariance (age as covariate) for repeated measures a significant time point to infarct groups interaction was observed for (Panel A) NIHSS and (Panel B) BI.

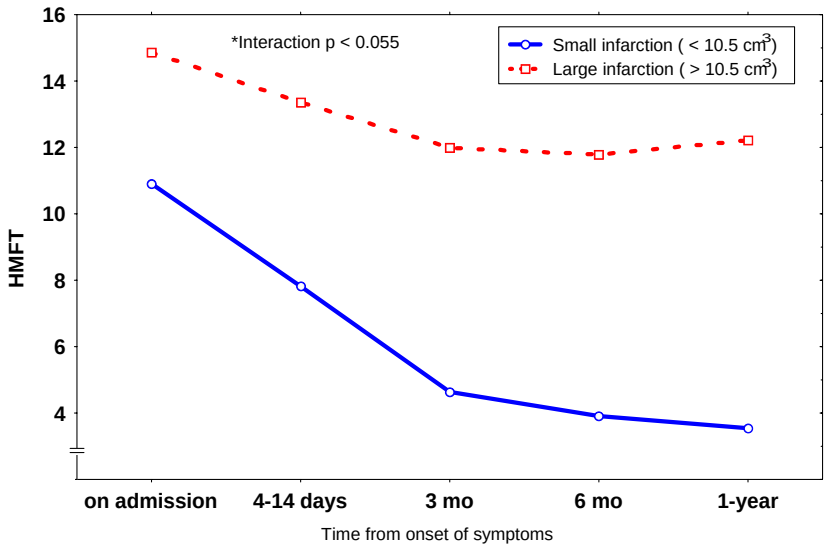

Figure 16. Neurological disability as measured by hand motor function test (HMFT) on admission, after 4-14 days, after three months, after six months and after one year from the onset of symptoms. In analysis of variance and covariance (age as a covariate) for repeated measures a significant time point to infarct group interaction was observed.

The volumes of the infarctions correlated with NIHSS, HMFT and BI in all consecutive neurological examinations (p less than 0.007 for correlation at all five time-points). See Table **16**.

Table 16. Spearman rank order correlations (R) between neurological function scores and quantified infarction volumes according to follow-up.

Neurological function scores	on admission R	4-14 days R	3-months R	6-months R	1-year R
NIHSS	0.737	0.774	0.629	0.593	0.665
P-value	< 0.0001	< 0.0001	< 0.0002	< 0.0001	< 0.0002
HMFT	0.492	0.491	0.494	0.520	0.519
P-value	< 0.0011	< 0.0011	< 0.0016	< 0.0011	< 0.0065
BI	0.576	- 0.629	- 0.605	- 0.458	- 0.559
P-value	< 0.0001	< 0.0001	< 0.0001	< 0.0049	< 0.0029

National Institutes of Health Stroke Scales (NIHSS), hand motor function tests (HMFT) and Barthel index (BI).

6 DISCUSSION

Very-high-speed computers are making it possible to scan a patient, archive the raw data for later review, analyze volumetric data and perform 3D-image analysis. This study represents an initial step towards improving the radiological assessment of different diseases of the respiratory, reproductive and central nervous systems by acquiring volumetric data and enhancing the interpretation with the help of computerized volumetric analysis. The Anatomatic™ and Medimag™ package used in this study represents an optimal application of interactive segmentation and 3D reconstruction algorithms comprising a friendly user-interface suitable for clinical use. Physicians have found Anatomatic™ to be valuable in clinical studies where volumetric analysis is important (Heinonen et al. 1998a).

However, problems requiring a solution for computerized quantification of any lesion are:

1. Lesions are often fuzzy with soft rather than hard boundaries,
2. There is significant variation in the conspicuity of lesions,
3. They may be small in size and large in number,
4. Many artifacts may arise from the scanner, patient motions and blood/CSF flow,
5. The true accuracy of any method cannot be determined because there is no ideal golden standard,
6. A major problem in quantification is the operator-dependency of lesion measurements, these being vulnerable to subjectivity in identifying lesions and determining threshold-intensity levels. Inter- and intra-observer studies are therefore essential in the evaluation of a new imaging and measurement tool (Miller et al. 1998).

6.1 TECHNICAL CONSIDERATIONS (I-VI)

6.1.1 SEGMENTATION TECHNIQUES (I)

Image analysis tools are classified as manual, semiautomatic and automatic (Dastidar et al. 1999 c). Anatomatic™ automatically defines the boundaries and combines the images corresponding to different tissues. Nevertheless it involves a certain amount of manual intervention and can thus be classified as semiautomatic (Heinonen et al. 1998a). Owing to the semiautomatic character of our software, it can be used in numerous applications and unexpected artifacts and anatomical anomalies do not cripple the system. Due to the variable size, shape and intensity of cerebral lesions and lesions located near the cerebrospinal fluid spaces, totally automated segmentation techniques cannot detect all lesions. The sensitivity of the analysis can be increased by manual intervention, but this is very time-consuming (Heinonen et al. 1998a). An ideal solution for a faster segmentation method would be to combine semi-automatic segmentation of the first slice and thereafter automatic segmentation of the rest of the MR slices. Even under this circumstance, the presence of an experienced radiologist or clinician is essential to evaluate the whole process and correct for possible errors. However, numerous neural networks and digital atlases are under development, which can be combined with automatic segmentation to obtain accurate results (Heinonen et al. 1999).

Recently several new semiautomatic and automatic segmentation techniques have been employed in clinical work. The new semiautomated segmentation technique Medical Image Display and Analysis Software (MIDAS) has been successfully applied for measuring ventricular volume (Dalton et al. 2002). Other semiautomated segmentation technique such as geometrically constrained region growth (GEORG), which requires user specification of lesion location, and directed multispectral segmentation (DMSS), requiring only the location of a single example lesion, have been studied and compared, both techniques showing equal accuracy and proving superior to the manual segmentation technique (Ashton et al. 2003). Automated segmentation techniques like MSA (multispectral automatic) based on Bayesian classification of brain tissue and the NIH image analysis semiautomatic technique based on lesion by lesion thresholding have been studied, the automatic technique proving superior in fast lesion load assessment (Achiron et al. 2002). Fully automatic pipeline image quantitative analysis based on robust image processing algorithms is being used in a large number of phase III drug trials (Zijdenbos et al. 2002). Automated segmentation techniques like SIENA (Structural Image Evaluation using Normalization of Atrophy) and SIENAX (an adaptation of SIENA for cross-sectional measurement) have been used to measure brain atrophy (Smith et al. 2002). A fully automated SPM99-based segmentation technique has been used to better recognize and follow up of white matter diseases (Jost et al. 2002). Marroquin and colleagues, in the year 2002, used another accurate and robust automatic 3D segmentation technique successfully in analyzing brain scans. The automated Exbrain v.2 algorithm has been used for serial intracranial volumetry (Lemieux et al. 2003). The segmentation technique ISODATA (Interactive Self Organizing Data Analysis) has been used in the analysis of acute infarction (Mitsias et al. 2002). It has been suggested that since semi-automated segmentation methods yield more accurate results than the automated segmentation methods but are time-consuming and prone to operator bias it is practical that the semiautomated method be used in postprocessing the automated

mode (Lee et al. 2003). Anatomatic™ software has these technical capabilities and hence we believe the software to be as good as the above-mentioned tcehniques if not better.

6.1.2 TIME USED TO PERFORM VOLUMETRIC ANALYSIS (I-VI)

In the present study, the time per patient for segmentation and volumetric analysis in nasal airway estimation, ovarian tumor volume estimation and fetal weight estimation was 30-50 minutes, 15-20 minutes and 5-10 minutes respectively, which we believe are optimal times for clinical studies although there has been no mention of such times in earlier literature. The reasonably fast segmentation and interaction times of 10 minutes and 5 minutes achieved with our software in MS are comparable with those in an earlier study (Udupa et al. 1997), where the time for segmentation was 5-40 minutes, and interaction time 1-15 minutes. This finding is also in accord with a similar earlier report on multiple sclerosis where segmentation time and interaction times were 30 minutes and 10 minutes respectively (O'Riordan et al. 1998). In our study with cerebral infarctions, when compared, manual segmentation time varied from 20 to 30 minutes and semiautomatic segmentation time varied from only 5-10 minutes in cerebral infarctions, demonstrating that with Anatomatic™ the volumetric analysis can be performed within a reasonable time.

6.1.3 SLICE THICKNESS AND GAP

In general any lesion detection depends on lesion size, slice thickness, lesion position relative to the slice, thickness of gap between slices and inherent contrast between lesion and surrounding structures (Bradley and Glenn 1987). Slice thickness and gap between the slices in CT/MRI have an important role in the reliable estimation of lesion volumes. Detection of small, low-contrast lesions has been shown to be the most sensitive to partial volume effects and to be ideal with thin slice acquistions. Detection of high-contrast lesions, on the other hand, is limited only by the presence of gap between slices. For example in MS patients with diffusely distributed disease the small low-contrast lesion (MS plaque) detection is superior for thin slices even with a gap rather than for thick contiguous slices (Bradley and Glenn 1987). In the intracranial area as one proceeds to estimate lesions situated higher up in the convexity area of the parietal region, lesion detection sensitivity decreases and the partial volume effects increase. In T2-weighted images the choice of slice gaps is an operator-selected parameter important in reducing contrast degradation. As the slice gap is reduced the contrast of T2-weighted images markedly degrades, though selective excitation pulses with better spatial resolution will diminish these contrast changes (Kucharczyk et al. 1988). In our study with MS disease a similar trend was found. Due to the technical restrictions on the 0.5 Tesla machine a thickness of 2 mm on 3D T2 FSE images was maintained. The above-mentioned problems of low-contrast lesion were partially overcome by using semiautomatic segmentation software where computer-aided lesion border detection was better than in conventional methods. In another study (Just et al. 1988), when phantoms containing fluids of T1 values were studied, a strong dependence on signal intensities emerged. In our study with MS T1 weighted studies were not volumetric in nature and a gap of 1-2 mm was kept between the slices. The volumes of lesions within the gaps were estimated separately and added to the main lesion volumes. In the abdominal region it has been found that thin interslice gaps and large imaging volumes are detrimental to the MR signal and contrast especially when using the body coil. In

one study (Schwaighofer et al. 1989) abdominal MRI was performed using a 40-cm imaging volume. Here it was found that increasing the interslice gap thickness increased the water signal without affecting the fat signal. Image contrast was nearly doubled when the interslice gap was increased from 10% to 75%. Also as the slices moved away from the central slice, fat and water signals slowly decreased to 12.5 cm offcenter. Signal loss was significant with an offsest greater than 12.5 cm. It is thus to be emphasized that to obtain proper contrast on T2 weighted images the optimal interslice gap should be used and the region of interest should be near the central slice. In our studies with ovarian tumors and fetal weight estimation the imaging volume was kept at a minimum and the interslice gap at an optimum (no gaps between the slices for those MRI sequences used for volume estimation).

6.1.4 INTER- AND INTRA-OBSERVER VARIATIONS (II-VI)

6.1.4.1 General

Significantly different inter-observer and intra-observer variabilities in MS load measurements have been seen at different field strengths on systems from different manufacturers (Filippi et al. 1997). They are relatively small when all examinations in the same study are done on the same 0.5 T, 1 T, or 1.5 T scanners from the same manufacturers, but when examinations are performed in different scanners, the variabilities begin to increase. Two explanations can be given for this: different manufacturers' technical and computerization solutions may result in different image contrast and resolution, and quality of analysis depends on observer's experience on machines with the same field strength (Filippi et al. 1997). In this study, performing all examinations in a particular disease group using the same 1.5 Tesla (ovarian tumors and fetal weight estimation) and a 0.5 T (multiple sclerosis, cerebral infarction) field strength scanner minimized this problem.

Inter- and intra-observer variabilities in volumetric estimations are dependent on the experience of the clinicians and radiologists involved in the study. Here we sought to obviate this problem by involving experts experienced in the fields of rhinology, neurology and neuroradiology who were also well-versed in the segmentation technique. A further factor is the extent of abnormalities present on the images. This is higher in the case of extended abnormalities in which it is difficult to analyze differences in size of the lesions and lower in cases of a few and well-circumscribed lesions (van Walderveen et al. 1995). It is also dependent on the time interval between the examinations i.e. higher with smaller intervals. In our study the time interval between the volumetric estimations was kept constant in all disease groups, i.e. 3 weeks.

6.1.4.2 Inter-observer studies:

In ovarian tumor volume estimation the inter-observer variability of 4% seems reasonable. No such studies have previously been performed. In multiple sclerosis, the average inter-observer variability has previously been less than 7% for volumetric estimation of MS lesions in various compartments of the brain (Jackson et al. 1993). In yet another study, the inter-observer variability for segmented volumes of MS lesions was found to be 3.9% (Filippi et al. 1995d). Using techniques similar to Anatomatic^{TM} in

one study (Parodi et al. 2002), the inter-observer variability of lesions in diffusion-weighted imaging technique and gadolinium-enhanced T1-weighted images was 10% and 8% respectively. In the same study, however, using manual segmentation techniques the interobserver variabilities using DWI and gadolinium T1 weighted were equally 30%. In our study the inter-observer variabilities of 1.5 % (for intracranial CSF space volumes) and 7% (for plaque volumes on T2 weighted images) are comparable to those in the former studies. In fact the inter-observer variability of 1.5% with volume estimation of intracranial CSF spaces can be considered excellent. In cerebral infarctions, with earlier segmentation techniques, the inter-observer reproducibility has ranged from 4-6% (Vaidyanathan et al. 1997a). With an inter-observer variability of 4% (i.e. less than in earlier studies) with right-sided cerebral infarctions, the volumetric estimations here would seem to be superior.

6.1.4.3 Intra-observer studies:

In nasal airway diseases**,** the accuracy of measurements with AR is heavily dependent on the technical performance of recordings. An acclimatization period of 20 minutes seems necessary before measurements because even slight exercise causes clinically significant changes in nasal volume. In an earlier study with AR and manual volume estimation, the intra-observer variation between four measurements of nasal volume in an area of 2-7 cm of the same nostril varied from ±8 % to ±32 % in the baseline phase (without using decongestants) the mean being ±16 %. In the post-decongestion phase the variations ranged from ±6 % to ± 24 % with a mean of ±14 %. The clinical reproducibility of AR is at a level of ±15 %, and the intra-observer variation is approximately 1.71 cm^3 or 0.3 cm^3 (Sipilä et al. 1996). If one restricts the AR to the nasal cavity and epipharynx, the measurements can be made with adequate reproducibility (Kunkel and Hochban 1994). Hitherto no volumetric studies using semiautomatic segmentation have been performed, and hence no inter- or intra- observer studies have been mentioned. In our study, the intra-observer variations were not performed.

In ovarian tumors, segmentation and volume analysis was here undertaken for the first time, so no earlier references regarding the intra-observer variations are to be found. The intraobserver variations of 2.5 % in this study seem optimal. In fetal weight estimations no variability studies were made.

In CNS disease estimation in MS, intra-observer variabilities involved in the volumetric estimation of T2-weighted MS plaques have varied in different studies from as low as 6% in experienced hands to as high as 14-20% in less experienced hands (Miller et al. 1998). Lesion volume measurements in MS are influenced by the use of different MR scanners and a patient included in a serial study should always be scanned with the same MR machine. In one study where the size and number of enhancing MS lesions were studied, a high level of intra-observer variabilities was observed. Here when the same scanner was used the intra-observer variability was as low as 1.3 %, whereas when different scanners were used it increased to as high as 8.9% (Filippi et al. 1997). Comparison of several quantitation techniques should be made in a multicenter longitudinal fashion in order to include variation caused by scanner and segmentation technique, in addition to biological activity (Barkhof et al. 1997). Linear extrapolation from data allowed the lesion volume at very small slice thicknesses to be estimated. It was found to be on an average 20% greater than that obtained using a slice thickness of 5 mm (Filippi et al. 1995 c). In our study the intra-observer variabilities of 1% (for intracranial CSF space volumes)

and 3% (for plaque volumes on T2-weighted images) are highly comparable to those in former studies. In cerebral infarctions, with earlier segmentation techniques the intra-observer reproducibility has ranged from 4-6% (Vaidyanathan et al. 1997a). With an intra-observer variability of 3% in the present study in the case of right-sided cerebral infarctions, the volumetric estimations seem to be superior.

6.1.5 USE OF DIFFERENT MRI SEQUENCES IN DISEASES STUDIED (II-VI)

The use of different sequences plays an important role in the assessment of clinical deficit and in the follow-up of patients. T1-weighted and 3 D T1 SPGR images are important sequences for image analysis. In ovarian tumors, Gd-chelate-enhanced 3D T1 SPGR was used in making volumetric estimation. When compared, no significant difference in volumetric estimations was found between those performed with 3D T1 SPGR and 3D T2 FSE weighted images. This proves that both sequences are equally sensitive and good for this purpose. In fetal weight estimation an accurate delineation of the fetal borders was obtained with T1-weighted images. In our study with MS we found only three cases where enhancing active MS lesions were found on gadolinium enhanced T1 images When compared, other fast MRI techniques like echo planar and turbo gradient spin echo imaging are less sensitive in detection of MS plaques than the conventional spin echo approach (Rovaris et al. 1997).

T2-weighted images also form an important part of image analysis. In ovarian tumors, axial 3D T2 FSE was used for volumetric estimation and gave a good estimate of the cystic and solid portion of the tumors in four out of six cases. In multiple sclerosis, 3D T2 FSE- weighted image analysis gave an accurate estimate of total lesion load (plaques seen both on T2 and T1 image). In right-sided cerebral infarctions, only 3D T2 FSE-weighted images were used for volumetric estimations and proved sufficiently sensitive to give good correlations between infarction volumes and neurological deficits.

New sequences like FLAIR and fast-FLAIR have been actively used in image analysis. In our study with MS patients, FLAIR images have been used as reference pictures when performing segmentation of T2-weighted lesions in multiple sclerosis and cerebral infarctions. They were not used for volumetric estimation because of their non-volumetric nature. FLAIR images result in greater conspicuity of MS plaques than T2 weighted fast spin echo images (Bastianello et al. 1997). The advantages of fast-FLAIR over the conventional T2-weighted images are higher sensitivity in detection of subcortical and periventricular plaques and greater reproducibility when assessing brain lesion volumes (Bastianello et al. 1997). However, fast-FLAIR images have the limitations of low sensitivity in detecting posterior fossa lesions (Gawne-Cain et al. 1998) and higher inter-scanner variability for lesion volume measurement than the conventional T2-weighted images (Filippi et al. 1999). In cerebral infarctions, FLAIR images offer an advantage in the detection of acute infarcts affecting the cortical ribbon improving the characterization of chronic infarctions and microangiopathic changes and thus leading to greater sensitivity to lesions (Brant-Zawadski et al. 1996). In our study with cerebral infarctions proton density images were taken as a part of dual-echo imaging instead of FLAIR due to shortcomings in the 0.5 T MR unit. Dual echo images were not analyzed because of their non-volumetric nature.

Magnetization transfer contrast images and MR spectroscopy also increase the sensitivity of lesion detection and morphology (Thomas 1996). Use of DWI and PWI has become routine in the early stages

of infarctions, but these could not be performed due to restrictions observed with our 0.5 Tesla machine. The differences in lesion volumes using these different sequences on MRI using semiautomatic segmentation need to be determined.

6.2 MEDICAL IMAGING (II-VI)

In this study, image segmentation and computerized volumetric analysis was performed for the first time in the evaluation of diseases of the nasal airways, in ovarian tumors, and in fetal weight estimation.

6.2.1 NASAL AIRWAY DISEASES (II)

Earlier, coronal HCT has been found to be the optimal imaging modality for the evaluation of diseases of the nasal cavity and paranasal sinuses (Yousem 1993). However, quantitative assessment of the nasal airways and lesions has been found to be difficult (Corsten et al. 1996). In the present study, the use of HCT and a semiautomatic segmentation technique was successfully evaluated in the quantification of airway spaces in nasal airway diseases, with good results.

CT before FESS operations has become routine. Here all anatomic variations and diseased areas are subjectively analyzed preoperatively. However, when the patient has to be followed up postoperatively, the changes seen need to be quantified in order to ensure an accurate assessment. Although AR-based volume estimation is being used in most ENT outpatient departments due to its simplicity in use, it is unreliable in predicting dimensions beyond large changes in a cross-sectional area and especially in the immediate proximity of a change in such an area (Tomkinson et al. 1996). Measurement of both the volumes in the area of constriction and beyond the constriction may be associated with systematic errors. As the nose presents a proximal constriction, this finding is of relevance and a factor limiting the clinical use of AR (Hamilton et al. 1995). Various factors affect the accuracy of measurements, for example a) magnitude of the change in cross sectional area; the smaller the change, the better is the estimate of the area beyond, and the smaller the disturbance surrounding the change and b) the rate of change in a cross-sectional area; if the change in area is gradual or stepped, the space is more accurately estimated.

As environmental conditions like air-conditioner fans and cafeteria noise may affect or distort findings, acoustic rhinometry should be performed in a relatively noise-protected environment to obtain good results (Corey et al. 1996). Changing postures contribute significantly to the source of variation in nasal cavity patency (50 to 100% coefficient of variation). The CT volume measurement cycle may also be affected by changes in posture, timing and the nasal cycle (Gilain et al. 1997). These effects on measurements with CT may be amplified in the presence of rhinitis, which is a likely accompaniment of sinusitis (Dastidar et al. 1999a). Hence decreased nasal cavity dimensions with changes in posture from standing to supine and to lateral recumbent positions must be taken into account in making measurement with AR and CT (Kase et al. 1994). No mention of the gap between the measurements between AR and CT has hitherto been made in the literature. In our study, the time gap kept between

the two readings first with AR and then with HCT may be taken to be optimal regarding functional changes in the mucosa of the nose, where it is assumed that practically the state of nasal mucosa remains the same within this 30-minute period This gap of 30 minutes was kept to allow the patient to shift from the ENT outpatient department to the CT scanner. Even a gap of 30 minutes might be suspected to be too long a time.

The use of CT to explore the nasal airways volume-nasal function relationship has upto now been limited to manual tracing on CT slices to achieve quantitative measures, a method which is extremely laborious. With HRCT and 3D HCT, image segmentation and hence accurate volume estimations have become possible. With this technique, the area behind the obstructions, under the turbinates, in the osteomeatal complex (OMC) (all of which cannot be distinguished with AR) can be reliably measured. Compared to the acoustic methods, there is no distortion in HCT and, in addition, the volumes of paranasal sinuses and concha bullosa in the turbinates can also be measured. With the advent of HCT, by initially taking thick slices, e.g. 3mm collimation and then reconstructing the slices to 1mm one can increase accuracy without having to increase the radiation doses, i.e. compared to 1mm HRCT, where the dose would increase considerably. In our study HCT gave optimal results. With the increasing use of multi-slice CT and its distinct advantage of retrospectively gaining extremely thin slice reformations with a decreasing amount of X-radiation the future of volume estimations is even more promising than with HCT (Blum 2002). Also the need for direct coronal scanning of the patient and thus an inconvenient patient position is obviated due to the high resolution reformatted images obtained from axially oriented images.

Reasonable correlation has been reported between AR and CT scans (D'Urzo et al. 1987, D'Urzo et al. 1988, Hilberg et al. 1989, Min and Jang 1995). In a previous study (Gilain et al. 1997) with CT and AR, the results showed a significant correlation between the volumes in the first part of the nasal cavity in the area of the nasal valve. Our study showed significantly similar volumes obtained with both techniques in the anterior and middle part of the nasal cavity. In contrast, a significant difference was found in the volumes of the posterior part of the nasal cavity. This poor statistical correlation led us to believe that the size of the nasal sinuses has no effect on the structural behavior of the nasal cavity. The fact that no correlations were found between right and left nasal cavities volumes suggests that they work as independent anatomic entities and have no effect on the overall functional insufficiency in diseased states. CT is now being used as a golden standard in the validation of acoustic rhinometry (Terheyden et al. 2000)

In a study with MRI (Corey et al. 1997) where five healthy subjects were evaluated with 2mm thin coronal sections the AR measurements were found to be higher than MRI measurements especially between the 2 cm and 6 cm area from the tip of the nose, and after the first four cm the correlation between the measurements by AR and MRI was poor. However, the poor visibility of the bony structures in MRI may be one factor to be considered in future if accurate volumes of air need to be assessed.

6.2.2 OVARIAN TUMORS (III)

In the evaluation of ovarian tumors, US, CT and MRI have been used with varying success. Even though ultrasound is an easy and inexpensive to approach, it is not ideal for volume measurements. In small-sized tumors, definition of tumor shape and size may be easy but is not comparable to that done by computerized segmentation techniques. Large irregular-shaped tumors cannot be measured accurately due to the limitations encountered with ultrasound transducers in regard to the size that can be visualized on the US screen. CT, due to its radiation hazards, is losing its role in the evaluation of gynecological tumors. MRI with its high sensitivity and specificity has become routine in this context. The use of MRI and volumetric estimation by means of image segmentation has been successful in the case of ovarian tumors.

In this study, the presence of ascites associated with ovarian tumors was a major hazard in the interpretation of MR images at segmentation. Ascites and cysts looked very similar on T2 weighted MRI sequences and the boundary between the two formed by the thin and smooth cyst wall was impossible to define. Thus, the tumor volume proved to be inaccurate in larger ascitic fluid accumulations. Volumetry misinterpreted the ascites as cyst fluid, which led to an overestimation of volume in two cases. Hence new MRI sequences like fast-FLAIR, MT and TI/T2- weighted fat suppression need to be tried out in order to define the cyst wall.

At laparotomy, volume estimation of ovarian tumors proved to be more difficult than expected in that the growths they tend to be irregular in shape. Volume measurement using the Archimedes principle, where the volume of water replaced by the extirpated tumor when immersed in a water-containing vessel is estimated, would have given a more accurate measurement. However, since cystic tumors are fragile and tend to rupture during removal, this kind of measurement could not be done. For example in an oval-shaped tumor the segmented volume was twice that estimated at laparatomy. After surgical treatment, where the residual disease is solid in 90% of cases and there is no possibility of cyst rupture during operation, our volumetric technique might be useful. 3D MRI-based volumetry seems to be most accurate in small- and moderate-sized tumors and thus seems a promising indication for ovarian cancer patients to evaluate the response to chemotherapy and thus improve the prognosis.

6.2.3 FETAL WEIGHT ESTIMATION (IV)

With US, the accuracy of fetal weight depends on how clearly the fetal borders can be defined. Certain conditions such as maternal obesity, oligohydroamnios and unfavorable fetal positions may lead to false measurements and weight estimation. In earlier studies, when three different sonographic circumference measurement techniques were compared in term fetuses, two of them, the diameter and ellipse circumference measurement techniques were found to be similar in predicting actual birth weights (Smulian et al. 1999). In our study, the correlations between the estimated and actual birth weights were comparable and even better than the accuracy of US-based weight prediction generally reported (Benaceraff et al. 1988, Hirata et al. 1990). Also accuracy depends on growth distribution. If the growth distribution is abnormal, as in diabetic pregnancy, the formulas developed to estimate weight might not be optimal. In our study, maternal diabetes did not lead to gross misestimations. Hadlock's formula was slightly better than Shepard's in predicting weight in these fairly tall fetuses,

which suggests that femoral length should be taken into account in estimations of macrosomal fetuses. With the introduction of new 3D ultrasound even more superior fetal weight estimations can be obtained compared to the 2D US (Schild et al. 2000).

In MRI the above-mentioned adverse factors do not affect accuracy. In a recent study (Kubik-Huch et al. 2000b), MRI was found useful in fetal imaging especially in assessing cerebral anomalies. MRI has been established as a safe and useful technique in evaluation of the fetus in utero (Laptook, 1990). Fetal weight estimation using MRI has been used in one study where there was an underestimation of weights (Baker et al. 1994a). Using image segmentation and volumetric analysis an optimal weight estimation of the fetuses was accomplished. MRI is an expensive means of estimating fetal weight in utero and thus its routine use is not yet recommended. However, in certain clinical conditions like diabetic pregnancy, use of MRI in fetal weight estimations can indeed be useful. Also when sonographic visualization is difficult, and one needs to get an accurate weight estimation MRI is recommended. It is believed that it will be a useful and reliable tool for clinical decisions. Out of the 20 patients studied with MRI here, motional blurring was observed in only 2 patients. This did not however prevent us from getting an accurate delineation of fetal borders in these cases. None of our subjects complained of discomfort; examining the subjects in a lateral supine position minimized this.

In the present study MRI was accurate in measuring fetal volume and consequently fetal weight. Fetal weight is derived when volume is multiplied by density. However the density is not universally defined and there may be a marked variation between fetuses. Using the earlier density of 1.03 as defined by Baker and associates (1994) in their study, a slight underestimation of fetal weight was observed in our material. However, with the density coefficient of 1.07, derived from the slope of the regression line in our study, an optimal weight estimation was observed. The Cavalieri method of stereology has been used successfully in fetal volume estimation (Garden et al. 1996). A serial measurement study assessing total fetal volume and differential growth of fetal organs using this method and MRI is a more sensitive means of assessing fetal intrauterine growth than US-estimated two-dimensional methods. With the Cavalieri method, fetal volume estimation with a coefficient error of less than 5% from 3 or 4 properly sampled MRI scans can be obtained (Robert's et al. 1994). In our study this aspect was not assessed. The use of MRI segmentation in evaluating the fetal morphology and fetal part weights has not yet been evaluated with Anatomatic^{TM}. Also in the future using segmentation MRI pelvimetry could be performed.

Use of different ultrafast MRI sequences is recommended. Ultrafast MR imaging traditionally means either echoplanar imaging on specially developed gradient systems or very short repetition time gradient-echo imaging on standard MRI scanners. Interleaved gradient-echoplanar imaging has been used to study in-vivo heart images acquired in 110 ms and with a resolution of 2.5 mm in standard body scanners However, the disadvantages of blurring of edges and increased noise leading to suboptimal images has discouraged the use of this technique (McKinnon et al. 1993). Sequences like HASTE, FISP and RARE have eliminated the need for fetal premedication with a concomitant improvement in image resolution and diminished blurring. Artifacts related to maternal respiratory motion no longer restrict the anatomic detail that can be had with MRI (Levine et al. 1996, Levine et al. 1998, Amin et al. 1999, Chung et al. 2000). In the recent literature knowledge of these sequences affecting the fetus or not has not been mentioned. This aspect needs to be studied in the future.

6.2.4 MULTIPLE SCLEROSIS (V)

In the analysis of neurological diseases, segmentation and volumetric estimation has previously been undertaken. In MS disease, planimetric evaluation of MRI has been found to be a useful supplement to clinical rating scales (Kappos et al. 1987). Several computer-assisted volumetric techniques have since been developed, e.g. manual outlining, semiautomatic lesions contouring and intensity-based thresholding techniques which have provided a quantitative and sensitive means of monitoring disease activity in MS in context of treatment trials (Grimaud et al. 1996). Our study represents a similar successful evaluation of MS lesion loads using a new semiautomatic segmentation software. The application of our new technique in quantifying intracranial CSF fluid spaces and cerebral volume as markers of cerebral atrophy were found to be optimal and fair correlation with neurological disability was observed.

The brain white matter bulk consists predominantly of axons (46%) followed by myelin (24%). The progressive atrophy in MS implies loss of these structures, especially axons (Ozawa et al. 1994, Loseff et al. 1996 a, Miller et al. 2002). Axonal injury has been explained by an inflammation (Fergusson et al. 1997, Trapp et al. 1998). However, brain atrophy in MS is not due simply to axonal loss involving macroscopic plaques but also involves the generalized degenerative process affecting various tissue components like NAWM (De Stefano et al. 2002). The development of brain atrophy occurs at all clinical stages, but especially during the progressive phase of the disease, and is associated with increasing disability (Filippi et al. 1996a, Loseff et al. 1998). Measuring brain atrophy (Loseff and Miller 1998) can objectively assess the effect of putative therapies aimed at preventing disability. The presence of brain atrophy is more prominent in patients with sustained deterioration of EDSS score (Loseff et al. 1996a). In our study, total and relative brain atrophy correlated significantly with EDSS (p values less than 0.005). Also mild inverse correlations were observed between brain volume and EDSS (p values less than 0.08). These findings are in agreement with the earlier studies mentioned.

To measure the level of brain atrophy in MS one needs to study the measures of brain volume and CSF volume also in control subjects. Normalized volumes are desirable for cross-sectional studies and absolute volume measures for serial investigation (Miller et al. 2002). Recently, in a study with MS where a cohort of normal control subjects (matched for age and sex) were also studied, brain atrophy was significantly more severe in MS patients (brain parenchymal fraction, white matter fraction and gray matter fraction were shown to be significantly reduced (p less than 0.001 for all fractions) (Chard et al. 2002). In another study with MS and controls the brain atrophy measures were significantly higher than in controls (p levels of less than 0.0001) (Vaidyanthan et al. 2002). In our study with SPMS we also found the brain atrophy measures in MS patients to be much greater than in controls (p less than 0.01). Using axial T2 images the majority of patients showed cerebral atrophy. Relative intracranial CSF space volumes and relative brain volume proved to be optimal markers of the condition.

In recent studies on brain atrophy, the brain parenchymal fraction (BPF), which is the ratio of brain parenchymal volume to the total volume within the surface contour is being used. BPF well correlates

inversely with the third ventricular width and total T1 hypointense lesion load (Bernel et al. 2002). The concept of fractional volumes of different brain structures like gray matter (fGM), white matter (fWM) and CSF spaces (fCSF) are being increasingly used to determine brain atrophy. All these mentioned volumes are normalized to total intracranial volumes to prevent error arising from individual head size variations. A significant decrease in fGM has been found in MS patients compared to normal volunteers (Quarantelli et al. 2003). Also the concept of normalized cortical volumes has been applied, where only the cortical volume has been measured, normalized to the total intracranial volume. A significant decrease in normalized cortical volumes has been found in the early stages of both RRMS and PPMS (De Stefano et al. 2003). In our study the so-called relative atrophy was the same as the fractional volumes of CSF (fCSF); fGM and fWM were not then measured.

In MS, T2-weighted image has been the most widely used technique and predicts the onset of definite MS (Morrissey et al. 1993). In several earlier studies, no notable associations were found between the extent of MS plaques on MRI and neurological disability as evaluated by EDSS (Franklin et al. 1988, Kiel et al. 1988, and Simons et al. 1998). The relation between enhancing lesions or hyperintense plaques on T2-weighted images and change in EDSS has been poor (Simons et al. 1998). Also hyperintense T2 plaques have correlated poorly with cognitive disability (Bagert et al. 2002). This is because the T2 image cannot differentiate between different stages of MS disease like active plaques, chronic plaques and irreversibly inactive plaques (black holes), thus lacking specificity. Highly significant correlations have been found between PD-weighted images and EDSS scores (Rovaris et al. 1998). In our study PD images were not analyzed because the sequence was not volumetric in nature. However a tendency to correlation was found between the volumes of T2-weighted lesions and total RFSS scores (p less than 0.03). The total T2 lesion load was measured from 3D T2 FSE images, where only T2 plaques between the level of the fourth ventricle and centrum semiovale were taken into account, and this could have led to minor volume errors, this being however due to the technical restrictions imposed by the 0.5 Tesla MRI machine. The fCSF was measured from the conventional T2 weighted axial images which covered the whole brain. To our knowledge the correlations between RFSS scores and volumetric measurement of segmented CSF spaces and MS plaques were elicited for the first time in this study.

There is a limitation to using T2-weighted MRI lesion volume alone. However, the detection of both hypointense and hyperintense MS plaques on fast-FLAIR images suggest a potential in combining information from two different images (T1- and T2-weighted images) into one single image (van Waesberghe et al. 1996). Also, combined analysis of MR-based chemical and imaging data (combined MRI and MRS) might allow improved non-invasive assessment of lesion pathology in order to better understand its relationship to the clinical features of multiple sclerosis (Matthews et al. 1996). MTR-derived measures correlate better with physical disability (Gass et al. 1994) and cognitive impairment (Rovaris et al. 1998) than conventional measures in MS. MS lesions show a dramatic drop in MT ratios in their enhancing active stage (Filippi et al. 1998b) and their short-term changes (3-12 months) range from a persistent and severe reduction to complete recovery (van Waesberghe et al. 1998). Very strong correlations have been found between the decreased MTR of various segmented tissue regions and clinical disability (Udupa et al. 2001). MTR could not be performed in our study due to restrictions with the 0.5 T MRI machines with which the patients were examined. Use of diffusion and perfusion-

weighted imaging has also been found useful in MS disease, but these sequences were lacking in our 0.5 T machine and so could not be studied.

In MS disease black holes or hypointense MS plaques on T1-weighted image represent axonal loss and tissue damage (van Waesberghe et al. 1997). T1-weighted MR images reveal major differences in the degree of hypointensity which correlates with the extent of axonal damage, and extracellular edema and the degree of demyelination or remyelination in biopsy-proven cases (Bruck et al. 1997). In contrast to earlier studies, where overall T1 plaque volume measurement correlated better with disability than T2 volume measurements (van Walderveen et al. 1995, Truyen et al. 1996), our study showed no correlations between the volumes of black holes in T1-weighted images and neurological disability, perhaps due to the small sample of patients. Gd-chelate enhancement of MS plaques demonstrates edematous changes in the blood brain barrier and is a highly sensitive measure of active MS disease, which may increase or decrease in follow-up (Stone et al. 1997). Only three out of 27 patients had enhancing active plaques on Gd-chelate-enhanced T1 images, the possible reason for this being the low disease activity during the MRI study (i.e. the number of patients with active lesions was 3). None of the patients complained of acute symptoms at the time of MRI. The stopping of steroids 6 months before the MRI examination and the fact that the patients had no clinical symptoms at the time was one of the inclusion criteria for the phase three drug trial to which our study belongs.

The serial measurement of cord cross sectional area is important. A lack of association between cord lesions and disability may be associated with limitations in MR resolution but also suggest that the mechanisms of disability in MS are complex and multifactorial (Kidd et al. 1993). The plaque/white matter ratio had a significantly negative correlation with the width of the cervical cord (Reider-Grosswasser et al. 1988). Quantified measurements of spinal cord atrophy (Loseff et al. 1996b) provide additional and specific information on demyelination and axonal loss in MS. Given its reproducibility, the magnitude of the change detected and the strong correlation with disability, the computerized quantification of spinal cord atrophy should prove to be a sensitive measure of progressive neurological deterioration and can easily be incorporated into imaging protocols aimed at monitoring therapy (Loseff et al.1998).

6.2.5 CEREBRAL INFARCTION (VI)

Up to now only few volumetric estimation studies using segmentation technique have been undertaken in patients with cerebral infarctions (Swanson et al. 1990). However, semiautomatic segmentation software has been successfully utilized for the first time in the literature in right-sided cerebral infarctions with neglect as the main symptom**.**

In two thirds of patients, infarct volume is established 24 to 36 hours after stroke onset (Pantano et al. 1999). In our study the volumes of MRI-based infarcts were measured between the 9^{th} and the 14^{th} day, so that quantitative analysis of the initial infarct volumes could not be performed.

CT-determined size of infarction has previously been used in the evaluation of short-term prognosis (Kinkel and Jacobs 1976; Rasmussen et al. 1992). A direct relationship has been established between infarct size and post-stroke Rankin score (Beleosesky et al. 1995). However, in unilateral lenticular

infarcts the size of the infarction did not correlate with the long-term prognosis (Giroud et al. 1997). Subsequently infarct volumes rather than the size were calculated. Large infarction volumes more than 50 cm^3 and 80 cm^3, found in two separate earlier studies (Andre and Pinheiro 1995, Saunders et al. 1995) have been associated with increased morbidity and mortality. In a recent study (Kuroda et al. 2001) the decreased regional cerebral blood flow on perfusion MRI in infarcted areas identified a higher risk of subsequent ischemic stroke during a follow-up period of 42.7 months. Also flow heterogeneity (FH) maps on MRI performed in the acute stages of infarction may enable more precise prediction of final infarct volume (Simonsen et al. 2002). DWI helps predict the size of lesion on T2 weighted images obtained after about 8 days in patients with a symptom onset of more than 4 hours, while in patients with symptoms of less than 4 hours perfusion imaging yielded additional information on the brain tissue with impaired perfusion (Wittsack et al. 2002). In our study with conventional MRI using 3D T2 FSE images, the median volumes of the infarctions ranged from 85.9 cm^3 with manual segmentation to 104.2 cm^3 with semiautomatic segmentation. The good correlations between the volumes and long-term prognosis (one year) in our study are in agreement with earlier reports (Saver et al. 1999, Iwamoto et al.1999) Volumes have been correlated positively with cognitive alterations and negatively with the global outcome as measured by Barthel index (Mauch et al. 1994). Regional infarct volumes have correlated significantly with motor impairment tests (Rogers et al. 1997). In our study the infarct volumes were positively correlated with the hand motor function test results and neglect. The volumes correlated negatively with the Barthel index. Reduction in infarct volume has been advocated as a biological surrogate or auxiliary outcome for human stroke trials to replace or supplement deficit, disability and global clinical scales (Saver et al. 1999).

New MRI sequences like fast FLAIR images provide more conspicuity of infarctions as compared with the conventional T1-, proton density- and T2-weighted spin echo images and a reduced scan time compared with the conventional FLAIR sequences. Lesion conspicuity is superior in 96% of lesions. The periventricular, cortical and pontine hyperintensities are more extensive on the fast FLAIR images (Alexander et al. 1996). Hence use of this sequence in the measurement of infarct volumes should be more accurate than with T1 weighted or T2 weighted sequences. Lesion conspicuity in T1 images are not sensitive enough in delineating the whole infarct, so they were not used for lesion volume estimation in our study.

New multiphasic perfusion CT imaging has been found to be useful and comparable utility to DWI and PWI MRI for predicting final infarct volume, infarct growth and clinical severity in acute ischemic stroke (Na et al. 2003). Both perfusion CT and PWI/DWI MRI have been found to be equivalent in the task of identification of cerebral penumbra in acute ischemic stroke patients and thus in the selection of patients suitable for thrombolytic therapy (Wintermark et al.2002).

During the one-year follow-up period, infarction volumes had a parallel effect on the NIHSS and BI but showed no effect on the HMFT neurological function score, probably because HMFT reflects the damage which larger infarcts cause to the corticospinal fibers from the area of representation of the hand.

In spite of the good correlations obtained here between infarct volumes and neurological dysfunction, there is some room for criticism. Traditional direct measurement of infarct volume is associated with an

overestimation of volumes during the development of edema during the first 3 days after ischemia, and the degree of vasogenic edema may be still profound during the 4^{th} and the 14^{th} days. Thus an approximate error of 20% in the volume may have occurred in our study. Here the indirect measurement of the noninfarcted parenchymal volume is useful (Lin et al. 1993).

The location of the cerebral infarction correlates with the long-term prognosis. For example in infarcts situated in the nucleus lentiformis, the long-term outcome for motor functions is excellent but slight cognitive disorders, problems with short-term memory and dysphasia persist for several months (Giroud et al. 1997). However, in another study by our group, the lesion localization and its correlation to symptoms were studied (Ahonen et al.1999). The lesions were shown to involve more than one lobe and/or included basal ganglia. Cortical infarcts were shown to extend to the subcortical white matter. Thus lesions were shown to be widely distributed and no conclusions could be drawn regarding the association between the location of infarcts and the specific neglect features in patients with right cerebral infarctions. This finding has been consistent in earlier studies (Coslett et al. 1990**).** Right hemisphere strokes, which mostly lie in the middle cerebral artery territory, tend to be very stereotyped in lesion localization, which may indeed have masked the importance of lesion location rather than the size of the lesion (Hier et al. 1983).

6.3 3D REPRESENTATION OF VOLUMETRIC MR IMAGES

Information regarding the location of a lesion in 3D and surrounding structures around a lesion and the probable compression of these structures is important from a clinical point of view. This can best be achieved with 3D reformations. A new software, Medimag^{TM}, was used during the course of our studies to create reliable 3D reformations of MR images. This was used in the case of ovarian tumors and cerebral infarction. No comparisons were made with the original axial, coronal or sagittal images. To evaluate the actual use of 3D visualization in all the above-mentioned disease groups, one still needs to compare the advantages of 3D over conventional MRI/CT images, and this will be a part of our future studies.

6.4 TRENDS IN THE FUTURE

Medical mage processing is still in its infancy; however, rapid growth in both hardware capabilities (especially with memory size and network communication speed) and software standards and techniques (radiologist workstations, DICOM and Java/WEB based systems) and their integration with existing radiological equipment have made these image processing techniques available to physicians everywhere (Wilkens and Rowberg 1995, Yuh et al. 1999).

In the nasal airways, the introduction of new multislice CT is offering improved temporal and spatial resolutions, retrospective determination of slice thickness to a level of 0.1 mm, and shorter acquisition times (Blum 2002). In airways volume estimation also multi-slice CT covers a greater volume of the focused area of interest than helical CT during a simple breath hold (Grenier et al. 2002). New real-

time dynamic cine MRI will allow efficient analysis of airway patency and function (Faust et al. 2001). In ovarian tumors and fetal weight estimation the increasing use of new fast MRI techniques like EPI will improve volume estimation capabilities.The use of new MRI sequences like HASTE and RARE using breath holding have increasingly shown better delineation of fetal borders (Levine et al. 1996, Levine et al 1998). In multiple sclerosis, MTR, DWI,fMRI and proton MRS are being and will be used more frequently to achieve reliable specific in vivo quantification of MS pathology (Fillippi et al.2003). Also targeted multiparametric MRI protocols should be used (Filippi and Grossman 2002). Quantitative diffusion-weighted MRI is in increasing use where the molecular self-diffusion coefficient D has been measured in both the MS lesions and normal-appearing white matter (Wilson et al. 2002). The increasing use of volumetric estimation of lesions seen on DWI in the very early stages of cerebral infarct has helped in improving prognosis in infarcts.The introduction of new multislice CT (perfusion CT) is offering a new simple and effective way of evaluating ischemic penumbra as effectively as DWI in the selection of patients with cerebral infarction for thrombolytic therapy (Wintermark et al.2002) New parallel MRI imaging techniques like sensitivity encoding (SENSE), array spatial sensitivity encoding (ASSET) and simultaneous acquisition of spatial harmonics (SMASH) have been introduced in clinical imaging. The aim of these techniques is to decrease the imaging time without losing the image resolution, increase the image resolution when the imaging time is kept the same and increase the number of image slice and the imaging region. They are being used in the assesement of intracranial and cardiac dynamics (Sodickson and Manning 1997, Pruessmann et al. 1999, Mori et al. 2002). It can be assumed that these techniques will be extremely helpful in making better volumetric estimations in the future.

According to clinical tests applied to MS and cerebral infarction patients, the volume of lesions does not always correlate with the clinical findings, which leads us to believe that the location of lesions is important. Also the volumes of lesions in specific locations help achieve good correlations with neurological dysfunctions (Brott et al. 1989). Therefore, we are in the process of developing a digital anatomic atlas, to be implemented with Anatomatic^{TM} in the future (Frey et al. 1999). Such a method would also allow automatic estimation of volumes anatomically in specific functional areas of the brain in addition to total quantification of lesions. The 3D software Medimag^{TM} has not been used routinely for 3D reformations. The advantage of these reformations over conventional MR images in the imaging of different diseases calls for assessment in the future.

Newer and faster semi- and fully automatic segmentation softwares have made lesion quantification easier, more reliable and user friendly. Segementation is now being used to determine cortical thickness of the brain, which is more sensitive than measurement of cortical volume for assessment of atrophy change in MS patients (Sailer et al.2003). In many new phase III drug trials, automatic segmentation softwares and digital anatomic atlases are being increasingly used in lesion quantification especially in MS and cerebral infarctions. Also, these techniques are being used. in neurodegenerative diseases like SLE and dementia

7 SUMMARY AND CONCLUSIONS

In this study we evaluated the use of a new semiautomatic segmentation technique, Anatomatic™, in volumetric estimation of structures and lesions in various diseases of the respiratory system, the reproductive system and the central nervous system. Also the use of the new 3D software Medimag™ was evaluated in the 3D representation of images.

The first aim was to evaluate the use of Anatomatic™ in volumetric measurements and that of Medimag™ software in 3D-image analysis in five different disease groups, i.e. nasal airway diseases, ovarian tumors, fetal weight estimation, multiple sclerosis and cerebral infarctions. After segmentation of all images in one HCT or MRI data set, the total and partial volumes were rendered automatically. In the test for calibration of the volumetric software, the validation test with five different-sized syringes using a head phantom giving an overall error of only 1.5% was considered optimal. In the test for repeatability of measurements, the very small variabilities in inter- and intra-observer tests in three different disease groups (ovarian tumors, multiple sclerosis and cerebral infarctions) showed the technique to have a good repeatability. In nasal airways (airway volumes), ovarian tumors (tumor volumes), fetal weight estimation (fetal volumes), MS disease (plaques and cerebral atrophy) and cerebral infarctions (infarction volumes) volumes of structures and lesions were rendered accurately. In addition we created 3D reformations from segmented HCT and MR images in various diseases (nasal airway diseases, ovarian tumors and cerebral infarctions) using Medimag™ software. In the sinonasal area, the complex anatomic structures of the nasal cavity and paranasal sinuses were well represented. Also in ovarian tumors and cerebral infarctions, accurate 3D reformation of lesions and images was demonstrated.

The second aim was to correlate the volumetric measurements obtained with segmented HCT/MRI and those achieved with acoustic rhinometry (nasal airway diseases), laparotomy (ovarian tumors) and abdominal ultrasound (fetal weight estimation). In nasal airway diseases, the volumes obtained by both techniques, i.e. segmented CT and AR, matched in the anterior and middle parts but not in the posterior portion of the nasal cavity. HCT was found to be a good method of validation for studies of acoustic rhinometry and, along with AR, can be used successfully in the field of rhinology. In ovarian tumors, the volumes obtained with segmented MRI and volumetric measurements at laparotomy matched correctly in only 50% (3 patients) due to the fact that the cysts could not be measured reliably during laparotomy, this by reason of the varying and very substantial size of tumor cysts and also due to their tendency to rupture during laparotomy. Also the presence of large ascitic fluid collections hindered visualization of the cystic membrane on segmented MRI, this leading to false volumetric measurements. In fetal weight estimations, the actual birth weights predicted with segmented MRI were more accurate than those obtained with US. MRI promises thus to be an reliable method of predicting birth weights especially in problematic cases such as in diabetic pregnancy.

The third aim was to correlate the volumetric measurements achieved with segmented MR images with neurological deficits in multiple sclerosis and cerebral infarctions. In secondary progressive MS, good correlations were found between cerebral atrophy and EDSS scores. Also significant associations emerged between the volumes of T2 plaques and total RFSS neurological function scores. In cerebral infarctions, infarction volumesshowed significant positive correlations with the NIHSS, HMFT function scores and degree of neglect and significant inverse correlations with BI function scores. In this study, the infarction volumes had a parallel effect on the NIHSS and BI neurological function scores during the one-year follow-up period. In contrast no effect was evident on HMFT neurological function score. Thus infarction volume predicted well the one-year outcome and prognosis. It helped understand the effect of volume of infarction on the course and prognosis of stroke.

In conclusion, we believe that our new, simple and fast microcomputer-applicable semiautomatic segmentation technique is a practical tool for the volumetric analysis of lesions in different diseases of the respiratory, reproductive, and central nervous system. Reliable lesion volume estimations and good correlations to clinical deficits lead us to believe that Anatomatic™ Segmentation software can be used for routine clinical work in different diseases.

ACKNOWLEDGEMENTS

This study was carried out at the Departments of Diagnostic Radiology, Neurology and Rehabilitation, and Otorhinolaryngology, Tampere University Hospital, Medical School, University of Tampere and at the Ragnar Granit Institute, Tampere University of Technology, Tampere, Finland.

I wish to express my sincere gratitude to my supervisor and teacher, Professor Erkki Laasonen, M.D., Ph.D. for introducing me to the topic of image segmentation. His professional guidance, personal involvement and continuos encouraging attitude made it possible to complete this study. My sincere gratitudes is also due to my supervisor, Professor Hannu Eskola, Ph.D. whose constant technical guidance and personal involvement formed an important contribution to this study.

I owe my warmest thanks to emeritus Professor Erkki Koivisto to introduce me to the world of scientific research. Without his fatherly advice during my early parts of the career, my career in the field of research would not have been possible. I owe my deepest gratitude to Docent Gabor Molnar, M.D., Ph.D and Docent Timo Kuurne M.D., Ph.D for their constant guidance and expertise which helped finish my thesis.

I wish to thank Docent Kaarina Partanen, M.D:, Ph.D. and Docent Tapani Tikkakoski, M.D., Ph.D., the official reviewers for their interest and careful review of the final manuscript. Their expert comments and constructive criticism proved extremely valuable.

I owe my warmest thanks to Professor Terho Lehtimäki. M.D., Ph.D. for constantly advising me on various important aspects of writing a good thesis. Through him I have learnt a great deal about the different aspects of proper statistical analysis.

I am indebted to Dr. Tomi Heinonen Ph.D. for letting me use his newly developed segmentation and 3D softwares in a medical environment. To his active involvement is due a large part of this study. I sincerely thank physicist Pertti Ryymin, without whom the technical part of this study would not have materialized.

My warm thanks are due to Docent Markus Rautiainen, M.D., Ph.D. for active involvement in this study. Also many thanks are due to emeritus Professor Heikki Puhakka for constantly encouraging me throughout the undertaking.

I am grateful to Emeritus Professor Harry Frey for actively involving himself throughout. His kindly and careful assistance was an invaluable help. I thank Professor Irina Elovaara, M.D., Ph.D. for her constructive criticism and comments and her indispensable advice and support during this entire study.

I thank all my co-authors for their collaboration: Pasi Kauppinen, Ph.D., Jura Numminen, M.D., Ph.D. Johanna Mäenpää, M.D., Ph.D.,Tapio Kuoppala, M.D., Ph.D, Jukka Uotila, M.D., Ph.D., Terttu Erilä, M.D., Ph.D., Marita Ukkonen , M.D. Jukka Peltola,M.D., Jukka Pekka Ahonen, M.D. and Mervi Jehkonen, M.D., Ph.D.

I wish to thank all my colleagues in the Department of Diagnostic Radiology,Tampere University Hospital for their constant support during the entire study. Also my warm thanks are due to the radiographers working in the MRI and CT departments.

I am grateful to Mr. Robert MacGilleon for revising the language of the thesis.I also wish to thank all personnel at the medical library of Tampere University Hospital. Also warm thanks are due to all personnel at the thesis committee for all their invaluable support.

And finally I want to thank my family, my wife Saila and our first baby who is due to be born soon. Also my deepest gratitude goes to my parents. Without their love and support this thesis would never have been possible.

This work was financially supported by the Medical Research Fund of Tampere University Hospital.

Tampere, 2004

Prasun Dastidar

REFERENCES

Achiron A, Gicquel S, Miron S, Faibel M (2002): Brain MRI lesion load quantification in multiple sclerosis: a comparison between automated multispectral and semi-automated thresholding computer-assisted techniques. Magn Reson Imaging 20:713-720

Acton PD, Mu M, Plossl K, Hou C, Siciliano M, Zhuang ZP, Oya S, Kung HF (1999): Single-photon emission tomography imaging of serotonin transporters in the non human primate brain with ((123)I OD). Eur J Nucl Med 26:1359-1362

Ahonen JP, Jehkonen M, Dastidar P, Molnar G, Häkkinen V (1999): Motor-evoked potentials in stroke patients with left hemi-neglect. Electroencephalogr Clin Neurophysiol 109:224-229

Alexander JA, Sheppard S, Davis PC, Salverda P (1996): Adult cerebrovascular disease: role of modified fluid-attenuated inversion-recovery sequences. AJNR Am J Neuroradiol 17:1507-1513

Amin RS, Nikolaidis P, Kawashima A, Kramer LA, Ernst RD (1999): Normal anatomy of the fetus at MR imaging. Radiographics 19: 201-214

Andersen O, Lycke J, Tollesson PO, et al. (1996): Linomide reduces the rate of active lesions in relapsing-remitting multiple sclerosis. Neurology 47:895-900

Andre C, Pinheiro RS (1995): The correlation of CT findings and in-hospital mortality after cerebral infarction. Arq Neuropsiquiatr 53:395-402

Anuweiri H, Prasana V (1992): Parallel architectures and algorithms for image component labeling. IEEE Trans. Pattern Anal Mach Intell 14:1014-1034

Apicella PL, Mirowitz SA (1995): Interactive multiplanar reformation of conventional two-dimensional MR images. Clin Imaging 19:279-282

Ashton EA, Takahashi C, Berg MJ, Goodman A, Totterman S, Ekholm S (2003): Accuracy and reproducibility of manual and semiautomated quantification. J Magn Reson Imaging 17:300-308

Bagert B, Camplair P, Bourdette D (2002): Cognitive dysfunction in multiple sclerosis: natural history, pathophysiology and management. CNS Drugs 16:445-455

Baker P, Johnson I, Gowland P, Hykin J, Harvey P, Freeman A (1994a): Fetal weight estimation by echo-planar magnetic resonance imaging. Lancet 343: 644-645

Baker P, Johnson I, Harvey P, Gowland P, Mansfield P (1994b): A three-year follow-up of children imaged *in utero* using echo-planar magnetic resonance. Am J Obstet Gynecol 170:32-33

Barker PA, Darby DG, Desmond PM, Yang Q, Gerraty RP; Jolley D, Donman GA, Tress BM, Davis SM (1998): Prediction of stroke outcome with echoplanar perfusion- and diffusion-weighted MRI. Neurology 51:418-426

Barkhof F, Scheltens P, Frequin ST, Nauta JJ, Tas MW, Valk J, Haumes OR (1992): Relapsing-remitting multiple sclerosis: sequential enhanced MR imaging vs. clinical findings in determining disease activity. AJR Am J Roentgenology 159:1041-1047

Barkhof F, Filippi M, Miller DH, Tofts P, Kappos L, Thompson AJ (1997): Strategies for optimizing MRI techniques aimed at monitoring disease activity in multiple sclerosis treatment trials. J Neurol 244:76-84

Bastianello S, Bozzao A, Paolillo A, Giugni E, Gasperini C, Koudriavtseva T, Millefiorni E, Horsfield MA, Colonnese C, Toni D, Fiorelli M, Pozzili C, Bozzao L (1997): Fast spin-echo and fast fluid-attenuated inversion recovery versus conventional spin-echo sequences for MR quantification of multiple sclerosis lesions AJNR Am J Neuroradiol 18:699-704

Baum K, Nehrig C, Girke W, Brau H, Schorner W (1990): Multiple sclerosis: relations between MRI and CT findings, cerebrospinal fluid parameters and clinical features. Clin Neurol Neurosurg 92:49-56

Beleoosesky Y, Streiffer JY, Burstin A, Grinblat J (1995): The importance of brain infarct size and location in predicting outcome after stroke. Age-Ageing 24: 515-518

Benaceraff B, Gelman R, Frigoletto F (1988): Sonographically estimated fetal weights: Accuracy and limitations. Am J Obstet Gynec 159:1118-1121

Benesch H, Felber SR, Finkstedt G, Kremser C, Stockhammer G and Aichner FT (1996): MR volumetry for monitoring intramuscular bromocriptine treatment in macroprolactinomas. J Comput Assist Tomogr 19:866-870

Berek JS, Bast RC Jr. (1995): Ovarian cancer screening: The use of serial complementary tumor markers to improve sensitivity and specificity for early detection. Cancer 76:2092-2096

Bernel RA, Bakshi R, Tjoa C, Pulli SR, Jacobs L (2002): Bicaudate ratio as a magnetic resonance imaging marker of brain atrophy in multiple sclerosis. Arch Neurol 59:275-280

Bilir E, Craven W, Hugg J, Gilliam F, Martin R, Faught E, Kuzniecky R (1998): Volumetric MRI of the limbic system: anatomic determinants. Neuroradiology 40:138-144

Blum A (2002): Volumic and multislice CT: principles, applications and future prospects. JBR-BTR 85:82-99

Bomans M, Hohne KH, Tiede U, Riemer M (1990): 3D segmentation of MR images of the head for 3-D display. IEEE Trans MI 9:177-183

Bradley WG and Glenn BJ (1987): The effect of variation in slice thickness and interslice gap on MR lesion detection. AJNR Am J Neuroradiol 8:1057-1062

Brant-Zawadski M, Atkinson D, Detrick M, Bradley WG, Scidmore G (1996): Fluid-attenuated inversion recovery (FLAIR) for assessment of cerebral infarction. Initial experience in 50 patients. Stroke 27:1187-1191

Brassow F, Spielmann RP, Heberhold C (1984): Computed tomographic volumetry of the pneumatic system of the ear. Comparison of normal subjects and patients with ear diseases. ROFO Fortschr Geb Rontgeenstr Nuklearmed 140:158-161

Brott T, Marler JR, Olinger CP, Adams HP Jr, Tomsick T, Barsan WG, Billre J, Eberle R, Hertzberg V, Walker M (1989): Measurements of acute cerebral infarction: lesion size by computed tomography Stroke 20:871-875

Bruck W, Bitsch A, Kolenda H, Bruck Y, Stiefel M, Lassmann H (1997): Inflammatory central nervous system demyelination: correlation of magnetic resonance imaging findings with lesion pathology. Ann Neurol 42.783-793

Calhoun PS, Kuszyk BS, Heath DG, Carley JC, Fishman EK (1999): Three-dimensional volume rendering of spiral CT data: theory and method. Radiographics 19:745-764

Carls FR, Schuknecht B, Sailer HF (1994): Orbital volumetry as a planning principle for reconstruction of the orbital wall. Fortschr Kiefer Gesichtschir 39:23-27

Chards DT, Griffin CM, Parker GJ, Kapoor R, Thompson AJ, Miller DH (2002): Brain atrophy in clinically early relapsing-remitting multiple sclerosis. Brain 125:327-337

Chakraborty A, Staib LH, Duncan JS (1996): Deformable boundary finding in medical images by integrating gradient and region information. IEEE Trans Med Imag 15:859-870

Chen CT, Tsao CK, Lin WC (1991): Medical image segmentation by a constraint satisfaction neural network. IEEE trans NS 38:678-686

Choi SM, Lee JE, Kim J, Kim MH (1997): Volumetric object reconstruction using the 3D MRF model based segmentation. IEEE Trans Med Imag 16: 887-892

Chung HW, Chen CY, Zimmerman RA, Lee KW, Lee CC, Chin SC (2000): T2 weighted fast MR imaging with true FISP versus HASTE: Comparative efficacy in the evaluation of normal fetal brain maturation. AJR Am J Roentgenol 175:1375-1380

Clanet M, Berry I, Boulanouar K (1997): Functional imaging in multiple sclerosis. Int MS J 4: 26-32

Clanet M, Cassol E, Manelfe C, Berry I (2003): Clinical-MRI correlations in the secondary progressive phase of MS: lessons from the treatment trials. J Neurol Sci 206:139-144

Comi G, Fillipi M, Martinelli V, Sirabian G, Visiani A, Campi A, Mammi S, Rovaris M, Canal N (1993): Brain MRI imaging correlates of cognitive impairment in multiple sclerosis. J Neurol Sci 115:66-73

Corsten MT, Bernard PA, Udjus K, Walker R (1996): Nasal fossa dimensions in normal and nasally obstructed neonates and infants: preliminary study. Int J Pediatr Otorhinolaryngol 36:23-30

Corey JP, Gungor A, Nelson RH, Velde T (1996): The effects of environmental noise on acoustic rhinometry. Am J Rhinol 10: 247-249

Coslett HB, Bowers D, Fitzpatrick E, Haws B, Heilman KM (1990): Directional hypokinesia and hemispatial inattention in neglect. Brain 113:475-486

Costello P, Andersen W, Blume D (1991): Pulmonary nodule: evaluation with spiral volumetric CT. Radiology 17: 875-876

Cox RD, Henri CJ, Rubin RK (1999): Transparent image access in distributed picture archiving and communications system: the master database broker. J Digit Imaging 12:175-177

Creasman WT (1994): Second-look laparatomy in ovarian cancer. Gynecol Oncol 55:122-127

Cree MJ, Olson JA, McHardy KC, Sharp PF, Forrester JV (1997): A fully automated comparative microaneurysm digital detection system. Eye 11:622-628

Dalton CM, Brex PA, Jenkins R, Fox NC, Miszkiel KA, Crum WR, O'Riordan JI, Plast GT, Thompson AJ, Miller DH (2002): Progressive ventricular enlargement in patients with clinically isolated syndromes is associated with early development of multiple sclerosis. J Neurol Neurosurg Psychiatry 73:141-147

Dastidar P, Heinonen T, Numminen J, Rautiainen M, Laasonen E (1999 a): Semi-automatic segmentation of computed tomographic images in volumetric estimation of nasal airway. Eur Arch Otorhinolaryngol 256:192-198

Dastidar P, Heinonen T, Ahonen JP, Jehkonen M, Lehtimäki T, Molnar G (1999 b): Volumes of cerebral infarctions correlated to one-year neurological prognosis in patients with right hemisphere infarction: a new application for a semiautomatic magnetic resonance imaging segmentation software. (Unpublished data)

Dastidar P, Heinonen T, Vahvelainen T, Elovaara I, Eskola H (1999 c): Computerized volumetric analysis of lesions in multiple sclerosis using new semiautomatic segmentation software. Med Biol Eng Comp 37:104-107

Denes G, Semenza C, Stoppa E, Lis A (1982): Unilateral spatial neglect and recovery from hemiplegia: a follow-up study. Brain 105:543-552

De Stefano N, Iannucci G, Sormani MP, Guidi L, Bartolozzi ML, Comi G, Federico A, Filippi M (2002): MR correlates of cerebral atrophy in patients with multiple sclerosis. J Neurol 249:1072-1077

De Stefano N, Matthews PM, Filippi M, Agosta F, De Luca M, Bartolli ML, Guidi L, Ghezzi A, Montanari E, Cifelli A, Frederico A, Smith SM (2003): Evidence of early cortical atrophy in MS: relevance to white matter changes and disability. Neurology 69:1157-1162

D'Urzo AD, Lawson VG, Vassal KP, Rebuck AS, Slutzky AS, Hoffstein V (1987): Airway area by acoustic response measurements and computerized tomography. Am Rev Respir Dis 135:392-395

D'Urzo AD, Rubinstein I, Lawson VG, Vassal KP, Rebuck AS, Slutsky AS, Hoffstein V (1988): Comparison of glottic measurements by acoustic reflection vs. computerized tomography. J Appl Physiol 64: 367-370

Elliott J, Connolly KJ (1984): A classification of hand movements. Dev Med Child Neurol 26:283-296

Ernst R, Le VT, Kawashima A, Caskey C, Zelitt D, Tamm E, Sandler CM (1999): A picture archiving and communications system featuring multiple monitors using Windows98. J Digit Imaging 12:106-108

Faust RA, Remley KB, Rimell FL (2001): Real-time, cine magnetic resonance imaging for evaluation of the pediatric airways. Laryngoscope 111:2187-2190

Fergusson B, Matyszak MK, Esisri MM, Perry VH (1997): Axonal damage in acute multiple sclerosis. Brain 120:393-399

Filippi M, Horsfield MA, Morrissey SP, MacManus DG, Rudge P, McDonald WI, Miller DH (1994): Quantitative brain MRI lesion load predicts the course of clinically isolated syndromes suggestive of multiple sclerosis. Neurology 44:635-641

Filippi M, Paty DW, Kappos L, Barkhof F, Compston DA, Thompson AJ, Zhao GJ, Wiles CM, McDonald WI, Miller DH (1995 a): Correlations between changes in disability and T2 weighted brain MRI activity in multiple sclerosis. A follow up study. Neurology 45:478-480

Filippi M, Horsfield MA, Tofts PS, Barkhof F, Thompson AJ, Miller DH (1995 b): Quantitative assessment of MRI lesion load in monitoring the evolution of multiple sclerosis. Brain 118: 1601-1612

Filippi M, Horsfield MA, Campi A, Mammi S, Pereira C, Comi G (1995 c): Resolution- dependent estimates of lesion volumes in magnetic resonance imaging studies of the brain in multiple sclerosis. Ann Neurol 38:749-754

Filippi M, Horsfield MA, Bressi S, Martinelli V, Baratti C, Reganati P, Campi A, Miller DH, Comi G (1995 d): Intra- and inter-observer agreement of brain MRI lesion volume measurements in multiple sclerosis. a comparison of techniques. Brain 118:1593-1600

Filippi M, Campi A, Dousset V (1995e): A magnetization transfer imaging study of normal -appearimg white matter in multiple sclerosis. Neurology 45:478-482

Filippi M, Campi A, Colombo B, Pereira C, Martinelli V, Boratti C, Comi G (1996a): A spinal cord MRI study of benign and secondary multiple sclerosis. J Neurol 243:502-505

Filippi M, Yousry T, Campi A (1996b): Comparison of triple dose verus standard dose gadolinimun_DTPA for detection of MRI enhancing lesions in patients with MS. Neurology 46:379-384

Filippi M, van Waesberghe JH, Horsfield MA (1997): Interscanner variation in brain MRI lesion load measurements in MS. Neurology 49:371-377

Filippi M, Mastronardo G, Rocca MA, Pereira C, Comi G (1998a): Quantitative volumetric analysis of brain magnetic resonance imaging from patients with multiple sclerosis. J Neurol Sci 158:148-153

Filippi M, Rocca MA, Rizzo G, Horsfield MA, Rovaris M, Minicucci L, Colombo B, Comi G (1998b): Magnetization transfer ratios in multiple sclerosis lesions enhancing after different doses of gadolinium. Neurology 50:1289-1293

Filippi M, Rocca MA, Gasperini C, Sormani MP, Bastianello S, Horsfield MA, Pozzili C, Comi G (1999): Interscanner variation in brain MRI lesion load measurements in MS using CSE, RARE and fast-FLAIR. AJNR Am J Neuroradiol 20:133-137

Filippi M, Grossman RI (2002): MRI techniques to monitor MS evolution: the present and the future. Neurology 23:1147-1153

Fillippi M, Rocca MA, Comi G (2003): The use of quantitative magnetic-resonance-baased techniques to monitor the evaluation of multiple sclerosis. Lancet Neurology 2:337-346

Fornage BD (1993): Measuring masses on cross-sectional images. Radiology 187:289

Forstner R, Graf A (1999): Diagnostic imaging in staging of gynecologic carcinomas. Radiologe 39:610-618

Franklin GM, Heaton RK, Nelson LM, Filley CM, Seibert C (1988): Correlation of neuropsychological and MRI findings in chronic progressive multiple sclerosis. Neurology 38:1826-1829

Frigui H, Krishnapuram R (1997): Clustering by competitive agglomeration. Pattern Recognition 30:1109-1119

Frey H, Lahtinen A, Heinonen T, Dastidar P (1999): Clinical application of MRI image processing in neurology. International Journal of Bioelectromagnetism IJBEM 1:47-53

Fullerton KJ, Mckenzie G, Stout RW (1988): Prognostic indices in stroke. QJM 250:147-162

Garden AS, Roberts N (1996): Fetal and fetal organ volume etsimations with magnetic resonance imaging. Am J Obstet Gynecol 175:442-448

Gass A, Barker GJ, Kidd D, Thorpe JW, MacManus D, Brennan A, Tofts PS, Thompson AJ, McDonald WI, Miller DH (1994): Correlation of magnetization transfer ratio with clinical disability in multiple sclerosis. Ann Neurol 36:62-67

Gawne-Cain ML, O'Riordan JI, Coles A, Newell B, Thompson AJ, Miller DH (1998): MRI lesion volume measurement in MS and its correlation with disability: a comparison of fast-FLAIR and spin echo sequences. J Neurol Neurosurg Psychiatry 64:197-203

Georgi P, Strauss L, Sturm V, Osterag H, Sinn H, Rommel T (1980): Pre and intraoperative volume determination of cranipharyngioma cysts. Nuklearmedizin 19:187-190

Gilain L, Coste A, Ricolfi F, Dahan E, Marliac D, Peynegre R, Harf A, Louis B (1997): Nasal cavity geometry measured by acoustic rhinometry and computed tomography. Arch Otolaryngol Head Neck Surg 123:401-405

Giroud M, Lemesle M, Madinier G, Billiar T, Dumas R (1997): Unilateral lenticular infarcts: radiological and clinical syndromes, aetiology, and prognosis. J Neurol Neurosurg Psychiatry 63:611-615

Goldszal AF, Davatzikos C, Pham DL, Yan MX, Bryan RN, Resnick SM (1998): An image processing system for qualitative and quantitative volumetric analysis of brain images. J Comput Assist Tomogr 22:827-837

Gonsalez CF, Swirsky-Sacchetti T, Mitchell D, Lublin FD, Knobler RL; Ehrlich SM (1994): Distribution patterns of multiple sclerosis brain lesions. J Neuroimag 4:188-195

Granger CV, Davis LS, Peffers NC, Sherwood CC, Barett J (1979): Stroke rehabilitation analysis of repeated Barthel index measures. Arch Phys Med Rehabil 60:14-17

Grenier PA, Beigelman-Aubry C, Fetita C, Preteux F, Brauner MW, Lenoir S (2002): New frontiers in CT imaging of airway disease. Eur Radiol 12:1022-1044

Grimaud J, Lai M, Thorpe J, Adeleine P, Wang L, Barker GJ, Plummer DL, Tofts PS, McDonald WI, Miller DH (1996): Quantification of MRI lesion load in multiple sclerosis: a comparison of three computer-assisted techniques. Magn Reson Imaging 14:495-505

Gupta L, Sortrakul T (1998): A Gaussian mixture image segmentation algorithm. Pattern Recognition 31:315-325

Hadlock F, harrist R, Sharman R, Deter R, Park S (1935): Estimation of fetal weight with the use of head body and femur measurements-a prospective study. Am J Obstet Gynecol 151: 333-337

Hageleit U, Will CH, Seidel D (1987): Automated measurements of cerebral atrophy in multiple sclerosis. Neurosurg Rev 10:137-140

Hamilton JW, Cook JA, Philips DE, Jones AS (1995): Limitations of acoustic rhinometry determined by a simple model. Acta Otolaryngol (stockh) 115:811-814

Haralick RM, Shapiro LG (1985): Image segmentation techniques. Comput Vision Graphics Image Process 29:100-132

Harris LD, Robb RA, Yuen TS, Ritman EL (1979): Display and visualization of three-dimensional reconstructed anatomic morphology: experience with the thorax, heart and coronary vasculature of dogs. J Comput Assist Tomogr 15: 439-446

Hasegawa Y, Fisher M, Latour LL, Dardzinski BJ, Sotak CH (1994): MRI diffusion mapping of reversible and irreversible ischemic injury in focal brain ischemia. Neurology 44: 1484-1490

Hassfield S, Muhling J (1998): Navigation in maxillofacial and craniofacial surgery. Comput Aided Surg 3:183-187

Hata T, Makihara K, Aoki S, Hata K, Kitao M (1990): Magnetic resonance imaging of the fetus: initial experience. Gynecol Obstet Invest 29:255-258

Heinonen T, Eskola H, Dastidar P, Laarne O, Malmivuo J (1997): Segmentation of T1 MR scans for reconstruction of resistive models. Comp Meth Prog Biomed 54:173-181

Heinonen T, Dastidar P, Eskola h, frey H, Ryymin P, laasonen E (1998a): Applicability of semiautomatic segmentation for volumetric analysis of brain lesions. J Med Eng and Tech 22:173-178

Heinonen T, Visala K, Blomqvist M, Eskola H, Frey H (1998b): 3D-visualization library for multimodal medical images. Comp Med Imag Graph 22:267-273

Heinonen T, Dastidar P, Frey H, Eskola H (1999): Applications of MR image segmentation. IJBEM 1: 35-46

Heilman KM; Bowers D, Coslett HB, Whelan H, Watson RT (1985): Directional hypokinesia: prolonged reaction times for leftward movements in patients with right hemisphere lesions and neglect. Neuroloy 35:855-859

Herman GT (1988): Three-dimensional imaging on a CT or MR scanner. JCAT Comput Assist Tomogr 12:450-458

Hier DB, Mondlock J, Caplan LR (1983): Behavioural abnormalities after right hemisphere stroke. Neurology 33:337-344

Hilberg O, Jackson AC, Swift DL, Pedersen OF (1989): Acoustic rhinometry: evaluation of nasal cavity by acoustic reflection. J Appl Physiol 66:295-303

Hilberg O, Jensen FT, Pedersen OF (1993): Nasal airway geometry: comparison between acoustic reflections and magnetic resonance scanning. J Appl Pysiol 75:2811-2819

Hirata G, Medearis A, Horenstein J, Bear M, Platt L (1990): Ultrasonographic estimation of fetal weight in the clinically macrosomic fetus. Am J Obstet Gynecol 162:238-242

Hoehne KH, Delapaz RL, Bernstein R, Taylor RC (1987): Combined surface display and reformatting for the three-dimensional analysis of tomographic data. Invest Radiol 22:658-664

Hofmann HM, Ebner F, Haas J, Einspieler R, Justich E, Lahousen M, Pickel H, Burghardt E (1988): Magnetic resonance imaging in clinical cervical cancer:pretherapeutic tumor volumetry. Baillieres Clin Obstet Gynecol 2:789-802

Hollett MD, Jehfrey B, Nino-Murcia M, Jorgensen MJ, Harris DP (1995): Dual-phase Helical CT of the liver: value of arterial phase scans in detection of small (1.5 cm) malignant neoplasms. AJR Am J Roentgenol 164: 879-884

Hölmberg V, Stephan KM, Netz J (1991): Transcranial stimulation of motor cortex in upper motor neuron syndrome: its relation to the motor deficit. Electroencephal Clin Neurophysiol 81:377-388

Hopper KD, Kasales CJ, Eggli KD, Tenhave TR, Belman NM, Potok PS, Van Slyke MA, Olt GJ, Close P, Lipton A, Harvey HA, Hartzel JS (1998): The impact of 3D quantification of tumor bulk determination on current methods of assessing response to treatment. J Comput Assist Tomogr 20:930-937

Hoskins WJ (1994): Epithelial ovarian carcinoma: Principles of primary surgery. Gynecol Oncol 55:91-96

Hricak H (1996): Magnetic resonance tumor volumetry in cervical cancer. Int J Rad Oncol Biol Phys 35:1113-1114

Hunter RW, Alexander NDE, Soutter WP (1992): Meta-analysis of surgery in advanced ovarian carcinoma: is maximum cytoreductive surgery an independent determinant of prognosis? Am J Obstet Gynecol 166:540-541

Huppert BJ, Brandt KR, Ramin KD, King BF (1999): Single shot fast spin echo MR imaging of the fetus: a pictorial assay. Radiographics 19:215-227

Igarashi M, O-Uchi T, Isago H, Wright WK (1983): Utricular and saccular volumetry in human temporal bones. Acta Otolaryngol 95:75-80

Ingle GT, Stevenson VL, Miller DH, Leary SM, Rovaris M, Barkhof F, Brochert B, Dousset V, Filiippi M, Montalban X, Kalkers NF, Polman CH, Rovira A, Thompson AJ (2002): Two year follow-up study of primary and transitional progressive multiple sclerosis. Mult Scler 8:108-114

Iwamoto T, Shimizu T, Akazawa M, Kikawada M, Nishimura T, Takasaki M (1999): Long-term prognosis of patients with initial cerebral thrombosis and MRI findings. Nippon Ronen Igakkai Zasshi 36:128-135

Jack CR Jr. (1994): MRI-based hippocampal volume measurements in epilepsy. Epilepsia 35 Suppl 6:21-29

Jackson EF, Narayana PA, Wolinsky JS, Doyle TJ (1993): Accuracy and reproducibility in volumetric analysis of multiple sclerosis lesions. J Comput Assist Tomogr 17:200-205

Jacquelin C, Aurengo A, Hejblum G (1997): Evolving descriptors for texture segmentation. Pattern Recognition 30:1069-1079

Jain A (1989): Fundamentals of digital image processing. Prentice-Hall, Inc. New York, USA

Jansen O, Schellinger P, Fiebach J, Hacke W, Sartor K (1999): Early recanalization in acute ischemic stroke saves tissue at risk defined by MRI. Lancet 353:2036-2037

Jehkonen M, Ahonen JP, Dastidar P, Koivisto AM, Laippala P, Vilkki J, Molnar G (2000): Visual neglect as a predictor of functional outcome one year after stroke. Acta Neurol Scand 101:195-201

Johnson I, Stehling M, Blamire A, Coxon R, Howseman A, Chapman B (1990): Study of internal structure of the human fetus *in utero* by echo-planar magnetic resonance imaging. Am J Obstet Gynecol 163:601-607

Johnson I (1995): Magnetic resonance imaging in obstetrics. Curr Obstet Gynaecol 5:25-29

Jost G, Hahnel S, Heiland S, Stippich C, Bellemann ME, Sa K (2002): An automated method for volumetric quantification magnetization transfer of the brain. Magn Reson Imaging 20: 593-597

Juottonen K, Laakso MP, Partanen K, Soininen H (1999): Comparative MR analysis of the entorhinal cortex and hippocampus in diagnosing Alzheimer disease. AJNR Am J Neuroradiol 20:139-144

Just M, Higer HP, Pfannenstiel P (1988): Errors in T1-determination using multislice technique and Gaussian slice profiles. Magn Reson Imaging 6:53-56

Kappos L, Stadt D, Keil W, Ratzka M, Heitzer T, Schneiderbanger-Grygier S (1987): An attempt to quantify magnetic resonance imaging in multiple sclerosis-correlation with clinical parameters. Neurosurg Rev 10: 133-135

Kase Y, Hilberg O, Pedersen OF (1994): Posture and nasal patency: Evaluation by acoustic rhinometry. Acta Otolaryngol 114:70-74

Kennedy DW, Zinreich J, Rosenbaum AE, Johns ME (1985): Functional endoscopic sinus surgery. Arch Otolaryngyol 111:576-582

Kertesz A, Harlock W, Coates R (1979): Computer tomographic localization, lesion size, and prognosis in aphasia and non-verbal impairment. Brain Lang 8:34-50

Kidd D, Thorpe JW, Thompson AJ, Kendall BE, Moseley IF, MacManus DG, McDonald WI, Miller DH (1993): Spinal cord MRI using multi-array coils and fast spin echo. Findings in multiple sclerosis. Neurology 43:2632-2637

Kiel MK, Greenspun B, Grossman RI (1988): Magnetic resonance imaging and degree of disability in multiple sclerosis. Arch Phys Med Rehab 69:11-13

Kinkell WR, Jacobs L (1976): Computed axial transverse tomography in cerebrovascular disease. Neurology 26:924-930

Kinsella G, Ford B (1985): Hemi-attention and the recovery patterns of stroke patients. Int Rehab Med 7:102-106

Kinoshita T, Ishii K, Naganuma H, Higashiiwai H (2000): MR findings of ovarian tumors with cystic components. Br J Radiol 73:333-339

Kischell ER, Kehtarnavaz N, Hillman GR, Levin H, Lilly M, Kent TA (1995): Classification of brain compartments and head injury lesions by neural networks applied to MRI. Neuroradiology 37:535-541

Knopman DS, Rubens AB (1986): The validity of computed tomographic scan findings for the localization of cerebral functions. Arch Neurol 43:328-332

Koudriavtseva T, Thompson AJ; Fiorelli M, Gasperini C, Bastianello S, Bozzao A, Paolillo A, Pisani A, Galgani S, Pozzilli C (1997): Gadolinium enhanced MRI predicts clinical and MRI disease activity in relapsing-remitting multiple sclerosis. J Neurol Neurosurg Psychiatry 62: 285-287

Krahe T, Scholaut KH, Poss T, Trier HG, Lackner K (1989): Computed tomographic volumetry of the orbit in endocrine orbitopathy. Rofo Forstschr Geb Rontgenstr Neuen Bildgeb Verfahr 151:597-601

Kucharzyck W, Crawley AP, Kelly WM, Henkelman RM (1988): Effect of multislice interference on image contrast in T2- and T1-weighted MR images. AJNR Am J Neuroradiol 9:443-451

Kunkel M, Hochban W (1994): Acoustic rhinometry: a new diagnostic procedure- experimental and clinical experience. Int J Oral Maxillofac Surg 23: 409-412

Kubik-Huch RA, Dorffler W, von Schulthess GK, Marinek B, Koch Seifert B, Haller U, Steinert HC (2000a): Value of (18F)-FDG positron emission tomography, computed tomography, and magnetic resonance imaging in diagnosing primary and secondary ovarian tumors. Eur Radiol 10:761-767

Kubik-Huch RA, Huisman TA, Wisser J, Gottstein–Alame N, Debatin JF, Seifert B, Ladd ME, Stallmach T, Marincek B (2000b): Ultrafast MR imaging of the fetus. AJR Am J Roentgenol 174:1599-1606

Kuroda S, Houkin K, Kamiyama H, Mitsumori K, Iwasaki Y, Abe H (2001): Long-term prognosis of medically treated patients with internal carotid or middle cerebral artery occlusion: can acetazolamide predict it? Stroke 2001 32:2110-2116

Kurtz AB, Tsimikas JV, Tempany CM, Hamper UM, Arger PH; Brewechsler RJ, Francis IR, Kuhlman JE, Siegelman ES, Mitchell DG, Silverman SG, Brown DL; Sheth S, Coleman BG, Ellis JH, Kurman I, Caudry DJ, McNeill BJ (1999): Diagnosis and staging of ovarian cancer: comparative values of Doppler and conventional US, CT, and MR imaging correlated with surgery and histopathologic analysis-report of the RadioDiagnostic Oncology Group. Radiology 212: 19-27

Kurtzke JF (1983): Rating neurologic impairment in multiple sclerosis. An expanded disability status scale (EDSS). Neurology 33:1444-1452

Kwok SH, Constantinides AG (1997): A fast recursive shortest spanning tree for image segmentation and edge detection. IEEE Trans Imag Proc 6:328-339

Laakso MP, Juottonen K, Partanen K, Vainio P, Soininen H (1997): MRI volumetry of the hippocampus: the effect of slice thickness on volume formation. Magn Reson Imaging 15:263-265

Lan LM, Yamashita Y, Tang Y, Sugahara T, Takahashi M, Ohba T, Okamura H (2000): Normal fetal brain development: MR imaging with a half-Fourier rapid acquisition with relaxation enhancement sequence. Radiology 215: 205-210

Laptook AR (1990): Magnetic resonance: safety considerations and future directions. Semin Perinatol 14:189-192

Lee Dh, Ko YT (1999): Advanced gastric carcinoma: the role of three-dimensional and axial imaging by spiral CT. Abdom Imaging 24:111-116

Lee JM, Yoon U, Nam SH, Kim JH, Kim IY, Lim SI (2003): Evaluation of automated and semi-automated skull-stripping algorithms using similarity index and segmentation error. Comput Biol Med 33: 495-507

Lei T, Sewchand W (1992): Statistical approach to X-ray CT imaging and its applications in image analysis - Part II: a new stochastic model-based image segmentation technique for X-ray CT image. IEEE Trans Med Imag 11:62-70

Leung CK, Lam FK (1997): Maximum a posteriori spatial probability segmentation. IEEE Proc Vis Image Signal Process 144:161-167

Levine DN (1990): Unawareness of visual and sensorimotor defects: A hypothesis. Brain Cogn 13:233-281

Levine D, Hatabu H, Gaa J, Atkinson MW, Edelman RR (1996): Fetal anatomy revealed with fast MR sequences. AJR Am J Roentgenol 167:905-908

Levine D, Barnes PD, Sher S, Semelka RC, Li W, McArdle CR, Worawattankul S, Edelman RR (1998): Fetal fast MR imaging : reproducibility, technical quality and conspicuity of anatomy. Radiology 206: 519-524

Li C, Goldgof DB, Hall LO (1993): Knowledge based classification and tissue labeling of MR images of human brain. IEEE Trans Med Imag 12:740-749

Li L, Gong J, Chen W (1997): Gray level image thresholding based on Fisher Linear Projection of two dimensional histogram. Pattern Recognition 30:743-749

Liang Z (1993): Tissue classification and segmentation of MR images. IEEE Eng Med Biol 93: 81-85

Lemieux L, Hammers A, Mackinnon T, Liu Rs (2003): Automatic segmentation of the brain and intracranial cerebrospinal fluid in T1-weighted volume MRI scans of the head, and its application to serial cerebral and intracranial volumetry. Magn Reson Med 49:872-884

Lin TN, He YY, Wu G, Khan M, Hsu CY (1993): Effect of brain edema on infarct volume in a focal cerebral ischemia model in rats. Stroke 24:117-121

Liszka G, Thalacker U, Somogyi A, Nemeth G (1997): Volume changes to the neck lymph node metastases in head and neck tumors. The evaluation of radiotherapeutic success. Strahlenther Onkol 173:428-430

Lodder J (1984): CT-detected hemorrhagic infarction: relation with the size of the infarct and the presence of midline shift. Acta Neurol Scand 70: 329-335

Loseff NA, Wang L, Lai HM, Yoo DS, Gawne-Cain ML, McDonald WI, Miller DH, Thompson AJ (1996 a): Progressive cerebral atrophy in multiple sclerosis. A serial MRI study. Brain 119:2009-2019

Loseff NA, Webb SL, O'Riordan JI, Page R, Wang L, Barker GJ, Tofts PS, McDonald WI, Miller DH, Thompson AJ (1996 b): Spinal cord atrophy and disability in multiple sclerosis. A new reproducible and sensitive MRI method with potential to monitor disease progression. Brain 119:701-708

Loseff NA, Miller DH (1998): Measures of brain and spinal cord atrophy in multiple sclerosis. J Neurol Neurosurg Psychiatry 64 (Suppl):102-105

Lowe TW, Weinreb J, Santos Ramos R, Cunningham FG (1985): Magnetic resonance imaging in human pregnancy. Obstet Gynecol 66:629-633

Mahoney FT, Barthel DW (1965): Functional evaluation: Barthel index. Rehabilitation 14:61-65

Mammi S, Filippi M, Martinelli V, Campi A, Colombo B, Scotti G, Canal N, Comi G (1996): Correlation between brain MRI lesion volume and disability in patients with multiple sclerosis. Acta Neurol Scand 94:93-96

Marroquin JL, Vemuri BC, Botello S, Calderon F, Fernando C, Bouzas A (2002): An accurate and efficient bayesian method for automatic segmentation of brain MRI. IEEE Trans Med Imaging 21:934-945

Mathews VP, Barker PB, Bryan RN (1992): Magnetic resonance evaluation of stroke. Magn Reson Quarterly 8:245-263

Matthews PM, Pioro E, Narayan S, De Stefano N, Fu L, Francis G, Antel J, Wolfson C, Arnold DL (1996): Assessment of lesion pathology in multiple sclerosis using quantitative MRI morphometry and magnetic resonance spectroscopy. Brain 119:715-722

Matsumae M, Kikinis R, Morocz I, Lorenzo AV, Albert MS, Black PM, Jolesz FA (1996): Intracranial compartment volumes in patients with enlarged ventricles assessed by magnetic resonance based image processing. J Neurosurg 84:972-981

Mauch E, Mayer G, Kornhuber A, Krapf H, Jurgens R, Hufnagl JM, Kornhuber HH (1994): The significance of quantitative computerized tomography in the long term prognosis of ischemic stroke. Rehabilitation (Stuttg) 33:212-220

McKinnon GC (1993): Ultrafast interleaved gradient-echo-planar imaging ona standard scanner. Magn Reson Med 30:609-616

Meier DS, Cothren RM, Vince DG, Cornhill JF (1997): Automated morphometry of coronary arteries with digital image analysis of intravascular ultrasound. Am Heart J 133:681-690

Mikolajczyk K, Szabatin M, Rudnicki P, Grodzki M, Burger C (1998): A JAVA environment for medical image data analysis: initial application for brain PET quantitation. Med Inform (London) 23:207-214

Miller AB, Hoogsstraten B, Staguet M, Winkler A (1981): Reporting rseults of cancer treatment. Cancer 47:207-214

Miller DH; Grossman RI, Reingold SC, McFarland HF (1998): “The role of magnetic resonance techniques in understanding and managing multiple sclerosis”. Brain 121:3-24

Miller DH, Barkhof F, Frank JA, Parker GJ, Thompson AJ (2002): Measurement of atrophy in multiple sclerosis: pathological basis, methodological aspects and clinical relevance. Brain 125:1676-1695

Min YG, Jang YJ (1995): Measurements of cross-sectional area of the nasal cavity by acoustic rhinometry and CT scanning. Laryngoscope 105:757-759

Mitchell JR, Karlik SJ, Lee DH, Fenster A (1994): Computer-assisted identification and quantification of multiple sclerosis lesions in MR imaging volumes in the brain. J Magn Reson Imaging 4:197-208

Mitsias PD, Jacobs MA, Hammond R, Pasnoor M, Santhakumar S, Papamitsikas NI, Soltanian-Zadeh H, Lu H, Chopp M, Patel SC (2002): Multiparamatric MRI ISODATA ischemic lesion analysis: correlation with clinical neurological deficit and single-parameter techniques. Stroke 2002 33:2839-2844

Mori H, Aoki S, Masumoto T, Yoshikawa T, Tago M, Shin M, Ohtomo K, Kabasawa H (2002): Two-dimensional magnetic resonance digital subtraction angiography using array spatial sensitivity encoding techniques in the assessment of intracranial hemodynamics. Radiat Med 20:223-229

Morrissey SP, Miller DH, Kendall B, Kingsley DP, Kelly MA, Francis DA, MacManus DG, McDonald WI (1993): The significance of brain magnetic resonance imaging abnormalities at presentation with clinically isolated syndromes suggestive of multiple sclerosis. A 5-year follow up study Brain 116:135-146

Moteki T, Ishiazaka H (2000): Diffusion-weighted EPI of cystic ovarain lesions: evaluation of cystic contents using apparent diffusion coefficients. J Magn Reson Imaging 12:1014-1019

Na DG, Ryoo JW, Lee KH, Moon CH, Yi CA, Kim EY, Lee SJ, Yi BY, Kim JH, Byun HS (2003): Multiphasic perfusion computed tomography in hyperacute ischemic stroke: comparison with diffusion and perfusion magnetic resonance imaging. J Comput Assist Tomogr 27:194-206

Ono I, Ohura T, Narumi E, Kawashima K, Matsuno I, Nakamura S, Ohhata N, Uchiyama Y, Watanabe Y, Tanaka F (1992): Three-dimensional analysis of craniofacial bones using three-dimensional computer tomography. J Craniomaxillofac Surg 20:49-60

Orthner H, Seler W (1975): Planimetric volumetry of human brains. Fortschr Neurol Psychiatr Grenzgeb 43:191-209

O'Riordan JI, Gawne-Cain M, Coles A, Wang L, Compston DA, Tofts P, Miller DH (1998): T1 hypointense lesion load in secondary progressive multiple sclerosis: a comparsion of pre versus post contrast loads and of manual versus post contrast loads and of manual versus semiautomated threshold techniques for lesion segmentation. Mult Scler 4: 408-412

Oyama H, Wakao F, Takahira Y (1998): The clinical advantages of editable real-time volume rendering in a medical virtual environment: Vol Med. Stud Health Technol Inform 50:341-345

Ozawa k, Suchanek G, Breitschopf H, Bruck W, Budka H, Jellinger K, Lassmann H (1994): Patterns of oligodendroglia pathology in multiple sclerosis. Brain 117:1311-1322

Pantano P, Caramia F, Bozzao L, Dieler C, von Kummer R (1999): Delayed increase in infarct volume after cerebral ischemia: correlations with thrombolytic treatment and clinical outcome. Stroke 30:502-507

Park KS, Lee NS (1987): A three-dimensional Fourier descriptor for human body representation/reconstruction from serial cross sections. Comput Biomed Res 20:125-140

Parnetti L, Lowenthal DT, Presciutti O, Pelliccioli GP; Palumbo R, Comi G, Chiarini P, Palumbo B, Tarducci R, Senin U (1996): 1H-MRS, MRI-based hippocampal volumetry, and 99m Tc-HMPAO-SPECT in normal aging, age-associated memory impairment, and probable Alzheimer's disease. J Am Geriatr Soc 44:209-211

Parodi RC, Sardanelli F, Renzetti P, Rosso E, Losacco C, Ferrari A, Levrero F, Pilot A, Inglese M, Mancardi GL (2002): Growing Region Segmentation software (GRES) for quantitative magnetic resonance imaging of multiple sclerosis: intra- and interobserver agreement : a comparison with manual contouring method. Eur Radiol 12:866-871

Paty DW, Li DK, Oger JJ, Kastrukoff L, Koopmans R, Tanton E, Zhao GJ (1994): Magnetic resonance imaging in the evaluation of clinical trials in multiple sclerosis. Ann Neurol Suppl 36:95-96

Pavlidis T (1988): Image Analysis. Ann Rev Comput Sci 3:121-146

Pelizzari CA. (1998): Image processing in stereotactic planning: volume visualization and image registration. Med Dosim 23:137-145

Peters H, Fischer C, Bogner U, Reiners C, Schleusener H (1996): Reduction in thyroid volume after radioiodine therapy of Grave's hyperthyroidism: results of a prospective, randomized multicenter study. Eur J Clin Invest 26:59-63

Piver MS, fanning J, Craig KA (1993): Ovarian cancer: in Knapp RC, Berkowitz RS (Eds), Gynecologic Oncology 2nd ed., McGraw-Hill, New York p.253

Poser CM, Paty DW, Scheinberg C, McDonald W, Davis FA, Ebers GC, Johnson KP, Sibley WA, Silberberg DH, Tourtelotte WW (1983): New diagnostic criteria for multiple sclerosis: Guidelines for research protocols. Ann Neurol 13:227-231

Price MA, Goldstein GD (1997): The use of a digital imaging system in a dermatologic surgery practice. Dermat Surg 23:31-32

Pruessmann KP, Weiger W, Scheidegger MB, Boesiger P (1999): SENSE: sensitivity encoding for fast MRI. Magn Reson Med 42:952

Quarantelli M, Ciarmiello A, Orra VB, Orefice G, Larobina M, Larobina R, Schiavone V, Salvatore E, Alfano B, Brunetti A (2003): Brain tissue volume changes in relapsing-remitting multiple sclerosis: correlation with lesion load. Neuroimage 18:360-366

Quint LE, Whyte RI, Kazarooni EA (1995): Stenosis of the central airways: evaluation by using helical CT with multiplanar reconstructions. Radiology 194: 871-877

Raff U, Newman FD (1992): Automated lesion detection and lesion quantitation in MR images using autoassociative memory. Med Phys 19:71-73

Raff U, Scherzinger AL, Vargas PF, Simon JH (1994): Quantitation of grey matter, white matter, and cerebrospinal fluid from spin-echo images using an artificial neural network technique. Med Phys 21:1933-1942

Ramac LC, Varshney PK (1997): Image thresholding based on Ali-Silvey distance measures. Pattern Recognition 30:1161-1174

Rasmussen D, Köhler O, Worm-Pettersen S, Blegvad N, Jacobson HL, Egeblad M, Frii SM, Nielsen NT (1992): Computed tomography in prognostic stroke evaluation. Stroke 23:506-510

Raya SP, Udupa JK, Barrett WA (1990): A PC-based 3D imaging system: algorithms, software, and hardware considerations. Comput Med Imaging Graph 14:353-370

Reider-Groswasser I, Kott E, Benmair J, Huberman M, Machtey Y, Gelertner I (1988): MRI parameters in multiple sclerosis patients. Neuroradiology 30:219-223

Reittner P, Tillich M, Luxenberger W, Weinke R, Preidler K, Kole W, Stammberger H, Szolar D (2002): Multislice CT-image guided endoscopic surgery using an electromagnetic tracking system. Eur Radiol 12: 592-596

Revol C, Jourlin M (1997): A new minimum variance region growing algorithm for image segmentation. Pattern Recognition Letters 18:249-258

Ritman EL, Harris LD, Padiyar R, Chevalier PA, Robb RA (1979): Non-invasive visualization and quantitation of cardiovascular structure and function. Physiologist 22:39-43

Robb RA, Hanson DP, Karwoski RA; Larson AG, Workman EL, Stacy MC (1989): ANALYZE: a comprehensive, operator-interactive software package for multidimensional medical image display and analysis. Comput Med Imaging Graph 13:433-454

Robb RA, Aharon S, Cameron BM (1997): Patient-specific anatomic models from three dimensional medical image data for clinical applications in surgery and endoscopy. J Digit Imaging 10:31-35

Roberts N, Garden AS, Cruz-Orive LM, Whitehouse GH, Edwards R (1994): Estimation of fetal volume by magnetic resonance imaging and stereology. Br J Radiol 67:1067-1077

Roithman R, Cole P, Chapnik J, Barreto SM, Szalai JP, Zamel N (1994): Acoustic rhinometry, rhinomanometry, and the sensation of nasal patency: a correlative study. J Otolaryngol 23:454-458

Roithman R, Cole P, Chapnik J, Zamel N (1995): Reproducibility of acoustic rhinometric measurements. Am J Rhinol 9:263-267

Rogers DC, Campbell CA, Stretton JL, Mackay KB (1997): Correlation between motor impairment and infarct volume after permanent and transient middle cerebral artery occlusion in the rat. Stroke 28:2060-2065

Ropele S, Strasser-Fuchs S, Augustin M, Stollberger R, Enzinger C, Hartung HP, Fazekas F (2000): A comparison of magnetization transfer ratio, magnetization transfer rate, and the native relaxation time of water protons related to relapsing-remitting multiple sclerosis. AJNR Am J Neuroradiol 21:1885-1891

Ropper AH (1986): Lateral displacement of the brain and level of consciousness in patients with an acute hemispheral mass. N Eng J Med 314:953-958

Rovaris M, Yousry TA, Calori G, Fesl G, Voltz R, Filippi M (1997): Sensitivity and reproducibility of fast-FLAIR, FSE, and TGSE sequences for the MRI assessment of brain lesion load in multiple sclerosis: a preliminary study. J Neuroimaging 7:98-102

Rovaris M, Filippi M, Falautano M, Minicucci L, Rocca MA, Martinelli V, Comi G (1998): Relation between MR abnormalities and patterns of cognitive impairment in multiple sclerosis. Neurology 50:1601-1608

Runmarker B, Andersen O (1993): Prognostic factors in a multiple sclerosis incidence cohort with twenty years of follow-up. Brain 116:117-134

Sahoo P, Soltani S, Wong A, Chen Y (1988): A survey of thresholding techniques. Comput. Vision Graphics Image Process 41:233-260

Sahoo P, Wilkins C, Yeager J (1997): Threshold selection using Renyi's Entropy. Pattern Recognition 30:71-84

Sailer M, Fischl B, Salat D, Tempelmann C, Schonfeld MA, Busa E, Bodammer N, Heinle HJ, Dale A (2003): Focal thinning of cerebral cortex in multiple sclerosis. Brain 126:1734-1744

Santarelli MF, Positano V, Landini L. (1997): Real time multimodal medical image processing: a dynamic volume-rendering application. IEEE Trans Inf Tech Biomed 1:171-178

Saunders DE, Clifton AG, Brown MM (1995): Measurement of infarct size using MRI predicts prognosis in middle cerebral artery infarction. Stroke 26:2272-2276

Satava RM (1996): Virtual endoscopy: diagnosis usiong 3-D visualization and virtual representation. Surg Endosc 10:173-174

Saver JL, Johnson KC, Homer D, Wityk R, Koroshetz W, Truskonski LL, Haley EC (1999): Infarct volume as a surrogate or auxillary outcome measure in ischemic stroke clinical trials. The RANTTAS Investigators. Stroke 30:293-298

Schellinger PD, Jansen O, Fiebach JB, Hacke W, Sartor K (1999): A standardized MRI stroke protocol: comparison with CT in hyperacute intracerebral hemorrhage. Stroke 30:765-768

Schild RL, Fimmers R, Hansmann M (2000): Fetal weight estimation by three-dimensional ultrasound. Ultrasound Obstet Gynecol 16:445-452

Schulz JB, Skalej M, Wedekind D, Luft AR, Abele M, Voigt K, Dichgans J, Klockgether T (1999): Magnetic resonance imaging-based volumetry differentiates idiopathic Parkinson's syndrome from multiple system atrophy and progressive supranuclear palsy. Ann Neurol 45: 65-74

Schlaug G, Benfield A, Baird AE, Siewert B, Lovblad KO, Parker RA, Edelman RR, Warach S (1999): The ischemic penumbra: operationally defined by diffusion and perfusion MRI. Neurology 53: 1528-1537

Schwaighofer BW, Yu KK, Mattrey RF (1989); Diagnostic significance of interslice gap and imaging volume in body MR imaging. AJR Am J Roentgenol 153:629-632

Seno H, Mizunuma M, Nishida M, Inoue M, Yanai A, Irimoto M (1999): 3D-CT stereoscopic imaging in maxillofacial surgery. J Comput Assist Tomogr 23:276-279

Senoh D, Tanaka H, Akiyama M, Yanagihara T, Hata T (1999): Saline infusion contrast intrauterine sonographic assessment of the endometrium with high-frequency, real-time miniature trasnsducer in normal menstrual cycle: a preliminary report. Hum Reproduc 14:2600-2603

Shan ZY, Yue GH, Liu JZ (2002): Automated histogram-based brain segmentation in T1-weighted three-dimensional magnetic resonance head images. Neuroimage 17:1587-598

Shepard M, Richards V, Berkowitz R, Warsof S, Hobbins J (1982): An evaluation of two equations for predicting fetal weight by ultrasound. Am J Obstet Gynecol 142:47-54

Shinozuka N, Okai T, Kohzuma S, Mukubo M, Shih CT, Maeda T, Kuwubara Y, Mizuno M (1987): Formulas for fetal weight estimation by ultrasound measurer based on neonatal specific gravities and volumes. Am J Obstet Gynecol 157:1140-1145

Sibbitt WL Jr., Sibbitt RR, Brooks WM (1999): Neuroimaging in neuropsychiatric systemic lupus erythematosus. Arthritis Rheum 42:2026-2038

Simons JH, Jacobs LD, Campion M, Wende K Simonian N (1998): Magnetic resonance studies of intramuscular Interferon B-la for relapsing multiple sclerosis. Ann Neurol 43:79-87

Simonsen CZ, Rohl L, Westergaard-Poulsen P, Gyldensted C, Andersen G, Ostergaard L (2002): Final infract size after acute stroke: prediction with flow heterogeneity. Radiology 225:269-275

Sipilä J, Nyberg-Simola S, Suonpää J, Laippala P (1996): Some fundamental studies on clinical measurement conditions in acoustic rhinometry. Rhinology 34:206-209

Smith SM, Zhang Y, Jenkinson M, Chen J, Matthews PM, Federico A, De Stefano N (2002): Accurate, robust and automated longitudinal and cross-sectional brain change analysis. Neuroimage 17:479-489

Smulian JC, Ranzini AC, Ananth CV, Rosenberg JC, Vintzileos AM (1999): Comparison of three sonographic circumference measurement techniques to predict birth weight. Obstet Gynecol 93:692-696

Sodickson DK, Manning WJ (1997): Simultaneous acquisition of spatial harmonics (SMASH): ultra-fast imaging with radiofrequency coil arrays. Magn Reson Med 38:591-603

Soltanian-Zadeh Hamid H, Windham JP, Peck DJ (1996): Optimal linear transformation for MRI feature extraction. IEEE Trans Med Imag 15:749-767

Stocchetti N, Croci M, Spagnoli D, Gilardoni F, Resta F, Colombo A (2000): Mass volume measurement in severe head injury: accuracy and feasibility of two pragmatic methods. J Neurol Neurosurg Psychiatry 68:14-17

Stehling MK, Mansfield P, Ordidge RJ, Coxon R, Chapman B, Blam P, Gibbs P, Johnson IR, Symonds EM; Worthington BS (1990): Echo-planar imaging of the human fetus in utero. Magn Reson Med 13:314-318

Stepanek V, Zavada M (1969): Practical applications of pulmonary X-ray volumetry, planimetry aand chest expansion coefficient. Cesk Radiol 23:224-230

Stone LA, Frank JA, Albert PS (1995): The effect of interferon beta on BBB disruptions demonstrated by contrast enhanced MRI in RRMS. Ann Neurol 37:611-619

Stroinska Kus B, Filipczak D (1990): The value of diagnostic and prognostic methods of encephalo-volumetry (EVM) in acute ischemic stroke. Neurol Neurochir Pol 24:146-152

Sueten P, Bellon E, Vandermeulen D, Smet M, Marchal G, Nuyts J, Mortelmans L (1993): Image segmentation: methods and applications in diagnostic radiology and nuclear medicine. Eur J Radiol 17:14-21

Sundaramoorthy G, Hoford JD, Hoffman EA, Higgins WE (1995): IMPROMPTU: a system for automatic 3D medical image analysis. Comput Med Imaging Graph19:131-143

Swanson RA, Morton MT, Tsao-Wu G, Savalos RA, Davidson C, Sharp FR (1990): A semiautomated method of measuring brain infarct volume. J Cerebr Blood Flow Metab 10:290-293

Szabo G, Hrabak K, Gyulai-Gaal S (1999): Sinus elevation and its control by 3D computer tomography. Fogorv Sz 92:41-44

Tamura R, Dooley S (1991): The role of ultrasonography in the management of diabetic pregnancy. Clin Obstet Gynecol 34:526-534

Taxt T, Lundervold A (1994): Multispectral analysis of the brain using magnetic resonance imaging. IEEE Trans Med Imag 13:470-481

Terheyden H, Maune S, Mertens J, Hillberg O (2000): Acoustic rhinometry:validation by three-dimensionally reconstructed computer tomographic scans. Appl Pyhsiol 89:1013-1021

Thomas JD (1996): Magnetization transfer in magnetic resonance imaging. Radiol Technol 67:287-306

Tomkinson A, Eccles R (1996): The identification of the potential limitations of acoustic rhinometry using computer-generated three dimensional reconstructions of simple models. Am J Rhinol 10:77-82

Trapp BD, Peterson J, Ranshoff RM, Rudick R, Mork S, Bo L (1998): Axonal transection in lesions of multiple sclerosis. N Eng J Med 338:278-285

Trievsky AL, Ptak T,Wu O (1997): Evaluation of MS lesions with full tensor diffusion weighted imaging and anisotropy mapping (abstract). Proceedings of the International Society for Magnetic Resonance in Medicine 1:666

Truyen L, van Waesberghe JH, van Walderveen MA, van Oosten BW, Polman CH, Hommes OR, Ader HJ, Barkhof F (1996): Accumulation of hypointense lesions ("black holes") on T1 spin-echo MRI correlates with disease progression in multiple sclerosis. Neurology 47:1469-1476

Tsuchiya K, Katase S, Seki T, Mizutani Y, Hachiya J (1996): Short communication: MR imaging of the fetal brain abnormalities using a HASTE sequence. Br J Radiol 69:668-670

Udupa JK, Hung HM, Chuang KS (1991): Surface and volume rendering in three-dimensional imaging: a comparison. J Digit Imaging 4:159-168

Udupa JK, Wei L, Samarasekara S, Miki Y, van Buchem MA, Grossman RI (1997): Multiple sclerosis lesion quantification using fuzzy-connected principles. IEEE Trans Med Imaging. 16: 598-669

Udupa JK (1999): Three-dimensional visualization and analysis in methodologies: a current perspective. Radiographics 19:783-806

Udupa JK, Nyul LG, Ge Y, Grossman RI (2001): Multiprotocol MR image segmentation in multiple sclerosis: experience with over 1,000 studies. Acad Radiol 8:1116-1126

Ukkonen M, Dastidar P, Heinonen T, Laasonen E, Elovaara I (2003): Volumetric estimation by MRI in primary progressive multiple sclerosis: volumes of plaques and atrophy correlated with neurologic disability. Eur J Neurol 10: 663-669

Utsonomiya H, Takano K, Okazaki M, Mitsudome A (1999): Development of the temporal lobe in infants and children: analysis by MR-based volumetry. AJNR Am J Neuroradiol 20:717-723

Vaidyanathan M, Clarke LP, Heidtman C, Velthuizen RP, Hall LO (1997a): Normal brain volume measurements using multispectral MRI segmentation. Magn Reson Imaging 15:87-97

Vaidyanathan M, Clarke LP, Hall LO, Heidtman C, Velthuizen R, Gosche K, Phupanich S, Wagner H, Greenberg H, Silbiger ML (1997b): Monitoring brain tumor response to therapy using MRI segmentation. Magn Reson Imaging 15:323-334

Vaidyanathan L, Tench CR, Morgan PS, Lin X, Blumhardt LD (2002): White matter T(1) relaxation times histograms and cerebral atrophy in multiple sclerosis. J Neurol Sci 197:45-50

van Waesberghe JHTM, Castelijns J, Weerts JGE, Nijeholt GJ, Hillegers JP, Polman CH, Barkhof F (1996): Disappearance of multiple sclerosis lesions with severely prolonged T1 on images obtained by a FLAIR sequence. Magn Reson Imaging 14:209-213

van Waesberghe JHTM, van Walderveen MAA, Castelijns J (1997): Natural history of hypointense lesions in multiple sclerosis. J Neurol 244 S 87, 248

van Waesberghe JHTM, van Walderveen MAA, Castelijns JA, Scheltens P, Lycklama A, Nijeholt GJ, Polman CH, Barkhof F (1998): Patterns of lesion development in multiple sclerosis: longitudinal observations with T1-weighted spin-echo and magnetization transfer MR. AJNR Am J Neuroradiol 19:675-683

van Walderveen MAA, Barkhof F, Hommes OR (1995): Correlating MR imaging and clinical disease activity in multiple sclerosis: relevance of hypointense lesions on short TR/short TE (T1 weighted) spin echo images. Neurology 45:1684-690

Vinitski S, Gonsalez C, Mohamed F, Iwanaga T, Knobler RL, Kahlili K, Mack J (1997): Improved intracranial lesion characterisation by tissue segmentation based on a 3D feature map. Magn Reson Med 37:457-469

Wade DT, Skilbeck CE, Langton Hewer R (1983a): Predicting Barthel Index score at 6 months after acute stroke. Arch Phys Med Rehabil 64:24-28

Wade DT, Langton-Hewer R, Wood VA; Skilbeck CE, Ismail HM (1983b): The hemiplegic arm after stroke: measurement and recovery. J Neurol Neurosurg Psychiatry 46:521-524

Watt A, Watt M (1992): Advanced animation and rendering techniques. Addison-Wesley, New York

Watt A (1993): 3D computer graphics, 2nd edition Reading. MA: Addison Wesley.

Weeks KJ, Montana GS (1997): Three-dimensional applicator system for carcinoma of the uterine cervix. Int J Radiat Oncol Biol Phys 37:455-463

Wilkens RF, Rowberg AH (1995): Future opportunities using technical advantages in picture processing and data transfer. J Rheumatol 22:2201-2203

Wilson B, Cockburn J, Halligan PW (1987): Development of a behavioural test of visuo-spatial neglect. Arch Phys Med 68: 98-102

Wilson M, Morgan PS, Blumhardt LD (2002): Quantitative diffusion characteristics of the human brain depend on MRI sequence parameters. Neuroradiology 44:586-591

Winfield D, Silbiger M, Brown GS, Clarke L, Dwyer S, Yaffe M, Stern F (1994): Technology transfer in digital mammography. Report of the Joint National Cancer Institute- National Aeronautics and Space Administration workshop of May 19-20,1993. Invest Radiol 29:507-515

Wintermark M, Reichhardt M, Cuisenaire O, Maeder P, Thiran JP, Schnyder P, Bogousslavsky J, Meuli R (2002): Comparison of admission perfusion computed tomography and qualitative diffusion- and perfusion-weighted magnetic resonance imaging in acute stroke patients. Stroke 33:2025-2031

Wittsack HJ, Ritzl A, Fink GR, Wenerski F, Siebler M, Seitz RJ, Modder U, Freund HJ (2002): MR imaging in acute stroke:diffusion-weighted and perfusion imaging parameters for predicting infarct size. Radiology 222:397-403

Yamamoto K, Shimuzu t, Tanaka Y, Narabayashi I (1999): Evaluation of utility of MR T2-weighted images using multislice echoplanar imaging of female pelvis: comparison with fat-supressed fast spin echo. Nippon Igaku Hoshasen Gakkai Zasshi 59:313-317

Yamashita Y, Namimoto T, Abe Y, Takahashi M, Iwanasa J, Miyazaki K, Okamura H (1997): MR imaging of the fetus by a HASTE sequence. AJR Am J Roentgenol 168:513-519

Yi CA, Na DG, Ryoo JW, Moon WJ, Lee KH, Lee SJ (2002): Multiphasic perfusion CT in acute middle cerebral artery ischemic stroke: prediction of final infract volume and correlation with clinical outcome. Korean J Radiology 3:163-170

YonedaY, Mori E, Yamashita H, Yamadori A (1994): MRI volumetry of medial temporal lobe structures in amnesia following herpes encephalitis. Eur Neurol 34:243-252

Yong TY, Fu KS (1986): Handbook of pattern recognitions and image processing. Academic press. New York

Youssem DM (1993): Imaging of sinonasal inflammatory disease. Radiology 188:303-314

Yuh EL, Jeffrey RB, Jr. Birdwell RL, Chen BH, Napel S (1999): Virtual endoscopy using perspective volume-rendered three-dimensional sonographic data: technique and clinical applications. AJR Am J Roentgenol 172:1193-1197

Zhu C, Jiang T (2003): Multicontext fuzzy clustering for separation of brain tissues in magnetic resonance images. Neuroimage 18:685-696

Zijdenbos AP, Forghani R, Evans AC (2002): Automatic pipeline analysis of 3-D MRI data for clinical application to multiple sclerosis. IEEE Trans Med Imaging 21:1280-1291

Zinreich ST (1992): Imaging of the nasal cavity and paranasal sinuses. Curr Opin Radiol 4:112-116

Zucker SW (1976): Region growing: childhood and adolescence. Comput Graphics Image Process 5:382-399